# Stochastic Reaction-Diffusion Methods for Modeling Gene Expression and Spatially Distributed Chemical Kinetics

*Samuel A. Isaacson*

A dissertation submitted in partial fulfillment

of the requirements for the degree of

Doctor of Philosophy

Department of Mathematics

New York University

September 2005

---

Charles S. Peskin

*Dedicated to my family. Their help and support has been greatly appreciated.*

# Acknowledgments

Foremost, I would like to thank my adviser Charles S. Peskin. Working with Charlie the past five years has been a wonderful experience. His enthusiasm was always uplifting, and his insight was a joy to see first hand. I've learned a great deal from my conversations with him and watching his thought process.

I would also like to thank my family. My father has always been there when I needed someone to discuss an idea with, and has given me many helpful suggestions over the years. I've had a great time learning from him throughout my entire life. My mother deserves thanks for all the hard work she has put in helping me with various annoying and unpleasant tasks the past several years. I had a great time living with my brother Will the past year. It was fun having the chance to hang out with him again. I'd also like to thank my brother Joe, getting together with him is definitely one of the best stress relievers I've encountered.

One of the best parts of attending Courant was the opportunity to see my grandfather on a regular basis. I had a great time talking to him these past five years. I'll never forget the wonderful Lincoln Center concerts my grandparents, aunt, uncle, and myself attended. I only wish I had managed to visit with my grandparents on more occasions.

At Courant I would like to thank a number of my fellow graduate students, former and current. Among Charlie's students; Boyce, Arjun, Yoichiro, Danny, and Paul, I've learned a lot from each of you, and had a great time talking over research with you all.

Finally, I'd like to thank several faculty members at Courant. I've had helpful discussions on several occasions with Dan Tranchina, Jerome Percus, and Eric Vanden-Eijnden, and appreciate their taking the time to talk. I would also like to thank Marsha Berger for letting me use her three–dimensional Cartesian mesh generation software. She was also very helpful in explaining how to use the program. While I was unable to find the time to put the three–dimensional gene expression results I have into this thesis, I have used her software on a number of occasions and found it invaluable.

# Preface

I've always enjoyed math and science, though in high school it was too easy, and hence often boring. I knew when I started college that I would pursue either mathematics or computer science. After taking a number of biology, physics, pure mathematics, computer science, and applied mathematics courses I realized that applied math held the most appeal to me. I particularly liked the idea of trying to use mathematics to solve problems in biology and medicine. Upon starting graduate school I focused on studying molecular cell biology. Here, every new insight into how cells work is another piece of information to aid in understanding disease.

I soon focused on studying the process of gene expression, and it is from there that thesis really begins.

*Samuel A. Isaacson*

*New York, New York*

# Abstract

In order to model fundamental cell biological processes including the transcription, translation, and nuclear membrane transport of biological molecules within a eukaryotic cell it is necessary to be able to approximate the stochastic reaction and diffusion of a small number of molecules in the complex three dimensional geometry of a cell. For this reason a method is developed that incorporates diffusion and active transport of chemicals in complex geometries into stochastic chemical kinetics simulations. Systems undergoing stochastic reaction and diffusion are modeled using a discrete state master equation. It is shown how the jump rates for spatial movement between mesh cells can be derived from the discretization weights of embedded boundary methods. Spatial motion is modeled as first order reactions between neighboring mesh cells using the predetermined jump rates. Individual realizations of the master equation can be created by the Gillespie Method, allowing numerical simulation of the underlying stochastic process. We investigate the numerical convergence properties of both the underlying embedded boundary methods, and the reaction–diffusion master equation model. Several continuum limits of the reaction–diffusion master equation are investigated. In addition, a proposed model for the problem of locating a point binding site by diffusive motion is studied. This problem is an

idealization of one proposed mechanism by which gene regulatory proteins may bind to specific sites on DNA. A model of transcription, translation, and nuclear membrane transport in eukaryotic cells is presented and solved using this stochastic reaction-diffusion master equation approach in order to demonstrate the feasibility of the method in studying fundamental spatially distributed cell biological processes.

# Contents

# List of Figures

# List of Tables

# List of Appendices

# Chapter 1

# Introduction

## 1.1 Why Choose This Problem

Over the last several decades there has been an explosive growth in the accumulated knowledge in the field of molecular cell biology. From the human genome project to the development of green fluorescent protein (GFP) markers for real–time cellular protein imaging, an enormous amount of new biological data has been generated. Much of this data is quantitative, allowing the development of detailed mathematical models of cellular processes, where before only qualitative models were possible. While working on extending to eukaryotes a recent mathematical model [12] of prokaryotic gene expression, I began to wonder how messenger ribonucleic acids (mRNAs) and proteins actually moved from one location to another within biological cells, and whether this movement could be important in the dynamics of cellular signaling networks. At the time, it turned out that this was very much an open problem in the biological literature. Moreover, several biological and modeling papers had just shown that

gene expression was in fact a very noisy, stochastic process [4],[33],[13] . I became interested in studying the roles that stochasticity and spatial movement could have in gene expression and cellular signaling. Looking at the existing literature, I soon realized that there appeared to be no well-developed method for modeling both stochastic and spatial dynamics of signaling networks within biological cells.

It was known, biologically, that mRNAs and proteins primarily moved either by diffusion, by active transport along microtubules and actin filaments, or by some combination of the two. What was not known for most signaling networks or the process of gene expression was which of these types of motion were used. Moreover, it was unknown how important this spatial motion actually was: did proteins and mRNA molecules simply diffuse quickly throughout the cellular environment and effectively become well–mixed on the time scale of any reaction events? If not, there were, and still are, many interesting questions about how proteins and mRNAs localize to specific regions of cells and locate specific binding targets. I was also curious about what effect the complex cellular architecture had on the spatial movement of proteins and mRNA. To investigate these problems, I began to work on developing a method for simulating the spatial processes of diffusion and active transport that could also account for the observed stochastic effects in certain signaling networks.

## 1.2 Importance of small numbers and spatial effects

Spatially homogeneous, deterministic mass–action kinetics is a standard model for the interactions of proteins, genes, and mRNAs within cellular networks. It assumes that the evolution of any chemical species can be represented by a continuously–varying concentration representing the number of that species within the cell divided by the cell volume. Fundamentally, however, the numbers of protein and mRNA molecules within cells are discrete integer variables. The notion of a continuously–varying concentration is only well–defined for a sufficiently large number of the molecules. Moreover, for systems in which spatial effects are important the population number must not only be large within the cell as a whole, but also locally within areas of interest. If the population number is sufficiently small, stochastic effects can have a noticeable impact on the behavior of the biological system.

The issue of stochasticity in gene expression was discussed in [4]. The authors subsequently demonstrated numerically that the variation of cell fates within a $\lambda$–phage infected population of bacterial cells can be explained as arising from a stochastically driven gene expression switch [5]. The presence of noise in prokaryotic transcription and translation was demonstrated experimentally in both [13] and [33]. More recently, experimental results demonstrating transcriptional noise in eukaryotic cells were presented in [7].

Spatial effects are present in many biological systems, and hence the spatially uniform, or well–mixed, assumption will not always hold. Systems in which spatial effects are known to play a role include Ash1 mRNA localiza-

tion in budding yeast [1], morphogen gradients across egg–polarity genes in Drosophila oocyte [1], and the synapse–specificity of long–term facilitation in Aplysia [25]. The exact processes by which proteins and mRNAs move between specific locations, and become localized, are not yet known definitively. Movement is believed to be composed of a mixture of diffusion and various forms of active transport. For example in [15], mRNA movement within the cytoplasm was found to exhibit diffusive motion, "corralled" diffusive motion, and active, directionally specific, transport. Probabilistic switching between these three types of movement was observed in most cases. Moreover, the fraction of time spent in each of the types of motion was found to differ depending on whether the mRNA was destined to be localized or not.

## 1.3 Methods and Modeling Developed Here

As mentioned in the previous sections, there are two primary means by which molecules move through biological cells: diffusion and active transport. Diffusion can be incorporated into deterministic mass–action kinetics through the use of reaction–diffusion partial differential equations. Molecular noise can be accounted for through the use of stochastic chemical kinetics, but the usual formulation of stochastic chemical kinetics assumes a spatially homogeneous cellular space [20]. Methods for incorporating diffusion into stochastic chemical kinetics are presented in [40] and [17], and go back as far as the model developed in [16]. In these methods, space is divided into a collection of equally–sized mesh cells. The state of the chemical system is then given by the number of each chemical species within each mesh cell. Using certain assumptions about

the nature of the diffusion process and the chemical reaction mechanisms, a reaction–diffusion master equation is then derived to give the probability of the system being in a particular state. In [17] all transition rates between mesh cells are identical, and formulas for the transition rates are calculated in this case. In [40] a discussion of the continuum–limit for the first several moments of the model is given, but no method is given for calculating the cell–based transition rates. Note that, to our knowledge, no prescription has yet been given for determining diffusive jump rates in complicated geometries, such as are present in biological cells.

We develop here a stochastic reaction–diffusion active transport model for mesh cells of arbitrary volume and shape, with varying spatial transition rates. Later, we specialize to considering only embedded boundary Cartesian mesh representations of the domain of interest. A method then is developed for calculating diffusive and active transport transition rates between mesh cells within a domain containing multiple complex boundaries embedded in the Cartesian mesh. The development of a convergent diffusive approximation within complex geometries is critical for use in individual (biological) cell models where the large number of organelles and membranes could have a significant effect on the overall dynamics of a chemical system. Diffusive transition rates are systematically calculated from terms in an embedded boundary discretization of the Fokker–Planck equation for a classically diffusing Brownian particle. We expect the reaction–diffusion master equation to be such a discretization in the case of no reactions and only one particle. Likewise, active transport rates are calculated from an embedded boundary discretization of a Fokker-Planck equation representing an advective transport model of active transport. The notion

of using a master equation as an approximation to a continuum equation was used in [41] to obtain approximations of the Fokker-Planck equation for a single particle moving in a one–dimensional potential. The master equation itself has a special structure, requiring a constraint on the weights of the discretization. Our method is found to conserve probability, and in the case of diffusion, to satisfy detailed balance. The underlying embedded boundary discretization converges at a rate between first and second order in practice. As an application of the method, a model of transcription, translation, nuclear transport, and the diffusive motion of expressed mRNAs and proteins within a two–dimensional eukaryotic cell was developed and simulated.

We note that the method we develop is an Eulerian method, using an underlying Cartesian mesh. We track the (integer) numbers of molecules of any given type within the different cells of the mesh, but we do not resolve the spatial location any more finely than that, not do we keep track of molecules as individuals. When a molecule of type A leaves mesh cell $i$ and enters mesh cell $j$, this registers in our methodology as a decrease by one in the number of molecules of type A in mesh cell $i$, and an increase by one in the number of molecules of type A in mesh cell $j$. If there was more than one molecule of type A in mesh cell $i$ before this event occurred, we do not care or keep track of *which* molecule of type A was the one that moved.

Other models of diffusive motion have been developed using Lagrangian methods that track the movement of each individual molecule within the system. For example, in [3] a Lagrangian method was developed for simulating stochastic–reaction diffusion systems within biological cells. These methods have the benefit of allowing exact local treatments of single–molecule diffusion,

but they introduce other challenges, in particular, how to handle the interactions between molecules. If the molecules are treated as points, they will never actually collide, and so the rate of a bimolecular reaction has to be modeled as a function of the distance between the molecules. It is not clear what function to use, or where to put the reaction product(s) once a simulated reaction has occurred.

reactions between particles, detection of particle collisions, and resolving particle–geometry interactions.

We begin in Chapter 2 by describing the different types of spatial and stochastic models that have previously been developed. We next give the formulation of our stochastic–reaction–diffusion master equation. This is followed by a discussion of our stochastic reaction–diffusion model's connections to deterministic reaction–diffusion models, Brownian motion, and reaction–diffusion models that track individual particles. We conclude by formulating a master equation that incorporates active transport into our stochastic reaction–diffusion model.

In Chapter 3 we derive expressions for the diffusive and active transport jump rates in the reaction–diffusion active transport model. We examine the numerical convergence of time independent and time dependent solutions to the discrete approximation to the Laplacian in two dimensions. From this approximation the diffusion jump rates are derived. The chapter concludes with a discussion of the convergence of our numerical method for approximating solutions to the reaction–diffusion master equation.

Chapter 4 presents our spatial model for transcription, translation, and nuclear transport. We assume that mRNAs and proteins are allowed to freely diffuse within the nucleus and cytoplasm, but must undergo a nuclear transport

process to cross the nuclear membrane. The time evolution of one realization of this model is demonstrated, and noisy oscillations in nuclear protein levels are observed.

Finally, in Chapter 5 we discuss the problem of whether the reaction–diffusion master equation model of the point binding interaction converges as the numerical mesh size is reduced. In the biological gene expression model of Chapter 4, binding to DNA is modeled as a chemical reaction involving a fixed target site, assumed located within a single mesh cell, and a diffusing regulatory protein. Several other methods by which this binding reaction can be modeled are studied, as is the behavior of solutions to the reaction–diffusion master equation model for this point interaction as the numerical mesh size is varied. The results we obtain do not give a good indication about whether the the master equation point binding model converges as the numerical mesh size goes to zero. We conclude with a discussion of an alternative continuum model of the point binding interaction, involving diffusion in a hierarchy of dimensions, for which we demonstrate a convergent discrete master equation approximation.

# Chapter 2

# Background and Formulation

## 2.1 Introduction

In this section we describe several physical models for representing a system of chemically reacting molecules. The models are presented in order from the most macroscopic to the most microscopic, and collectively give a hierarchy of different physical descriptions. Figure 2.1 shows an expanded hierarchy of physical theories and models that can be used to study chemically reacting biological systems. Quantum Mechanics provides the most microscopic and fundamental representation of such systems. Unfortunately, it is severely limited with current technology in both the number of interacting atoms and the timescale which can be realistically simulated. To study more complicated problems, such as protein folding and protein–DNA interactions, Molecular Dynamics simulations are commonly used [35]. Here, heuristic force fields for molecular interactions are defined and then used in Newtonian Mechanics simulations. Typically, Gaussian noise is added to the equations of motion to account for thermal forcing,

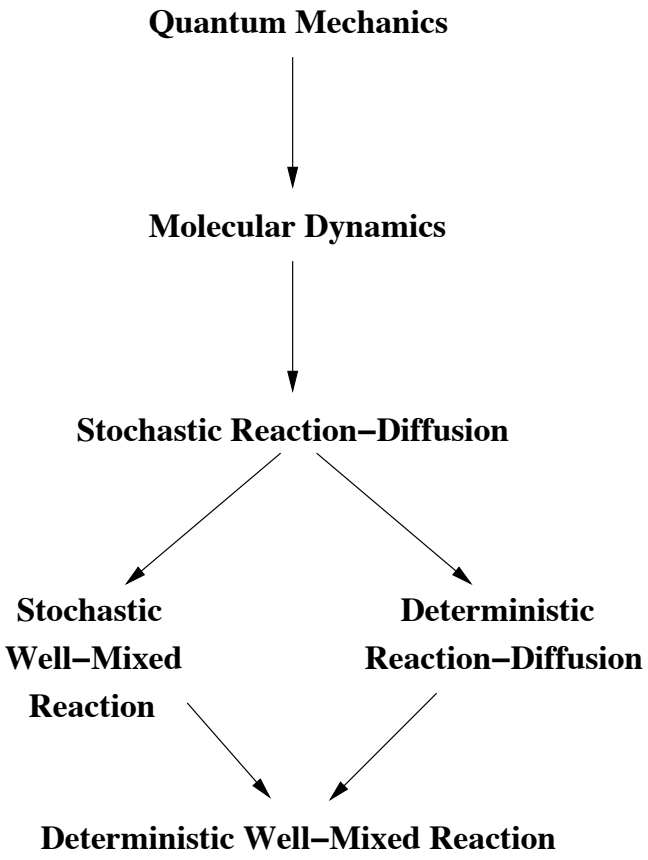


Figure 2.1: Hierarchy of physical models useful in studying chemical reactions.

and simulations are performed in the over–damped regime. Recently, a number of methods for incorporating Quantum Mechanical effects into Molecular Dynamics simulations have been developed. These techniques allow small subsets of interactions to be resolved Quantum Mechanically as needed, see for example [36]. As of 2002, state of the art Molecular Dynamics simulations could only resolve at most microsecond timescales, and at most on the order of $100,000$ atoms [35], hence, a coarser description is needed to describe the interactions of multiple biological molecules.

At a more macroscopic level than Molecular Dynamics, stochastic well–

mixed chemical kinetics [21] [31], deterministic reaction–diffusion chemical kinetics, and deterministic well-mixed chemical kinetics (i.e. mass action), have all been used to study the populations of chemical species within single cells. Stochastic chemical kinetics assumes all chemicals are uniformly distributed, i.e. well–mixed, at all times within the volume of interest. It describes the evolution of the random variables for the number of each chemical species as a functions of time. One benefit to this description is the ability to resolve accurately fluctuations in the number of a given biochemical species, an important effect in studying processes at the single cell level [7]. In contrast, deterministic reaction–diffusion partial differential equations ignore fluctuations in the number of each chemical species, but instead resolve spatial gradients in chemical concentration within the cell. Such gradients are present, and can play an important role in many biological signaling and transport processes [37] [27]. The most macroscopic type of description typically considered is deterministic mass–action chemical kinetics. Here, biological cells are assumed to be well–mixed environments, where fluctuations in chemical concentrations can be ignored.

We begin this chapter by reviewing the previous three descriptions of chemical processes at the cellular level, and then describe how both spatial and stochastic effects can be combined in a more microscopic physical model, stochastic reaction–diffusion chemical kinetics. This description, while more macroscopic than Molecular Dynamics, provides a fundamentally more accurate description of chemical processes within cells then the levels below it in Figure 2.1. We discuss the relation between stochastic reaction–diffusion models and the more macroscopic descriptions, while also motivating how one can completely specify diffusion related parameters of the stochastic reaction–diffusion

model through its relation to single particle Brownian motion. Finally, we also present an analogous method for describing stochastic chemical reactions in advective flows, which we use as a model of active transport in biological cells.

## 2.2 Deterministic Mass–Action Chemical Kinetics

### 2.2.1 Well–Mixed Mass Action

Well–mixed mass action kinetics assumes that all chemical species can be described by spatially uniform, continuously varying in time, chemical concentrations. Rates laws give the instantaneous change in concentration of each chemical species per unit time, and lead to ordinary differential equations for the time evolution of each chemical species' concentration. These rate laws are approximations to more exact quantum and statistical mechanical models of the chemical system, and only in certain special cases can they be derived explicitly from these more exact representations. (See, for example, [14] and [29] for derivations from quantum mechanical models, and [32] for derivations from kinetic theory hard sphere models).

We now formulate the mathematical description of deterministic chemical kinetics. The chemical system is assumed to be composed of $L$ distinct chemical species, with concentrations $C^l(t)$, $l = 0 \dots L$. The state vector for the chemical system is then $\boldsymbol{C}(t) = \big(C^1(t), \dots, C^L(t)\big)$. Later, when we consider stochastic models, the state of the chemical system will be described by the number of

each chemical species,

$$\boldsymbol{M}(t) = \left(M^1(t), \ldots, M^L(t)\right) = V\boldsymbol{C}(t),$$

where $V$ gives the total volume in which the chemical system is reacting. Assume there are $K$ possible reactions, with the function $\tilde{a}^k(\boldsymbol{C}(t))$ denoting the rate of the $k$'th reaction, $k = 1 \ldots K$. The stoichiometry of the chemical reactions are given by the vector $\boldsymbol{\nu}_k = \left(\nu_k^1, \ldots, \nu_k^L\right)$, defined to be the change in the number of each chemical species that results from one occurrence of reaction $k$ (i.e., $\boldsymbol{M}(t) \to \boldsymbol{M}(t) + \boldsymbol{\nu}_k$). Note that the change in concentration, per unit time, of the $l$'th species due to the $k$'th reaction is then given by $\nu_k^l \tilde{a}^k(\boldsymbol{C}(t))$. With these definitions, the total change in concentration, per unit time, of the $l$'th chemical species is then given by the sum of the rates of change in the concentration caused by all the different chemical reactions:

$$\frac{d\boldsymbol{C}^l}{dt}(t) = \sum_{k=1}^{K} \nu_k^l \tilde{a}^k(\boldsymbol{C}(t)). \tag{2.1}$$

As a simple example, consider the bimolecular reaction A + B $\to$ C, with bimolecular rate constant $\alpha$. Let $l = 1$ denote species A, $l = 2$ denote species B, and $l = 3$ denote species C. There is only one reaction, so $K = 1$, with $\nu_1 = (-1, -1, 1)$, and $\tilde{a}^1(A, B, C) = \alpha AB$. The equations of evolution for the chemical system are then

$$\begin{aligned}
\frac{dA}{dt} &= -\alpha A(t)B(t) \\
\frac{dB}{dt} &= -\alpha A(t)B(t) \\
\frac{dC}{dt} &= \alpha A(t)B(t)
\end{aligned}$$

### 2.2.2 Reaction–Diffusion Models

Deterministic reaction–diffusion models incorporate diffusion, through Fick's law, into well–mixed mass action kinetics. It is assumed that all molecules of each chemical species diffuse independently, and that all chemical reactions are local. Reactions are pointwise, and generally only depend on the chemical concentration of each species at that point. With these assumptions, the total change in amount of a chemical species, within a region, per unit time is given by the diffusive flux into the region added to the total change in the amount of that species throughout the region cause by chemical reactions.

Denote by $\boldsymbol{F}^l(\boldsymbol{x},t)$ the diffusive flux of chemical species $l$ at the point $\boldsymbol{x}$. Fick's Law states that

$$\boldsymbol{F}^l(\boldsymbol{x},t) = -D^l \nabla C^l(\boldsymbol{x},t),$$

where $D^l$ is the diffusion coefficient of species $l$. The total amount of chemical species $l$ will then satisfy a conservation equation within any arbitrary small closed region, $B$,

$$\frac{d}{dt}\int_B C^l(\boldsymbol{x},t)\,d\boldsymbol{x} = -\int_{\partial B} \boldsymbol{F}^l(\boldsymbol{x},t)\cdot\boldsymbol{\eta}(\boldsymbol{x},t)\,dS + \int_B \sum_{k=1}^{K} \nu_k^l a^k(\boldsymbol{C}(\boldsymbol{x},t),\boldsymbol{x})\,d\boldsymbol{x}.$$

Here $\boldsymbol{\eta}(\boldsymbol{x})$ denotes the normal to the boundary of $B$. The first term on the right hand side gives the total change in the amount of the $l$'th chemical species due to diffusion into the region, while the second term gives the change in amount within the region due to chemical reactions. Applying the divergence theorem,

$$\frac{d}{dt}\int_B C^l(\boldsymbol{x},t)\,d\boldsymbol{x} = \int_B D^l \Delta C^l(\boldsymbol{x},t)\,d\boldsymbol{x} + \int_B \sum_{k=1}^{K} \nu_k^l a^k(\boldsymbol{C}(\boldsymbol{x},t),\boldsymbol{x})\,d\boldsymbol{x}.$$

Taking the time derivative inside the first integral, and noting that $B$ is an arbitrary region, we obtain the reaction–diffusion partial differential equations

(PDEs),

$$\frac{\partial C^l}{\partial t}(\boldsymbol{x},t) = D^l \Delta C^l(\boldsymbol{x},t) + \sum_{k=1}^{K} \nu_k^l a^k(\boldsymbol{C}(\boldsymbol{x},t),\boldsymbol{x}), \quad l = 1 \ldots L. \tag{2.2}$$

### 2.2.3 Reaction–Diffusion Active Transport

Many cellular processes involve the active transport of molecules along microtubules or actin filaments. A well–known example is the active transport of vesicles along axonal microtubules in neurons [1]. We present here a model, similar to the macroscopic one–dimensional transport model of [38], that incorporates active transport into the reaction–diffusion mass–action model. The general process by which cargo is moved along microtubules is through binding to molecular motors, which can subsequently "walk" along the microtubule towards a desired target. As the microtubule density is fairly high within eukaryotic cells, we model their effect as an underlying direction field along which molecular motors can proceed with a specified velocity.

With these assumptions, let $\boldsymbol{v}(\boldsymbol{x})$ denote the velocity a given motor will have at location $x$. The simplest model one could assume would be that the microtubules form a specified direction field, $\boldsymbol{\phi}(\boldsymbol{x})$, along which motors progress with a fixed speed, $v$. Note that $v$ may be positive or negative depending on the direction a given motor walks along the microtubules. In this case, $\boldsymbol{v}(\boldsymbol{x}) = v\,\boldsymbol{\phi}(\boldsymbol{x})$. The system of reaction–advection–diffusion equations describing the chemical concentrations would then be

$$\frac{\partial C^l(\boldsymbol{x},t)}{\partial t} + \nabla \cdot \left( C^l(\boldsymbol{x},t)\, \boldsymbol{v}^l(\boldsymbol{x}) \right) = D^l \Delta C^l + \sum_{k=1}^{K} \nu_k^l\, \tilde{a}^k(\boldsymbol{C}(\boldsymbol{x},t),\boldsymbol{x}), \quad l = 1 \ldots L. \tag{2.3}$$

In general, except for chemical species representing microtubule bound motor

proteins or microtubule bound complexes of motor proteins and cargo, $\boldsymbol{v}^l(\boldsymbol{x}) \equiv 0$. Further, note that the model will include multiple chemical states for each motor protein. For example, motors can be bound to cargo or unbound, and in each of these states can either be bound to a microtubule and undergoing active transport, or freely diffuse. These different states, and the reactions representing transitions between them, are absorbed into the state vector, $\boldsymbol{C}(\boldsymbol{x}, t)$, and the reaction terms, $a^k(\boldsymbol{C}(\boldsymbol{x}, t), \boldsymbol{x})$. Note that no single equation in the coupled system (2.3) will contain both the advective and diffusive terms, since any given component of $\boldsymbol{C}(\boldsymbol{x}, t)$ can only undergo one of the two types of motion.

## 2.3 Stochastic Chemical Kinetics

### 2.3.1 Physical Basis and Formulation

Consider a well–mixed chemical system in a finite closed volume $V$. That is: the probability of a given particle of the system being in an arbitrary subregion of volume $dV$ is $dV/V$. Further, let each individual particle's velocity be a Maxwell–Boltzmann distributed random variable. With these assumptions Gillespie showed in [21] that a chemical system can be represented as an integer valued, continuous time Markov Process satisfying a master equation.

Let $\boldsymbol{M}(t) = \left(M^1(t), \ldots, M^L(t)\right)$ denote the state vector of the chemical system. $M^l(t)$ will be the random variable representing the number of molecules of chemical species $l$ at time $t$. Define $\boldsymbol{m} = \left(m^1, \ldots, m^L\right)$ to be a possible value of $\boldsymbol{M}(t)$. Denote by $\mathrm{S}^l$ the *name* of the $l$'th species. Assume there are $K$ possible reactions, with the function $a^k(\boldsymbol{m})$ giving the probability per unit time of reaction $k$ occurring when $\boldsymbol{M}(t) = \boldsymbol{m}$. For example, letting $k$ label the

unimolecular (first order) reaction $S^i \to S^j$, then $a^k(\boldsymbol{m}) = \alpha\, m^i$, where $\alpha$ is the rate constant in units of number of occurrences of the reaction per molecule of $S^i$ per unit time. Letting $k'$ denote the index of the bimolecular reaction $S^i + S^j \to S^n$, where $i \neq j$, then $a^{k'}(\boldsymbol{m}) = \beta\, m^i m^j$. Here $\beta$ is the rate constant in units of number of occurrences of the reaction per molecule of $S^i$ and per molecule of $S^j$, per unit time. Note that if species $i$ and $j$ are the same, then $a^{k'}(\boldsymbol{m}) = (\beta/2)\, m^i(m^i - 1)$. Let $\boldsymbol{\nu}_k = \left(\nu_k^1, \ldots, \nu_k^L\right)$ be the change in $\boldsymbol{M}$ that results from one occurrence of reaction $k$ (i.e., $\boldsymbol{M}(t) \to \boldsymbol{M}(t) + \boldsymbol{\nu}_k$). The integers $\left(\nu_k^1, \ldots, \nu_k^L\right)$ define the stoichiometry of the $k$'th reaction. In the notation of Appendix A, $a^k(\boldsymbol{m}) = W_{\boldsymbol{m}+\boldsymbol{\nu}_k, \boldsymbol{m}}$, assuming $\boldsymbol{\nu}_i \neq \boldsymbol{\nu}_k$ for all $i \neq k$. (If two or more reactions have identical stoichiometry, their rates are added to obtain the corresponding transition rate $W$. Also, if there are no reactions leading from state $\boldsymbol{m}'$ to $\boldsymbol{m}$, then $W_{\boldsymbol{m},\boldsymbol{m}'}$ is zero.) Note that the $\nu_k^l$ may be positive or negative integers (or zero). Then if

$$P(\boldsymbol{m}, t) \equiv \text{Prob}\{\boldsymbol{M}(t) = \boldsymbol{m} | \boldsymbol{M}(0) = \boldsymbol{m}_0\},$$

the master equation for the time evolution of the probability of the system will be

$$\frac{dP(\boldsymbol{m})}{dt} = \sum_{k=1}^{K} \left( a^k(\boldsymbol{m} - \boldsymbol{\nu}_k) P(\boldsymbol{m} - \boldsymbol{\nu}_k) - a^k(\boldsymbol{m}) P(\boldsymbol{m}) \right), \tag{2.4}$$

where we drop the argument $t$ for notational convenience, and where $P(\boldsymbol{m}, 0) = 1$ if $m = m_0$ and zero otherwise. This is a coupled set of ODEs over all possible integer values of the components of the vector $\boldsymbol{m}$. The derivation of this equation follows from the results of Appendix A. We shall subsequently refer to (2.4) as the chemical master equation. Assuming all the $\boldsymbol{\nu}_k$ are distinct, in

the notation of Appendix A the master equation is

$$\frac{dP(\boldsymbol{m})}{dt} = \sum_{k=1}^{K} \left( W_{\boldsymbol{m},\boldsymbol{m}-\boldsymbol{\nu}_k} P(\boldsymbol{m}-\boldsymbol{\nu}_k) - W_{\boldsymbol{m}+\boldsymbol{\nu}_k,\boldsymbol{m}} P(\boldsymbol{m}) \right). \tag{2.5}$$

In both (2.4) and (2.5) the first term in the sum corresponds to all possible transitions into state $\boldsymbol{m}$ from some pre–state, $\boldsymbol{m}-\boldsymbol{\nu}_k$, while the second term corresponds to all possible transitions out of state $\boldsymbol{m}$ to $\boldsymbol{m}+\boldsymbol{\nu}_k$.

### 2.3.2 Moments

We derive here the equations satisfied by the moments for an arbitrary component of $\boldsymbol{M}$, $M^l$. To find this system of ODEs consider an arbitrary moment, defined by

$$\left\langle \left(M^l\right)^n \right\rangle \equiv \sum_{\boldsymbol{M}} \left(M^l\right)^n P(\boldsymbol{M}).$$

In this equation, the sum is over all possible values of the state vector $\boldsymbol{M}$. Note that in many practical models $M^l$ has a finite maximum value; we assume that $P(\boldsymbol{m})$ is defined to be zero for values of $m^l$ larger than that maximum. An equation for the time evolution of $\left(M^l\right)^n$ can be obtained by multiplying (2.4)

by $\left(m^l\right)^n$, and summing over all possible values of $\boldsymbol{m}$. This gives

$$\begin{aligned}
\frac{d\left\langle \left(M^l\right)^n \right\rangle}{dt} &= \sum_{\boldsymbol{m}} \left(m^l\right)^n \frac{dP(\boldsymbol{m})}{dt}, \\
&= \sum_{\boldsymbol{m}} \sum_{k=1}^{K} \left( \left(m^l\right)^n a^k(\boldsymbol{m}-\boldsymbol{\nu}_k) P(\boldsymbol{m}-\boldsymbol{\nu}_k) - \left(m^l\right)^n a^k(\boldsymbol{m}) P(\boldsymbol{m}) \right), \\
&= \sum_{k=1}^{K} \sum_{\boldsymbol{m}} \left( \left(m^l + \nu_k^l\right)^n - \left(m^l\right)^n \right) a^k(\boldsymbol{m}) P(\boldsymbol{m}), \\
&= \sum_{k=1}^{K} \sum_{\boldsymbol{m}} \sum_{l=0}^{n-1} \binom{n}{l} \left(\nu_k^l\right)^{n-l} \left(m^l\right)^l a^k(\boldsymbol{m}) P(\boldsymbol{m}), \\
&= \sum_{k=1}^{K} \sum_{l=0}^{n-1} \binom{n}{l} \left(\nu_k^l\right)^{n-l} \left\langle \left(M^l\right)^l a^k(\boldsymbol{M}) \right\rangle . \qquad (2.6)
\end{aligned}$$

Letting $n = 1$ in (2.6) we find that the mean of $m^l$ satisfies

$$\frac{d\left\langle M^l \right\rangle}{dt} = \sum_{k=1}^{K} \nu_k^l \left\langle a^k(\boldsymbol{M}) \right\rangle . \qquad (2.7)$$

Setting $n = 2$ in (2.6), the second moment of $M^l$ satisfies

$$\frac{d\left\langle \left(M^l\right)^2 \right\rangle}{dt} = \sum_{k=1}^{K} \left( \left(\nu_k^l\right)^2 \left\langle a^k(\boldsymbol{M}) \right\rangle + 2\nu_k^l \left\langle M_l\, a^k(\boldsymbol{M}) \right\rangle \right).$$

A similar analysis shows that $\langle M_l\, M_{l'} \rangle$, satisfies

$$\frac{d\left\langle M_l\, M_{l'} \right\rangle}{dt} = \sum_{k=1}^{K} \nu_k^l \left\langle M_{l'}\, a^k(\boldsymbol{M}) \right\rangle + \nu_k^{l'} \left\langle M_l\, a^k(\boldsymbol{M}) \right\rangle + \nu_k^l \nu_k^{l'} \left\langle a^k(\boldsymbol{M}) \right\rangle .$$

### 2.3.3 Relation to Deterministic Chemical Kinetics

We now consider the relationship between the deterministic mass action chemical kinetic equations and the chemical master equation. Define $\boldsymbol{C} \equiv \boldsymbol{M}/V$, to be the vector of random variables for the concentration of each species. Let $\tilde{a}^k$ denote the concentration dependent form of the rate $a^k$. $\tilde{a}^k$ and $a^k$ are related

by $\tilde{a}^k(\boldsymbol{c}) = a^k(V\boldsymbol{c})/V$, and vice–versa $a^k(\boldsymbol{m}) = \tilde{a}^k(\boldsymbol{m}/V)V$. Note that $\tilde{a}^k(\boldsymbol{c})$ is the expected number of occurrences of reaction $k$ *per unit volume* per unit time when the vector of concentrations is $\boldsymbol{c}$. Using equation (2.7) the mean of $C^l$, $\langle C^l \rangle$, then satisfies

$$\frac{d\langle C^l \rangle}{dt} = \sum_{k=1}^{K} \nu_k^l \langle \tilde{a}^k(\boldsymbol{C}) \rangle . \tag{2.8}$$

If the averaging operation commutes with the functions $\tilde{a}^k$, then one obtains the equations for classical deterministic chemical kinetics (see (2.1)),

$$\frac{d\langle C^l \rangle}{dt} = \sum_{k=1}^{K} \nu_k^l \, \tilde{a}^k\big( \langle \boldsymbol{C} \rangle \big),$$

however, in general $\langle \tilde{a}^k(\boldsymbol{C}) \rangle \neq \tilde{a}^k\big( \langle \boldsymbol{C} \rangle \big)$, unless $\tilde{a}^k$ is linear. One does expect that asymptotically, as the population sizes become very large, $\langle \tilde{a}^k(\boldsymbol{C}) \rangle \approx \tilde{a}^k\big( \langle \boldsymbol{C} \rangle \big)$. For one discussion of the validity of this approximation see [22].

### 2.3.4 Gillespie Method

The number of the ODEs comprising the master equation are very large even for simple chemical systems. Direct solution methods become impractical, so that instead Monte Carlo methods are used. These methods create realizations of the underlying stochastic process, $\boldsymbol{M}(t)$, governed by the master equation. Statistics from many realizations can be used to calculate moments of $\boldsymbol{M}(t)$ and the distribution, $P(\boldsymbol{m}, t)$. In [20] Gillespie presented two equivalent methods that produce exact realizations of $\boldsymbol{M}(t)$. We shall describe only one of them here.

Gillespie's First Reaction Method is based on calculating a sample of the random time of occurrence of each reaction independently, as if no other reactions were possible. The reaction with the minimal time to its next occurrence

is then executed, and the system state updated. This process is then repeated until the simulation reaches the desired final time. In detail, let

$$p(\tau, k|\boldsymbol{m}, t)\, d\tau \equiv \text{ Prob}\{ \text{ reaction } k \text{ occurs in the interval } [t+\tau, t+\tau+d\tau)\,, \\ \text{ignoring that another reaction could occur first}\}.$$

Then in [20] it is shown that

$$p(\tau, k|\boldsymbol{m}, t) = a^k(\boldsymbol{m})\, e^{-a^k(\boldsymbol{m})\,\tau}. \tag{2.9}$$

Knowing $\boldsymbol{m}$ at time $t$, for each reaction $k$, a time $\tau_k$ at which reaction $k$ would occur can be generated by inverting the probability distribution corresponding to probability density (2.9). The time at which reaction $k$ would occur is given by $t + \tau_k$, where

$$\tau_k = \frac{1}{a^k(\boldsymbol{m})} \ln \frac{1}{r_k},$$

$r_k$ being a uniformly distributed random number in $[0, 1]$. The overall time–evolution algorithm is then:

1. Initialize, $t = 0$, set initial molecule numbers, $\boldsymbol{m} = \boldsymbol{m}_0$
2. Calculate $a^k(\boldsymbol{m})$, for all $k$
3. For each $k$, generate $\tau_k = \left(\ln\left(1/r_k\right)\right)/a^k(\boldsymbol{m})$
4. Execute the reaction, $k'$, with the smallest $\tau_k$, update $\boldsymbol{m} := \boldsymbol{m} + \boldsymbol{\nu}_{k'}$
5. Set the time to, $t := t + \tau_{k'}$
6. Return to 2.

Optimized versions of Gillespie's algorithms that substantially decrease the computational work were developed by Gibson and Bruck [19]. Their Next Reaction Method is equivalent to the First Reaction Method, but requires only one random number per reaction event. By using a special data structure they reduce finding the reaction with the minimum $\tau_k$ to a constant work operation, and updating following a reaction to logarithmic work in the number of reactions, $K$. For all subsequent Monte Carlo simulations discussed we use the Next Reaction Method.

## 2.4 Stochastic Reaction–Diffusion Chemical Kinetics

We now come to the new methodology proposed in this thesis, see also [23] our forth coming paper. As mentioned in the introduction, the reaction–diffusion master equation goes back to [16]. In this section we formulate the reaction–diffusion master equation, and discuss its connections to several other types of reaction–diffusion models. A new model for the stochastic reaction–diffusion and active transport of molecules is also presented.

### 2.4.1 Mathematical Formulation

Let the domain of interest be a closed volume $V$. Divide the domain into a collection of computational cells indexed by $i = 1 \dots N$. Assume that the size of each cell can be chosen such that within each cell, independently, the master equation formulation of chemical kinetics holds (see Section 2.3.1). In other

words, the individual computational cells are small enough that each such cell may be regarded as well mixed. Transitions of particles *between* cells are then modeled as first order reactions.

Let $M_i^l(t)$ denote the random variable for the number of particles of species $l$ in computational cell $i$, $l = 1 \dots L$. Define $\boldsymbol{M}^l(t) = \left(M_1^l, \dots, M_N^l\right)^T$ to be the spatial vector of species $l$, and $\boldsymbol{M}(t) = \left(\boldsymbol{M}^1, \dots, \boldsymbol{M}^L\right)$ to be the state matrix of the system. As for the well–mixed case, let

$$P(\boldsymbol{m}, t) \equiv \text{Prob}\{\boldsymbol{M}(t) = \boldsymbol{m} | \boldsymbol{M}(0) = \boldsymbol{m}_0\},$$

where we have again dropped the dependence on $t$ for convenience. Let $\boldsymbol{M}_i(t) = \left(M_i^1, \dots, M_i^L\right)$, define $\boldsymbol{e}_i^l$ to be the matrix all of whose elements are zero except for the element, $(i, l)$ which is one, and let $\boldsymbol{e}_i$ be the column vector which has a 1 in its $i$'th entry and is 0 elsewhere. $\boldsymbol{e}_i\boldsymbol{\nu}_k$ will denote the matrix formed by the product of the column vector $\boldsymbol{e}_i$ with the row vector $\boldsymbol{\nu}_k$. This matrix will be zero everywhere except for the $i$'th row, which will be equal to $\boldsymbol{\nu}_k$. It corresponds to the change in $\boldsymbol{M}(t)$ due to one occurrence of reaction $k$ at location $i$ (i.e., $\boldsymbol{M}(t) \to \boldsymbol{M}(t) + \boldsymbol{e}_i\boldsymbol{\nu}_k$). Let $k_{ij}^l$ denote the jump rate for each individual molecule of the $l$'th chemical species into cell $i$ from cell $j$, for $i \neq j$. Since diffusion is treated as a first order reaction, and since the molecules are assumed to diffuse independently, the total probability per unit time at time $t$ for one molecule of species $l$ to jump from cell $j$ to cell $i$ is $k_{ij}^l M_j^l(t)$.

The master equation for the time evolution of $P(\boldsymbol{m}, t)$ is then

$$\begin{aligned}\frac{dP(\boldsymbol{m})}{dt} = &\sum_{i=1}^{N}\sum_{j=1}^{N}\sum_{l=1}^{L}\left(k_{ij}^l\left(m_j^l + 1\right)P(\boldsymbol{m} + \boldsymbol{e}_j^l - \boldsymbol{e}_i^l) - k_{ji}^l m_i^l P(\boldsymbol{m})\right) \\ &+ \sum_{i=1}^{N}\sum_{k=1}^{K}\left(a_i^k(\boldsymbol{m}_i - \boldsymbol{\nu}_k)P(\boldsymbol{m} - \boldsymbol{e}_i\boldsymbol{\nu}_k) - a_i^k(\boldsymbol{m}_i)P(\boldsymbol{m})\right).\end{aligned} \tag{2.10}$$

This is a coupled set of ODEs over all possible integer values of the matrix $\boldsymbol{m}$. Notice the important point that the reaction probabilities per unit time, $a_i^k(\boldsymbol{m})$, may now depend on spatial location. For example, in an eukaryotic cell some reactions may occur only in the nucleus and others may occur only in the cytoplasm.

Equation (2.10) is separated into two sums. The first term corresponds to diffusive motion between cells $i$ and $j$ of a given species, $l$. The second is just the components of the chemical master equation, but applied at each individual cell. At this point no specification has been made as to where the rates $k_{ij}^l$ come from, or what their values should be.

### 2.4.2 Relation to Deterministic Reaction–Diffusion

For deterministic reaction–diffusion, let $C^l(\boldsymbol{x}, t)$ denote the concentration and $D^l$ the diffusion constant of the $l$'th species. Let $\tilde{a}^k(\boldsymbol{C}(\boldsymbol{x}, t), \boldsymbol{x})$ denote the spatially varying concentration dependent form of $a_i^k$ (see Section 2.3.1). Then

$$\frac{\partial C^l(\boldsymbol{x}, t)}{\partial t} = D^l \Delta C^l + \sum_{k=1}^{K} \nu_k^l \, \tilde{a}^k(\boldsymbol{C}(\boldsymbol{x}, t), \boldsymbol{x}).$$

To see the relation to the stochastic formulation let $C_i^l(t) = M_i^l(t)/V_i$ be the random variable for the chemical concentration of species $l$, in cell $i$. Let $\tilde{a}_i^k$ denote the concentration dependent form of $a_i^k$. $\tilde{a}_i^k$ and $a_i^k$ are related by $\tilde{a}_i^k(\boldsymbol{c}) = a_i^k(V_i\boldsymbol{c})/V_i$, and vice–versa $a_i^k(\boldsymbol{m}) = \tilde{a}_i^k(\boldsymbol{m}/V_i)V_i$. Since the reaction–diffusion master equation has the same general form as the chemical master equation (2.4), with the diffusive terms thought of as additional reactions, we

may use equation (2.8) to determine the average of $C_i^l$. We then find

$$\frac{d\left\langle C_i^l\right\rangle}{dt} = \sum_{j=1}^{N}\left(\frac{V_j}{V_i}k_{ij}^l\left\langle C_j^l\right\rangle - k_{ji}^l\left\langle C_i^l\right\rangle\right) + \sum_{k=1}^{K}\nu_k^l\left\langle \tilde{a}_i^k\left(C_i\right)\right\rangle.$$

Suppose the rates $k_{ij}^l$ could be chosen so that the first term is a discretization of $D^l\Delta C^l$. The only difference between the deterministic reaction–diffusion PDEs and the means of the stochastic formulation in the continuum limit would then be the non–commutativity of the reaction terms with averaging; diffusion would be identical.

### 2.4.3 Relation to Brownian Motion

Returning to the reaction–diffusion master equation (2.10), we expect that the diffusive jump rates should be independent of the chemical reactions present within a given chemical system. Therefore, we now consider a spatially distributed chemical system with no reactions. In this case, we expect each particle of each chemical species to independently undergo Brownian motion in the continuum limit as the computational cell size approaches zero. Since, by construction, the diffusive motion of each particle of each chemical species is independent in the reaction–diffusion master equation formulation, it is sufficient to further restrict ourselves to a system consisting of only one chemical species containing just one particle. With these choices, the reaction–diffusion master equation reduces to

$$\frac{dP(\boldsymbol{m})}{dt} = \sum_{i=1}^{N}\sum_{j=1}^{N} k_{ij}\left(m_j+1\right)P(\boldsymbol{m}+\boldsymbol{e}_j-\boldsymbol{e}_i) - k_{ji}m_iP(\boldsymbol{m}). \tag{2.11}$$

Since $\boldsymbol{M}(t)$ is describing one particle, $M_i(t)$ will be zero for all $i$ except the location at which the particle currently is. Let $\boldsymbol{X}(t)$ be the Brownian motion

process of the particle. Then define

$$Q_i(t) \equiv P(\boldsymbol{e}_i, t) \approx \text{Prob}\{\boldsymbol{X}(t) \in V_i | \boldsymbol{X}(0) = \boldsymbol{x}_0\},$$

with $\boldsymbol{e}_i$ denoting, as before, the unit vector along the $i$'th Cartesian coordinate axis of $\mathbb{R}^N$. With this definition, $Q_i(t)$ is the probability that the particle is in the $i$'th computational cell. Letting $\boldsymbol{m} = \boldsymbol{e}_i$, equation (2.11) implies

$$\frac{dQ_i}{dt} = \sum_{j=1}^{N} k_{ij}\, Q_j - k_{ji}\, Q_i. \tag{2.12}$$

Define a probability density for the particle's position by $p_i(t) \equiv Q_i(t)/V_i$. Then $p_i$ satisfies

$$\frac{dp_i}{dt} = \sum_{j=1}^{N} \frac{V_j}{V_i} k_{ij}\, p_j - k_{ji}\, p_i. \tag{2.13}$$

Again if the rates form a discretization of $D\Delta p$, for $p$ the continuum single particle density, then the continuum limit as cell size goes to zero would be

$$\frac{\partial p}{\partial t}(\boldsymbol{x}, t) = D\Delta p. \tag{2.14}$$

This is the Fokker–Planck equation for a single classical Brownian particle.

With these continuum limits, and those of the previous section, constructing an operator, $L_h$, of the form

$$(L_h p)_i = \sum_{j=1}^{N} \frac{V_j}{V_i} k_{ij}\, p_j - k_{ji}\, p_i, \tag{2.15}$$

where $L_h \to D\Delta$ as $h \to 0$, will determine the $k_{ij}$. (Here $h$ represents the maximum length scale associated with a computational cell). The diffusion jump rates will then be $k_{ij}$, provided $k_{ij} \geq 0$ (see Appendix A).

### 2.4.4 Relation to Individual Particle Models

We now discuss the relation between the reaction–diffusion master equation formulation (2.10) and reaction–diffusion models that track the position of each individual molecule. We show how the reaction–diffusion master equation can be thought of as a discrete approximation to a continuous Fock Space formulation. Specifically, we relate equation (2.10) to the spatially continuous representation studied in [11], equation (51), where a Fock Space representation is used to model the reaction $\mathrm{A} + \mathrm{A} \to \mathrm{B}$. Instead of considering an arbitrary reaction–diffusion system, for notational simplicity, we study the reaction $\mathrm{A} + \mathrm{B} \rightleftarrows \mathrm{C}$. We denote by $k_+$ the forward reaction rate with units volume/time, and by $k_-$ the reverse reaction rate with units time$^{-1}$. The domain in which the reaction may occur is taken to be the periodic box $\Omega = [-L/2, L/2)^3$.

We divide $\Omega$ into a standard Cartesian mesh, comprised of cubes of length $h$. To ease the transition from the reaction–diffusion master equation to the Fock Space representation we use a slightly different notation than in Section 2.4.1. Let

$$\boldsymbol{i} = (i_1, i_2, i_3) \in I^3$$

be the multi–index labeling a given mesh cell in $\Omega$, with $I^3$ representing the three–dimensional index space. We denote by $a_{\boldsymbol{i}}$ the number of molecules of chemical species A at location $\boldsymbol{i}$, and define

$$\boldsymbol{a} = \{a_{\boldsymbol{i}} \mid \boldsymbol{i} \in I^3\}.$$

(We similarly define $\boldsymbol{b}$, and $\boldsymbol{c}$). The notation $\boldsymbol{a} + 1_{\boldsymbol{i}}$, will represent $\boldsymbol{a}$ with one added to $a_{\boldsymbol{i}}$. The diffusive jump rate for species A, from mesh cell $\boldsymbol{j}$ to mesh cell $\boldsymbol{i}$, is denoted by $k^{\mathrm{A}}_{\boldsymbol{ij}}$, with $k^{\mathrm{B}}_{\boldsymbol{ij}}$ and $k^{\mathrm{C}}_{\boldsymbol{ij}}$ defined similarly. Using these definitions,

the reaction–diffusion master equation can be rewritten as

$$\frac{dP}{dt}(\boldsymbol{a},\boldsymbol{b},\boldsymbol{c},t) = (L_h P + R_h P)(\boldsymbol{a},\boldsymbol{b},\boldsymbol{c},t), \tag{2.16}$$

where the diffusion operator, $L_h$, is

$$\begin{aligned}(L_h P)(\boldsymbol{a},\boldsymbol{b},\boldsymbol{c},t) = \\ \sum_{\boldsymbol{i}\in I^3}\sum_{\boldsymbol{i}'\in I^3}\Big(&\left[k^{\mathrm{A}}_{\boldsymbol{i}\boldsymbol{i}'}\,(a_{\boldsymbol{i}'}+1)\,P(\boldsymbol{a}+1_{\boldsymbol{i}'}-1_{\boldsymbol{i}},\boldsymbol{b},\boldsymbol{c},t) - k^{\mathrm{A}}_{\boldsymbol{i}'\boldsymbol{i}}\,a_{\boldsymbol{i}}P(\boldsymbol{a},\boldsymbol{b},\boldsymbol{c},t)\right] \\ &+\left[k^{\mathrm{B}}_{\boldsymbol{i}\boldsymbol{i}'}\,(b_{\boldsymbol{i}'}+1)\,P(\boldsymbol{a},\boldsymbol{b}+1_{\boldsymbol{i}'}-1_{\boldsymbol{i}},\boldsymbol{c},t) - k^{\mathrm{B}}_{\boldsymbol{i}'\boldsymbol{i}}\,b_{\boldsymbol{i}}P(\boldsymbol{a},\boldsymbol{b},\boldsymbol{c},t)\right] \\ &+\left[k^{\mathrm{C}}_{\boldsymbol{i}\boldsymbol{i}'}\,(c_{\boldsymbol{i}'}+1)\,P(\boldsymbol{a},\boldsymbol{b},\boldsymbol{c}+1_{\boldsymbol{i}'}-1_{\boldsymbol{i}},t) - k^{\mathrm{C}}_{\boldsymbol{i}'\boldsymbol{i}}\,c_{\boldsymbol{i}}P(\boldsymbol{a},\boldsymbol{b},\boldsymbol{c},t)\right]\Big),\end{aligned}$$

and the reaction operator, $R_h$, is defined as

$$\begin{aligned}(R_h P)(\boldsymbol{a},\boldsymbol{b},\boldsymbol{c},t) = \\ \sum_{\boldsymbol{i}\in I^3}\Big(&\frac{k_+(a_{\boldsymbol{i}}+1)(b_{\boldsymbol{i}}+1)}{h^3}P(\boldsymbol{a}+1_{\boldsymbol{i}},\boldsymbol{b}+1_{\boldsymbol{i}},\boldsymbol{c}-1_{\boldsymbol{i}},t) - \frac{k_+ a_{\boldsymbol{i}}b_{\boldsymbol{i}}}{h^3}P(\boldsymbol{a},\boldsymbol{b},\boldsymbol{c},t) \\ &+ k_-(c_{\boldsymbol{i}}+1)P(\boldsymbol{a}-1_{\boldsymbol{i}},\boldsymbol{b}-1_{\boldsymbol{i}},\boldsymbol{c}+1_{\boldsymbol{i}},t) - k_- c_{\boldsymbol{i}}P(\boldsymbol{a},\boldsymbol{b},\boldsymbol{c},t)\Big).\end{aligned}$$

We now change variables to convert to the Fock Space representation. Denote by $a$ the *total* number of molecules of chemical species A within $\Omega$, i.e.

$$a = \sum_{\boldsymbol{i}\in I^3} a_{\boldsymbol{i}}.$$

(Define $b$ and $c$ similarly). We introduce a new set of variables, $\boldsymbol{j}^a = (\boldsymbol{j}^a_1,\ldots,\boldsymbol{j}^a_a)$, where $\boldsymbol{j}^a_l \in I^3$ labels the mesh cell in which the $l$'th molecule of chemical species A is located. Note that we use $a$ as a superscript to indicate that there are $a$ total *vectors*, $\boldsymbol{j}^a_l$, that comprise the components of $\boldsymbol{j}^a$. Therefore, $\boldsymbol{j}^a$ is a vector of dimension $3a$ . With $\boldsymbol{j}^b$ and $\boldsymbol{j}^c$ defined similarly, let $f^{(a,b,c)}(\boldsymbol{j}^a,\boldsymbol{j}^b,\boldsymbol{j}^c,t)$ denote the probability that at time $t$ there are $a$ particles of species A located within

the mesh cells given by $\boldsymbol{\jmath}^a$, $b$ particles of species B located within the mesh cells given by $\boldsymbol{\jmath}^b$, and $c$ particles of species C located within the mesh cells given by $\boldsymbol{\jmath}^c$. Note that the particles are assumed to be labeled, so that each $\boldsymbol{\jmath}^a_l$ always represents the same particle.

The set of all permutations of the index vectors comprising $\boldsymbol{\jmath}^a$ is defined as

$$\sigma(\boldsymbol{\jmath}^a) = \{\left(\boldsymbol{\jmath}^a_{\sigma_1}, \ldots, \boldsymbol{\jmath}^a_{\sigma_a}\right) \mid (\sigma_1, \ldots, \sigma_a) \text{ is any permutation of } (1, \ldots, a)\}.$$

($\sigma(\boldsymbol{\jmath}^b)$ and $\sigma(\boldsymbol{\jmath}^c)$ are defined similarly). With these definitions, we symmetrize $f^{(a,b,c)}$. Physically, this assumption means that molecules of the same chemical species are assumed identical, and hence the order in which such molecules are labeled is irrelevant. Note that this assumption is implicit in the reaction–diffusion master equations (2.10) and (2.16) to begin with. The symmetrized probability is defined as

$$F^{(a,b,c)}(\boldsymbol{\jmath}^a, \boldsymbol{\jmath}^b, \boldsymbol{\jmath}^c) = \frac{1}{a!\, b!\, c!} \sum_{\substack{\tilde{\boldsymbol{\jmath}}^a \in \sigma(\boldsymbol{\jmath}^a), \\ \tilde{\boldsymbol{\jmath}}^b \in \sigma(\boldsymbol{\jmath}^b), \\ \tilde{\boldsymbol{\jmath}}^c \in \sigma(\boldsymbol{\jmath}^c)}} f^{(a,b,c)}(\tilde{\boldsymbol{\jmath}}^a, \tilde{\boldsymbol{\jmath}}^b, \tilde{\boldsymbol{\jmath}}^c). \tag{2.17}$$

Dividing the right hand side by $a!\, b!\, c!$ sets the state space of $F^{(a,b,c)}$ to be the same as that of $f^{(a,b,c)}$. By this we mean that $F^{(a,b,c)}(\boldsymbol{\jmath}^a, \boldsymbol{\jmath}^b, \boldsymbol{\jmath}^c)$ is defined for all possible vectors, $(\boldsymbol{\jmath}^a, \boldsymbol{\jmath}^b, \boldsymbol{\jmath}^c) \in I^{3a} \times I^{3b} \times I^{3c}$. If this normalization were not included, than $F^{(a,b,c)}(\boldsymbol{\jmath}^a, \boldsymbol{\jmath}^b, \boldsymbol{\jmath}^c)$ would define a probability for a subset of these values. Note that $F^{(a,b,c)}$ is symmetric under permutations of the components of each vector $\boldsymbol{\jmath}^a$, $\boldsymbol{\jmath}^b$, and $\boldsymbol{\jmath}^c$, so that for any permutation $(\sigma_1, \ldots, \sigma_a)$,

$$F^{(a,b,c)}(\boldsymbol{\jmath}^a_{\sigma_1}, \ldots, \boldsymbol{\jmath}^a_{\sigma_a}, \boldsymbol{\jmath}^b, \boldsymbol{\jmath}^c) = F^{(a,b,c)}(\boldsymbol{\jmath}^a, \boldsymbol{\jmath}^b, \boldsymbol{\jmath}^c),$$

with similar relations holding for permutations in the components of $\boldsymbol{\jmath}^b$ and $\boldsymbol{\jmath}^c$.

Using these definitions, the probability of being in any given state is then completely specified by the collection of probabilities,

$$\{F^{(a,b,c)}(\cdot,\cdot,\cdot) \mid a,\ b, \text{ and } c \text{ take all possible values}\}.$$

The total probability that the system is in any state at all

$$\sum_{\substack{a=0,\\ b=0,\\ c=0}}^{\infty} \sum_{\substack{\boldsymbol{j}^a \in I^3,\\ \boldsymbol{j}^b \in I^3,\\ \boldsymbol{j}^c \in I^3}} F^{(a,b,c)}(\boldsymbol{j}^a, \boldsymbol{j}^b, \boldsymbol{j}^c, t) = 1.$$

We now relate $F^{(a,b,c)}$ to the reaction–diffusion master equation. Consider any state, $(\boldsymbol{a}, \boldsymbol{b}, \boldsymbol{c})$, and any corresponding set of particle positions, $\left(\boldsymbol{j}^a, \boldsymbol{j}^b, \boldsymbol{j}^c\right)$ such that

$$a_{\boldsymbol{i}} = \left|\{\boldsymbol{j}_l^a \mid \boldsymbol{j}_l^a = \boldsymbol{i}, l = 1 \ldots a\}\right|.$$

(Similar relations holding for $b_{\boldsymbol{i}}$ and $c_{\boldsymbol{i}}$). Here $|\cdot|$ denotes the cardinality of a set. Denote by $\tilde{\sigma}(\boldsymbol{j}^a)$ the set of all *distinct* permutations of the components of $\boldsymbol{j}^a$. Note that $\tilde{\sigma}(\boldsymbol{j}^a) \subseteq \sigma(\boldsymbol{j}^a)$, and by Theorem B.0.1 has cardinality

$$|\tilde{\sigma}(\boldsymbol{j}^a)| = a! \prod_{\boldsymbol{i} \in I^3} \frac{1}{a_{\boldsymbol{i}}!}. \tag{2.18}$$

With $\tilde{\sigma}(\boldsymbol{j}^b)$ and $\tilde{\sigma}(\boldsymbol{j}^c)$ defined similarly, let

$$\tilde{\sigma}(\boldsymbol{j}^a, \boldsymbol{j}^b, \boldsymbol{j}^c) = \tilde{\sigma}(\boldsymbol{j}^a) \times \tilde{\sigma}(\boldsymbol{j}^b) \times \tilde{\sigma}(\boldsymbol{j}^c).$$

The cardinality of this set gives the total number of distinct permutations of the components of $\left(\boldsymbol{j}^a, \boldsymbol{j}^b, \boldsymbol{j}^c\right)$ that correspond to the state $(\boldsymbol{a}, \boldsymbol{b}, \boldsymbol{c})$, assuming $\boldsymbol{j}^a$ precedes $\boldsymbol{j}^b$, and $\boldsymbol{j}^b$ precedes $\boldsymbol{j}^c$. We subsequently denote this quantity by

$$C_{\boldsymbol{a},\boldsymbol{b},\boldsymbol{c}} = \left|\tilde{\sigma}(\boldsymbol{j}^a, \boldsymbol{j}^b, \boldsymbol{j}^c)\right| = a!\, b!\, c! \prod_{\boldsymbol{i} \in I^3} \frac{1}{a_{\boldsymbol{i}}!\, b_{\boldsymbol{i}}!\, c_{\boldsymbol{i}}!}.$$

Several identities involving $C_{\boldsymbol{a},\boldsymbol{b},\boldsymbol{c}}$ will be subsequently be needed and are collected here:

$$a_{\boldsymbol{i}} = (a_{\boldsymbol{i}'} + 1)\,\frac{C_{\boldsymbol{a}+1_{i'}-1_i,\boldsymbol{b},\boldsymbol{c}}}{C_{\boldsymbol{a},\boldsymbol{b},\boldsymbol{c}}}, \tag{2.19}$$

$$\left(\frac{(a+1)\,(b+1)}{c}\right) c_{\boldsymbol{i}} = (a_{\boldsymbol{i}} + 1)\,(b_{\boldsymbol{i}} + 1)\,\frac{C_{\boldsymbol{a}+1_i,\boldsymbol{b}+1_i,\boldsymbol{c}-1_i}}{C_{\boldsymbol{a},\boldsymbol{b},\boldsymbol{c}}}, \tag{2.20}$$

$$\left(\frac{c+1}{ab}\right) a_{\boldsymbol{i}} b_{\boldsymbol{i}} = (c_{\boldsymbol{i}} + 1)\,\frac{C_{\boldsymbol{a}-1_i,\boldsymbol{b}-1_i,\boldsymbol{c}+1_i}}{C_{\boldsymbol{a},\boldsymbol{b},\boldsymbol{c}}}. \tag{2.21}$$

The probability of being in any state $(\boldsymbol{a},\boldsymbol{b},\boldsymbol{c})$, $P(\boldsymbol{a},\boldsymbol{b},\boldsymbol{c},t)$, is equivalent to the probability of being in any collection of particle positions within the set $\tilde{\sigma}(\boldsymbol{j}^a,\boldsymbol{j}^b,\boldsymbol{j}^c)$. (Assuming $\left(\boldsymbol{j}^a,\boldsymbol{j}^b,\boldsymbol{j}^c\right)$ is one collection of particle positions that are consistent with the state $(\boldsymbol{a},\boldsymbol{b},\boldsymbol{c})$). Therefore,

$$P(\boldsymbol{a},\boldsymbol{b},\boldsymbol{c},t) = \sum_{\substack{\left(\tilde{\boldsymbol{j}}^a,\tilde{\boldsymbol{j}}^b,\tilde{\boldsymbol{j}}^c\right)\\ \in\tilde{\sigma}(\boldsymbol{j}^a,\boldsymbol{j}^b,\boldsymbol{j}^c)}} f^{(a,b,c)}(\tilde{\boldsymbol{j}}^a,\tilde{\boldsymbol{j}}^b,\tilde{\boldsymbol{j}}^c,t).$$

Using Theorem B.0.2, and then the definition of $F^{(\boldsymbol{a},\boldsymbol{b},\boldsymbol{c})}$,

$$\begin{aligned}\sum_{\substack{\left(\tilde{\boldsymbol{j}}^a,\tilde{\boldsymbol{j}}^b,\tilde{\boldsymbol{j}}^c\right)\\ \in\tilde{\sigma}(\boldsymbol{j}^a,\boldsymbol{j}^b,\boldsymbol{j}^c)}} f^{(a,b,c)}(\tilde{\boldsymbol{j}}^a,\tilde{\boldsymbol{j}}^b,\tilde{\boldsymbol{j}}^c) &= \frac{C_{\boldsymbol{a},\boldsymbol{b},\boldsymbol{c}}}{a!\,b!\,c!}\sum_{\substack{\left(\tilde{\boldsymbol{j}}^a,\tilde{\boldsymbol{j}}^b,\tilde{\boldsymbol{j}}^c\right)\\ \in\sigma(\boldsymbol{j}^a,\boldsymbol{j}^b,\boldsymbol{j}^c)}} f^{(a,b,c)}(\tilde{\boldsymbol{j}}^a,\tilde{\boldsymbol{j}}^b,\tilde{\boldsymbol{j}}^c),\\ &= C_{\boldsymbol{a},\boldsymbol{b},\boldsymbol{c}}\,F^{(a,b,c)}(\boldsymbol{j}^a,\boldsymbol{j}^b,\boldsymbol{j}^c).\end{aligned}$$

Therefore,

$$P(\boldsymbol{a},\boldsymbol{b},\boldsymbol{c},t) = C_{\boldsymbol{a},\boldsymbol{b},\boldsymbol{c}}\,F^{(a,b,c)}(\boldsymbol{j}^a,\boldsymbol{j}^b,\boldsymbol{j}^c,t).$$

Plugging this expression into equation (2.16), and dividing by $C_{\boldsymbol{a},\boldsymbol{b},\boldsymbol{c}}$, we obtain the equations of evolution satisfied by $F^{(a,b,c)}$,

$$\frac{dF^{(a,b,c)}}{dt}(\boldsymbol{j}^a,\boldsymbol{j}^b,\boldsymbol{j}^c,t) = \left(\tilde{L}_h F^{(a,b,c)} + \tilde{R}_h F^{(a,b,c)}\right)\left(\boldsymbol{j}^a,\boldsymbol{j}^b,\boldsymbol{j}^c,t\right). \tag{2.22}$$

Before deriving $\tilde{L}_h$ and $\tilde{R}_h$, we must first introduce new notations for removing and adding elements to a position vector, $\boldsymbol{j}^a$. Let $\boldsymbol{j}^a \setminus \boldsymbol{j}^a_l$ denote $\boldsymbol{j}^a$ with the $l$'th particle removed, i.e.,

$$\boldsymbol{j}^a \setminus \boldsymbol{j}^a_l = \left(\boldsymbol{j}^a_1, \ldots, \boldsymbol{j}^a_{l-1}, \boldsymbol{j}^a_{l+1}, \ldots, \boldsymbol{j}^a_a\right).$$

Similarly, $\boldsymbol{j}^a \setminus \{\boldsymbol{i}\}$ will denote removing any one component of $\boldsymbol{j}^a$ that has the value $\boldsymbol{i}$. Note that since we are only considering a symmetrized density, it does not matter which component with the value $\boldsymbol{i}$ is removed. Adding an additional particle to $\boldsymbol{j}^a$ is denoted by $\boldsymbol{j}^a \cup \boldsymbol{j}^a_{a+1}$, i.e.,

$$\boldsymbol{j}^a \cup \boldsymbol{j}^a_{a+1} = \left(\boldsymbol{j}^a_1, \ldots, \boldsymbol{j}^a_a, \boldsymbol{j}^a_{a+1}\right).$$

To add the specific value $\boldsymbol{i}$ for the new particle's position, the notation $\boldsymbol{j}^a \cup \{\boldsymbol{i}\}$ is used.

With the preceding definitions, and using identity (2.19), the diffusion operator, $\tilde{L}_h$, is

$$\begin{aligned}
&\left(\tilde{L}_h F^{(a,b,c)}\right)\left(\boldsymbol{j}^a, \boldsymbol{j}^b, \boldsymbol{j}^c, t\right) = \\
&\sum_{\boldsymbol{i}\in I^3}\sum_{\boldsymbol{i}'\in I^3}\Bigg(\left[k^{\mathrm{A}}_{\boldsymbol{i}\boldsymbol{i}'}\, a_{\boldsymbol{i}} F^{a,b,c}\left(\boldsymbol{j}^a \setminus \{\boldsymbol{i}\}\cup\{\boldsymbol{i}'\}, \boldsymbol{j}^b, \boldsymbol{j}^c\right) - k^{\mathrm{A}}_{\boldsymbol{i}'\boldsymbol{i}}\, a_{\boldsymbol{i}} F^{(a,b,c)}\left(\boldsymbol{j}^a, \boldsymbol{j}^b, \boldsymbol{j}^c\right)\right] \\
&\qquad + \left[k^{\mathrm{B}}_{\boldsymbol{i}\boldsymbol{i}'}\, b_{\boldsymbol{i}} F^{(a,b,c)}\left(\boldsymbol{j}^a, \boldsymbol{j}^b \setminus \{\boldsymbol{i}\}\cup\{\boldsymbol{i}'\}, \boldsymbol{j}^c\right) - k^{\mathrm{B}}_{\boldsymbol{i}'\boldsymbol{i}}\, b_{\boldsymbol{i}} F^{(a,b,c)}\left(\boldsymbol{j}^a, \boldsymbol{j}^b, \boldsymbol{j}^c\right)\right] \\
&\qquad + \left[k^{\mathrm{C}}_{\boldsymbol{i}\boldsymbol{i}'}\, c_{\boldsymbol{i}} F^{(a,b,c)}\left(\boldsymbol{j}^a, \boldsymbol{j}^b, \boldsymbol{j}^c \setminus \{\boldsymbol{i}\}\cup\{\boldsymbol{i}'\}\right) - k^{\mathrm{C}}_{\boldsymbol{i}'\boldsymbol{i}}\, c_{\boldsymbol{i}} F^{(a,b,c)}\left(\boldsymbol{j}^a, \boldsymbol{j}^b, \boldsymbol{j}^c\right)\right]\Bigg).
\end{aligned} \tag{2.23}$$

Using the fact that $a_{\boldsymbol{i}}$ gives the number of particle positions within $\boldsymbol{j}^a$ that have the value $\boldsymbol{i}$,

$$k^{\mathrm{A}}_{\boldsymbol{i}'\boldsymbol{i}}\, a_{\boldsymbol{i}} F^{(a,b,c)}\left(\boldsymbol{j}^a, \boldsymbol{j}^b, \boldsymbol{j}^c\right) = \sum_{l\in\{\tilde{l}\,|\,\boldsymbol{j}^a_{\tilde{l}}=i\}} k^{\mathrm{A}}_{\boldsymbol{i}'\boldsymbol{j}^a_l} F^{(a,b,c)}\left(\boldsymbol{j}^a, \boldsymbol{j}^b, \boldsymbol{j}^c\right). \tag{2.24}$$

Similarly,

$$k^{\mathrm{A}}_{\boldsymbol{i}\boldsymbol{i}'}\, a_{\boldsymbol{i}} F^{(a,b,c)}\big(\boldsymbol{j}^a \setminus \{\boldsymbol{i}\} \cup \{\boldsymbol{i}'\}, \boldsymbol{j}^b, \boldsymbol{j}^c\big) = \sum_{l \in \{\tilde{l} | \boldsymbol{j}^a_{\tilde{l}} = i\}} k^{\mathrm{A}}_{\boldsymbol{j}^a_l \boldsymbol{i}'} F^{(a,b,c)}\big(\boldsymbol{j}^a_1, \ldots, \boldsymbol{j}^a_{l-1}, \boldsymbol{i}', \boldsymbol{j}^a_{l+1}, \ldots, \boldsymbol{j}^a_a, \boldsymbol{j}^b, \boldsymbol{j}^c\big).$$

Finally, noting that for the previous two equations

$$\sum_{\boldsymbol{i} \in I^3} \sum_{l \in \{\tilde{l} | \boldsymbol{j}^a_{\tilde{l}} = i\}} (\cdot) = \sum_{l=1}^{a} (\cdot)\,, \tag{2.25}$$

we find that equation (2.23) simplifies to

$$\begin{aligned}
\Big(\tilde{L}_h F^{(a,b,c)}\Big)\big(\boldsymbol{j}^a, \boldsymbol{j}^b, \boldsymbol{j}^c, t\big) = \sum_{\boldsymbol{i}' \in I^3} \Bigg( & \\
& \sum_{l=1}^{a} \Big[ k^A_{\boldsymbol{j}^a_l \boldsymbol{i}'} F^{(a,b,c)}\big(\boldsymbol{j}^a_1, \ldots, \boldsymbol{j}^a_{l-1}, \boldsymbol{i}', \boldsymbol{j}^a_{l+1}, \ldots, \boldsymbol{j}^a_a, \boldsymbol{j}^b, \boldsymbol{j}^c\big) - k^A_{\boldsymbol{i}' \boldsymbol{j}^a_l} F^{(a,b,c)}\big(\boldsymbol{j}^a, \boldsymbol{j}^b, \boldsymbol{j}^c\big) \Big] \\
& + \sum_{l=1}^{b} \Big[ k^B_{\boldsymbol{j}^b_l \boldsymbol{i}'} F^{(a,b,c)}\big(\boldsymbol{j}^a, \boldsymbol{j}^b_1, \ldots, \boldsymbol{j}^b_{l-1}, \boldsymbol{i}', \boldsymbol{j}^b_{l+1}, \ldots, \boldsymbol{j}^b_b, \boldsymbol{j}^c\big) - k^B_{\boldsymbol{i}' \boldsymbol{j}^b_l} F^{(a,b,c)}\big(\boldsymbol{j}^a, \boldsymbol{j}^b, \boldsymbol{j}^c\big) \Big] \\
& + \sum_{l=1}^{c} \Big[ k^C_{\boldsymbol{j}^c_l \boldsymbol{i}'} F^{(a,b,c)}\big(\boldsymbol{j}^a, \boldsymbol{j}^b, \boldsymbol{j}^c_1, \ldots, \boldsymbol{j}^c_{l-1}, \boldsymbol{i}', \boldsymbol{j}^c_{l+1}, \ldots, \boldsymbol{j}^c_c\big) - k^C_{\boldsymbol{i}' \boldsymbol{j}^c_l} F^{(a,b,c)}\big(\boldsymbol{j}^a, \boldsymbol{j}^b, \boldsymbol{j}^c\big) \Big] \\
& \Bigg).
\end{aligned} \tag{2.26}$$

Since the volume of each mesh cell is identical, the diffusion operators for each particle of each of the three chemical species simply correspond to discretizations of the Laplacian scaled by the corresponding diffusion coefficient, as given by equation (2.15). Denote by $(\Delta_h)^a_l$ the discrete Laplacian acting on the $\boldsymbol{j}^a_l$ coordinates. The total Laplacian acting on all of the $\boldsymbol{j}^a$ coordinates is then defined to be

$$\Delta^a_h = \sum_{l=1}^{a} (\Delta_h)^a_l\,.$$

With $\Delta_h^b$ and $\Delta_h^c$ definined similarly, equation (2.26) can be simplified to

$$\left(\tilde{L}_h F^{(a,b,c)}\right)\left(\boldsymbol{j}^a,\boldsymbol{j}^b,\boldsymbol{j}^c,t\right) = \left(D^{\mathrm{A}}\Delta_h^a + D^{\mathrm{B}}\Delta_h^b + D^{\mathrm{C}}\Delta_h^c\right) F^{(a,b,c)}\left(\boldsymbol{j}^a,\boldsymbol{j}^b,\boldsymbol{j}^c,t\right). \tag{2.27}$$

Using equations (2.20) and (2.21), the reaction operator, $\tilde{R}_h$, is

$$\begin{aligned}
&\left(\tilde{R}_h F^{(a,b,c)}\right)\left(\boldsymbol{j}^a,\boldsymbol{j}^b,\boldsymbol{j}^c\right) = \\
&\quad \frac{k_+}{h^3}\sum_{\boldsymbol{i}\in I^3}\Bigg[\left(\frac{(a+1)\,(b+1)}{c}\right) c_{\boldsymbol{i}} F^{(a+1,b+1,c-1)}\left(\boldsymbol{j}^a\cup\{\boldsymbol{i}\},\boldsymbol{j}^b\cup\{\boldsymbol{i}\},\boldsymbol{j}^c\setminus\{\boldsymbol{i}\}\right) \\
&\qquad\qquad - a_{\boldsymbol{i}} b_{\boldsymbol{i}} F^{(a,b,c)}\left(\boldsymbol{j}^a,\boldsymbol{j}^b,\boldsymbol{j}^c\right)\Bigg] \\
&\quad +k_-\sum_{\boldsymbol{i}\in I^3}\Bigg[\left(\frac{c+1}{ab}\right) a_{\boldsymbol{i}} b_{\boldsymbol{i}} F^{(a-1,b-1,c+1)}\left(\boldsymbol{j}^a\setminus\{\boldsymbol{i}\},\boldsymbol{j}^b\setminus\{\boldsymbol{i}\},\boldsymbol{j}^c\cup\{\boldsymbol{i}\}\right) \\
&\qquad\qquad - c_{\boldsymbol{i}} F^{(a,b,c)}\left(\boldsymbol{j}^a,\boldsymbol{j}^b,\boldsymbol{j}^c\right)\Bigg].
\end{aligned} \tag{2.28}$$

Defining

$$\delta_{\boldsymbol{i}\boldsymbol{j}} = \begin{cases} 1, & \boldsymbol{i}=\boldsymbol{j}, \\ 0, & \text{else}, \end{cases}$$

then

$$a_{\boldsymbol{i}} b_{\boldsymbol{i}} F^{(a,b,c)}\left(\boldsymbol{j}^a,\boldsymbol{j}^b,\boldsymbol{j}^c\right) = \sum_{l\in\{l'|\boldsymbol{j}^a_{l'}=\boldsymbol{i}\}}\sum_{\tilde{l}=1}^{b}\delta_{\boldsymbol{j}^a_l\boldsymbol{j}^b_{\tilde{l}}} F^{(a,b,c)}\left(\boldsymbol{j}^a,\boldsymbol{j}^b,\boldsymbol{j}^c\right). \tag{2.29}$$

Similarly,

$$\begin{aligned}
&a_{\boldsymbol{i}} b_{\boldsymbol{i}} F^{(a-1,b-1,c+1)}\left(\boldsymbol{j}^a\setminus\{\boldsymbol{i}\},\boldsymbol{j}^b\setminus\{\boldsymbol{i}\},\boldsymbol{j}^c\cup\{\boldsymbol{i}\}\right) = \\
&\qquad\qquad \sum_{l\in\{l'|\boldsymbol{j}^a_{l'}=\boldsymbol{i}\}}\sum_{\tilde{l}=1}^{b}\delta_{\boldsymbol{j}^a_l\boldsymbol{j}^b_{\tilde{l}}} F^{(a-1,b-1,c+1)}\left(\boldsymbol{j}^a\setminus\boldsymbol{j}^a_l,\boldsymbol{j}^b\setminus\boldsymbol{j}^b_{\tilde{l}},\boldsymbol{j}^c\cup\boldsymbol{j}^a_l\right).
\end{aligned} \tag{2.30}$$

We now expand each term in (2.28) into a sum over particle indexes using equations (2.24), (2.29), and (2.30). Reusing equation (2.25), we obtain the

final expression for the reaction operator,

$$\begin{aligned}
\left(\tilde{R}_h F^{(a,b,c)}\right)\left(\boldsymbol{\jmath}^a,\boldsymbol{\jmath}^b,\boldsymbol{\jmath}^c\right) = \\
\frac{k_+}{h^3}\Bigg[\left(\frac{(a+1)\,(b+1)}{c}\right)\sum_{l=1}^{c} F^{(a+1,b+1,c-1)}\left(\boldsymbol{\jmath}^a\cup\boldsymbol{\jmath}_l^c,\boldsymbol{\jmath}^b\cup\boldsymbol{\jmath}_l^c,\boldsymbol{\jmath}^c\setminus\boldsymbol{\jmath}_l^c\right) \\
-\sum_{l=1}^{a}\sum_{\tilde{l}=1}^{b}\delta_{\boldsymbol{\jmath}_l^a\boldsymbol{\jmath}_{\tilde{l}}^b}\,F^{(a,b,c)}\left(\boldsymbol{\jmath}^a,\boldsymbol{\jmath}^b,\boldsymbol{\jmath}^c\right)\Bigg] \\
+k_-\Bigg[\left(\frac{c+1}{ab}\right)\sum_{l=1}^{a}\sum_{\tilde{l}=1}^{b}\delta_{\boldsymbol{\jmath}_l^a\boldsymbol{\jmath}_{\tilde{l}}^b}\,F^{(a-1,b-1,c+1)}\left(\boldsymbol{\jmath}^a\setminus\boldsymbol{\jmath}_l^a,\boldsymbol{\jmath}^b\setminus\boldsymbol{\jmath}_{\tilde{l}}^b,\boldsymbol{\jmath}^c\cup\boldsymbol{\jmath}_l^a\right) \\
-\sum_{l=1}^{c}F^{(a,b,c)}\left(\boldsymbol{\jmath}^a,\boldsymbol{\jmath}^b,\boldsymbol{\jmath}^c\right)\Bigg].
\end{aligned} \tag{2.31}$$

Note that the terms

$$\frac{(a+1)\,(b+1)}{c}$$

and

$$\frac{c+1}{ab}$$

are due to the normalization of $F^{(a,b,c)}$ chosen in equation (2.17). If in equation (2.17) division by $a!\,b!\,c!$ was left out, then the preceding terms would disappear. We note that it is this later definition that is used in [11], equation (51).

Up to this point, our calculations have been exact and mathematically rigorous. We now speculate on the relation between the discrete reaction–diffusion master equation (2.16) and the continuum, Fock Space formulation of [11]. This is investigated by taking a formal continuum limit, $h \to 0$, for the equation of evolution of $F^{(a,b,c)}$, equation (2.22). We shall recover a final model of the same type as equation (51) of [11]. Note, however, that the subsequent analysis is not

mathematically rigorous, and does not necessarily give the mathematically correct continuum limit. (Assuming such a limit even exists). What the analysis does show is the formal connection between the two formulations. Moreover, it motivates the possibility of deriving from the more microscopic representation used in [11] a discrete reaction–diffusion master equation type model.

We begin by rescaling the probability $F^{(a,b,c)}\left(\boldsymbol{j}^a, \boldsymbol{j}^b, \boldsymbol{j}^c\right)$ to obtain a probability density, $\rho_h^{(a,b,c)}\left(\boldsymbol{q}^a, \boldsymbol{q}^b, \boldsymbol{q}^c\right)$. Here, $\left(\boldsymbol{q}^a, \boldsymbol{q}^b, \boldsymbol{q}^c\right)$ are taken to be spatial position vectors that correspond to the cell centers of each box labeled by the components of $\left(\boldsymbol{j}^a, \boldsymbol{j}^b, \boldsymbol{j}^c\right)$. We then define

$$\rho_h^{(a,b,c)}\left(\boldsymbol{q}^a, \boldsymbol{q}^b, \boldsymbol{q}^c\right) \approx \frac{1}{h^{3(a+b+c)}} F^{(a,b,c)}\left(\boldsymbol{j}^a, \boldsymbol{j}^b, \boldsymbol{j}^c\right). \tag{2.32}$$

With this definition, we are assuming that the probability density for a particle to be at the center of a given mesh cell is approximately the probability of the particle being in that mesh cell divided by the volume of the mesh cell. Plugging this rescaling into equation (2.22), the equation of evolution for $\rho_h^{(a,b,c)}$ is then

$$\frac{d\rho_h^{(a,b,c)}}{dt}\left(\boldsymbol{q}^a, \boldsymbol{q}^b, \boldsymbol{q}^c\right) = \left(\tilde{L}_h \rho_h^{(a,b,c)} + \hat{R}_h \rho_h^{(a,b,c)}\right)\left(\boldsymbol{q}^a, \boldsymbol{q}^b, \boldsymbol{q}^c\right). \tag{2.33}$$

Note that the diffusion operator, $\tilde{L}_h$, is unchanged from equation (2.22). This is due to the linearity of the operator and that the operator does not change particle numbers. In contrast to this, the reaction operator is altered giving the

new operator,

$$\begin{aligned}
\Big(\tilde{R}_h\rho_h^{(a,b,c)}\Big)\big(\boldsymbol{q}^a,\boldsymbol{q}^b,\boldsymbol{q}^c\big) = \\
k_+\Bigg[\left(\frac{(a+1)\,(b+1)}{c}\right)\sum_{l=1}^{c}\rho_h^{(a+1,b+1,c-1)}\big(\boldsymbol{q}^a\cup\boldsymbol{q}_l^c,\boldsymbol{q}^b\cup\boldsymbol{q}_l^c,\boldsymbol{q}^c\setminus\boldsymbol{q}_l^c\big) \\
-\sum_{l=1}^{a}\sum_{\tilde{l}=1}^{b}\delta_h\big(\boldsymbol{q}_l^a-\boldsymbol{q}_{\tilde{l}}^b\big)\,\rho_h^{(a,b,c)}\big(\boldsymbol{q}^a,\boldsymbol{q}^b,\boldsymbol{q}^c\big)\Bigg] \\
+k_-\Bigg[\left(\frac{c+1}{ab}\right)\sum_{l=1}^{a}\sum_{\tilde{l}=1}^{b}\delta_h\big(\boldsymbol{q}_l^a-\boldsymbol{q}_{\tilde{l}}^b\big)\,\rho_h^{(a-1,b-1,c+1)}\big(\boldsymbol{q}^a\setminus\boldsymbol{q}_l^a,\boldsymbol{q}^b\setminus\boldsymbol{q}_{\tilde{l}}^b,\boldsymbol{q}^c\cup\boldsymbol{q}_l^a\big) \\
-\sum_{l=1}^{c}\rho_h^{(a,b,c)}\big(\boldsymbol{q}^a,\boldsymbol{q}^b,\boldsymbol{q}^c\big)\Bigg].
\end{aligned} \tag{2.34}$$

Here we have introduced the rescaled function, $\delta_h\big(\boldsymbol{q}_l^a-\boldsymbol{q}_{\tilde{l}}^b\big)=h^{-3}\delta_{\boldsymbol{\jmath}_l^a\boldsymbol{\jmath}_{\tilde{l}}^b}$.

We now consider the formal continuum limit of (2.33). The particle position vectors, $\big(\boldsymbol{q}^a,\boldsymbol{q}^b,\boldsymbol{q}^c\big)$, now become arbitrary points within the periodic box, $\Omega$. We assume that the discrete particle density, $\rho_h^{(a,b,c)}$ converges to a continuum density, $\rho^{(a,b,c)}$. Denote by $\Delta_l^a$ the continuum three–dimensional Laplacian, acting on the $l$'th particle of species $a$. Letting,

$$\Delta^a=\sum_{l=1}^{a}\Delta_l^a,$$

we find that the diffusion operator, $\tilde{L}_h$ goes over into the continuum diffusion operator

$$\Big(\tilde{L}\rho^{(a,b,c)}\Big)\big(\boldsymbol{q}^a,\boldsymbol{q}^b,\boldsymbol{q}^c\big)=\big(D^{\mathrm{A}}\Delta^a+D^{\mathrm{B}}\Delta^b+D^{\mathrm{C}}\Delta^c\big)\,\rho^{(a,b,c)}\big(\boldsymbol{q}^a,\boldsymbol{q}^b,\boldsymbol{q}^c\big). \tag{2.35}$$

Assuming the discrete delta function, $\delta_h\big(\boldsymbol{q}_l^a-\boldsymbol{q}_{\tilde{l}}^b\big)$, will converge to the continuum delta function, $\delta\big(\boldsymbol{q}_l^a-\boldsymbol{q}_{\tilde{l}}^b\big)$, the reaction operator, $\tilde{R}_h$, converges to the

continuum reaction operator

$$\begin{aligned}
\Big(\tilde{R}\rho^{(a,b,c)}\Big)\big(\boldsymbol{q}^a,\boldsymbol{q}^b,\boldsymbol{q}^c\big) = \\
k_+\Bigg[\left(\frac{(a+1)\,(b+1)}{c}\right)\sum_{l=1}^{c}\rho^{(a+1,b+1,c-1)}\big(\boldsymbol{q}^a\cup\boldsymbol{q}^c_l,\boldsymbol{q}^b\cup\boldsymbol{q}^c_l,\boldsymbol{q}^c\setminus\boldsymbol{q}^c_l\big) \\
-\sum_{l=1}^{a}\sum_{\tilde{l}=1}^{b}\delta\big(\boldsymbol{q}^a_l-\boldsymbol{q}^b_{\tilde{l}}\big)\,\rho^{(a,b,c)}\big(\boldsymbol{q}^a,\boldsymbol{q}^b,\boldsymbol{q}^c\big)\Bigg] \\
+k_-\Bigg[\left(\frac{c+1}{ab}\right)\sum_{l=1}^{a}\sum_{\tilde{l}=1}^{b}\delta\big(\boldsymbol{q}^a_l-\boldsymbol{q}^b_{\tilde{l}}\big)\,\rho^{(a-1,b-1,c+1)}\big(\boldsymbol{q}^a\setminus\boldsymbol{q}^a_l,\boldsymbol{q}^b\setminus\boldsymbol{q}^b_{\tilde{l}},\boldsymbol{q}^c\cup\boldsymbol{q}^a_l\big) \\
-\sum_{l=1}^{c}\rho^{(a,b,c)}\big(\boldsymbol{q}^a,\boldsymbol{q}^b,\boldsymbol{q}^c\big)\Bigg].
\end{aligned} \tag{2.36}$$

This definition can be rewritten in the form of the reaction operator from [11] by defining the reaction rate terms,

$$\begin{aligned}
\alpha_+\big(\boldsymbol{q}^a_l,\boldsymbol{q}^b_{l'},\boldsymbol{q}^c_{\tilde{l}}\big) &= k_+\delta\big(\boldsymbol{q}^a_l-\boldsymbol{q}^b_{l'}\big)\delta\big(\boldsymbol{q}^a_l-\boldsymbol{q}^c_{\tilde{l}}\big), \\
\alpha_-\big(\boldsymbol{q}^a_l,\boldsymbol{q}^b_{l'},\boldsymbol{q}^c_{\tilde{l}}\big) &= k_-\delta\big(\boldsymbol{q}^a_l-\boldsymbol{q}^b_{l'}\big)\delta\big(\boldsymbol{q}^a_l-\boldsymbol{q}^c_{\tilde{l}}\big).
\end{aligned}$$

Equation (2.36) then becomes

$$\begin{aligned}
\left(\tilde{R}\rho^{(a,b,c)}\right)\left(\boldsymbol{q}^a,\boldsymbol{q}^b,\boldsymbol{q}^c\right) = \\
&\left[\left(\frac{(a+1)\,(b+1)}{c}\right)\sum_{l=1}^{c}\Bigg(\right. \\
&\quad\left.\int_\Omega\int_\Omega \alpha_+\left(\boldsymbol{q}_1,\boldsymbol{q}_2,\boldsymbol{q}_l^c\right)\rho^{(a+1,b+1,c-1)}\left(\boldsymbol{q}^a\cup\boldsymbol{q}_1,\boldsymbol{q}^b\cup\boldsymbol{q}_2,\boldsymbol{q}^c\setminus\boldsymbol{q}_l^c\right)d\boldsymbol{q}_1 d\boldsymbol{q}_2\Bigg)\right. \\
&\quad\left.-\sum_{l=1}^{a}\sum_{\tilde{l}=1}^{b}\int_\Omega \alpha_+\left(\boldsymbol{q}_l^a,\boldsymbol{q}_{\tilde{l}}^b,\boldsymbol{q}_3\right)\rho^{(a,b,c)}\left(\boldsymbol{q}^a,\boldsymbol{q}^b,\boldsymbol{q}^c\right)d\boldsymbol{q}_3\right] \\
+&\left[\left(\frac{c+1}{ab}\right)\sum_{l=1}^{a}\sum_{\tilde{l}=1}^{b}\Bigg(\right. \\
&\quad\left.\int_\Omega \alpha_-\left(\boldsymbol{q}_l^a,\boldsymbol{q}_{\tilde{l}}^b,\boldsymbol{q}_3\right)\rho^{(a-1,b-1,c+1)}\left(\boldsymbol{q}^a\setminus\boldsymbol{q}_l^a,\boldsymbol{q}^b\setminus\boldsymbol{q}_{\tilde{l}}^b,\boldsymbol{q}^c\cup\boldsymbol{q}_3\right)d\boldsymbol{q}_3\Bigg)\right. \\
&\quad\left.-\sum_{l=1}^{c}\int_\Omega\int_\Omega \alpha_-\left(\boldsymbol{q}_1,\boldsymbol{q}_2,\boldsymbol{q}_l^c\right)\rho^{(a,b,c)}\left(\boldsymbol{q}^a,\boldsymbol{q}^b,\boldsymbol{q}^c\right)d\boldsymbol{q}_1 d\boldsymbol{q}_2\right].
\end{aligned} \tag{2.37}$$

The equation of evolution, equation (2.33), now becomes

$$\frac{d\rho^{(a,b,c)}}{dt}\left(\boldsymbol{q}^a,\boldsymbol{q}^b,\boldsymbol{q}^c\right) = \left(\tilde{L}\rho^{(a,b,c)} + \tilde{R}\rho^{(a,b,c)}\right)\left(\boldsymbol{q}^a,\boldsymbol{q}^b,\boldsymbol{q}^c\right). \tag{2.38}$$

A key point about the preceding analysis is that the formulation given by the operators (2.35) and (2.37) with equation (2.38) provides a possible *initial* model of the chemical reaction $\mathrm{A}+\mathrm{B}\leftrightarrows\mathrm{C}$, for many different possible choices of $\alpha_+$ and $\alpha_-$. We are formally using point reactions to represent binding interactions, but there is no reason that $\alpha_+$ could not allow binding within a certain binding radius. Likewise, there is no reason that unbinding might not produce two particles a fixed separation apart. In fact, such interaction models are commonly used in stochastic reaction–diffusion formulations that track individual particles [3]. While the preceding analysis is not rigorous, it does provide a mechanism to

start with a more microscopic particle interaction model and then, through an appropriate discretization mechanism, try to obtain a reaction–diffusion master equation model. (By specifying the reaction interaction terms, and then applying the preceding analysis in the reverse order).

With regards to the specific particle interactions derived above for $\alpha_+$ and $\alpha_-$, we note that the critical steps in the derivation are the assumption that the discrete delta functions go over into continuum delta functions, and that the solutions to the discrete equations approach well-defined solutions to the continuum equations. Unfortunately, just giving a precise mathematical meaning to the continuum equation is difficult because of the delta function coefficients. The definition of solutions to PDEs with delta function coefficients has been previously considered, but only in certain special cases has been made mathematically rigorous, see for example [2]. It is not clear that equation (2.38) really is well–defined as formulated, let alone the limit of the discrete model. While these issues are interesting possible research directions, they are beyond the scope of our current discussion.

## 2.5 Stochastic Reaction–Diffusion Active Transport Chemical Kinetics

We now extend the reaction–diffusion master equation (2.10) to incorporate active transport along microtubules and actin filaments. The biological model for active transport is the same as that presented in Section 2.2.3. Here, we represent the advective motion of active transport as a system of first–order reactions corresponding to jumps between mesh cells. Note the similarity of this

approach to the representation of diffusion introduced above. Considering the motion of a single microtubule–bound motor along the microtubule direction field, we obtain a corresponding Fokker–Planck equation for the probability density of the motor's position. An appropriate discretization of this equation then determines the jump rates to use in the reaction–diffusion active transport master equation.

Denote by $\kappa_{ij}^l$ the *active transport* jump rate for each individual molecule of the $l$'th chemical species into cell $i$ from cell $j$, for $i \neq j$. Since active transport is treated as a first order reaction, and since individual molecules are assumed to move independently, the total probability at time $t$ for one molecule of species $l$ to jump by active transport from cell $j$ to $i$ is $\kappa_{ij}^l M_j^l(t)$. The reaction–diffusion active transport master equation is then

$$\begin{aligned}\frac{dP(\boldsymbol{m})}{dt} =& \sum_{i=1}^{N}\sum_{j=1}^{N}\sum_{l=1}^{L}\left(k_{ij}^l\left(m_j^l+1\right)P(\boldsymbol{m}+\boldsymbol{e}_j^l-\boldsymbol{e}_i^l)-k_{ji}^l m_i^l P(\boldsymbol{m})\right)\\ &+\sum_{i=1}^{N}\sum_{j=1}^{N}\sum_{l=1}^{L}\left(\kappa_{ij}^l\left(m_j^l+1\right)P(\boldsymbol{m}+\boldsymbol{e}_j^l-\boldsymbol{e}_i^l)-\kappa_{ji}^l m_i^l P(\boldsymbol{m})\right) \qquad (2.39)\\ &+\sum_{i=1}^{N}\sum_{k=1}^{K}\left(a_i^k(\boldsymbol{m}_i-\boldsymbol{\nu}_k)P(\boldsymbol{m}-\boldsymbol{e}_i\boldsymbol{\nu}_k)-a_i^k(\boldsymbol{m}_i)P(\boldsymbol{m})\right).\end{aligned}$$

The only difference between equation (2.39) and equation (2.10) is the addition of the middle line above, corresponding to motion by active transport. Note that the form of the active transport term is the same as that for diffusion, just with different specific jump rates.

The active transport jump rates, as was done for the diffusive jump rates, can be determined through comparison to either the corresponding continuum reaction–diffusion active transport model, or through comparison to a single particle active transport model. Recall the deterministic reaction–diffusion ac-

tive transport model given by equation (2.3). Letting $C_i^l(t) = M_i^l(t)/V_i$, and using equation (2.7) to calculate the mean of equation (2.39), we find that the mean of the concentration of the $l$'th chemical species is given by

$$\frac{d\left\langle C_i^l\right\rangle}{dt} - \sum_{j=1}^{N}\left(\frac{V_j}{V_i}\kappa_{ij}^l\left\langle C_j^l\right\rangle - \kappa_{ji}^l\left\langle C_i^l\right\rangle\right) = \sum_{j=1}^{N}\left(\frac{V_j}{V_i}k_{ij}^l\left\langle C_j^l\right\rangle - k_{ji}^l\left\langle C_i^l\right\rangle\right) + \sum_{k=1}^{K}\nu_k^l\left\langle\tilde{a}_i^k\left(C_i\right)\right\rangle.$$

Suppose the rates $\kappa_{ij}^l$ could be chosen so that the active transport term,

$$\sum_{j=1}^{N}\left(\frac{V_j}{V_i}\kappa_{ij}^l\left\langle C_j^l\right\rangle - \kappa_{ji}^l\left\langle C_i^l\right\rangle\right),$$

is a discretization of $-\nabla\cdot\left(C^l(\boldsymbol{x},t)\boldsymbol{v}^l(\boldsymbol{x})\right)$. Then, as for the purely diffusive case, in the continuum limit the only difference between the deterministic reaction–diffusion active transport model and the mean concentrations of the stochastic model would be the non–commutativity of the reaction terms with averaging; both diffusion and active transport would be identical between the two models.

Alternatively, we can simplify equation (2.39) as in Section 2.4.3. Restricting to movement due solely to active transport (no diffusion), we assume the active transport jump rates are independent of the chemical reactions present within a given chemical system. Therefore, we now consider a chemical system involving no reactions. The movement by active transport of each individual particle of each chemical species will then be independent. It is therefore sufficient to consider the active transport, in the presence of no reactions, of just one particle of one chemical species. With these assumptions, equation (2.39) then reduces to

$$\frac{dP(\boldsymbol{m})}{dt} = \sum_{i=1}^{N}\sum_{j=1}^{N}\kappa_{ij}\left(m_j+1\right)P(\boldsymbol{m}+\boldsymbol{e}_j-\boldsymbol{e}_i) - \kappa_{ji}m_iP(\boldsymbol{m}). \tag{2.40}$$

As $\boldsymbol{M}(t)$ is describing one particle, $M_i(t)$ will be zero for all $i$ except the location at which the particle is. Let $\boldsymbol{X}(t)$ be the process giving the position of the particle at time $t$. Then define

$$Q_i(t) \equiv P(\boldsymbol{e}_i, t) \approx \text{Prob}\{\boldsymbol{X}(t) \in V_i | \boldsymbol{X}(0) = \boldsymbol{x}_0\},$$

$\boldsymbol{e}_i$ denoting, as before, the unit vector along the $i$'th Cartesian coordinate axis of $\mathbb{R}^N$. Letting the probability density to be at the center of mesh cell $i$ be $p_i(t) \equiv Q_i(t)/V_i$, and following the analysis of Section 2.4.3, we find that $p_i$ satisfies

$$\frac{dp_i}{dt} - \sum_{j=1}^{N} \frac{V_j}{V_i} \kappa_{ij}\, p_j - \kappa_{ji}\, p_i = 0. \tag{2.41}$$

Therefore, if the rates again formed a discretization of the advection operator, $-\nabla \cdot (\boldsymbol{v}(\boldsymbol{x})$, then in the continuum limit as cell size goes to zero equation (2.41) would become

$$\frac{\partial p}{\partial t}(\boldsymbol{x}, t) + \nabla \cdot (p(\boldsymbol{x}, t)\boldsymbol{v}(\boldsymbol{x})) = 0. \tag{2.42}$$

This is simply an advection equation, exactly what one would expect for the motion in a velocity field, $\boldsymbol{v}(\boldsymbol{x})$, of a single particle.

With this continuum limit, and that for the mean concentrations, we see that constructing an operator, $A_h$, of the form

$$(A_h p)_i = \sum_{j=1}^{N} \frac{V_j}{V_i} \kappa_{ij}\, p_j - \kappa_{ji}\, p_i, \tag{2.43}$$

where $A_h \rightarrow -\nabla \cdot (\boldsymbol{v}(\boldsymbol{x})$, will determine the $\kappa_{ij}$. (Again, here $h$ represents the maximum length scale associated with a computational cell). The active transport jump rates will then be $\kappa_{ij}$, provided $\kappa_{ij} \geq 0$ (see Appendix A). We shall see in Section 3.2 that we obtain different scalings for the active transport and diffusion jump rates.

The preceding model is a more macroscopic formulation of active transport than is often used. By using advection to model active transport, we are assuming that the active transport mechanism is deterministic. Our method therefore approximates determinisitic advective motion by a stochastic process. In the continuum limit as the mesh width approaches zero, the stochastic process will become deterministic. We note that one could also couple more microscopic stochastic active transport models, as in [41] and [42], to the reaction–diffusion master equation if needed.

# Chapter 3

# Numerical Method

## 3.1 Determining the Diffusive Jump Rates

From the results of Section 2.4.1, an appropriate spatial discretization of either the classical deterministic formulation of reaction–diffusion, or the Fokker–Planck equation for a single Brownian particle would determine the jump rates in (2.10). We note that in choosing the jump rates to recover either one of these two formulations, the macroscopic diffusion of the mean concentration from the reaction–diffusion master equation, or the microscopic Brownian motion of independent particles, we will also recover the other formulation. Previous authors [17] [40] have used the requirement of obtaining macroscopic diffusion of the mean concentrations given by the reaction–diffusion master equation to derive diffusive jump rates in the special case of a uniform Cartesian mesh. In this case, it has been shown that the jump rates, with mesh width $h$, can be given by

$$\frac{D}{h^2}$$

for jumps between neighboring mesh cells, and are zero for jumps between non-neighboring cells. This result has been known from as far back as [16]. In this section, instead of focusing on recovering macroscopic diffusion of the mean concentrations, we focus on the mathematically equivalent requirement of reproducing single particle Brownian motion. We note that if we assume molecules are only moving by diffusion, then the requirement of recovering single particle Brownian motion in the continuum limit is a physical necessity for the reaction–diffusion master equation. With this choice we can derive valid jump rates for diffusion within complex geometries, allowing us to extend the existing methodology to handle arbitrary boundaries. This result is important since many problems of practical interest contain geometrically complex domains, such as the movement of molecules within biological cells where there are many barriers due to organelles and membranes.

To discretize the Laplacian, and hence obtain the diffusive jump rates, boundary conditions must be specified for the domain of interest; this is discussed in Section 3.1.1. Section 3.1.2 derives the embedded boundary method to discretize the Fokker–Planck equation, and calculates the corresponding diffusive jump rates for the reaction–diffusion master equation. Some consequences of the specific discretization chosen are also presented. In Section 3.1.3 the complete algorithm for solving the reaction–diffusion master equation is summarized. Convergence of the embedded boundary discretization is demonstrated for several examples in Section 3.1.4, while Section 3.1.5 discusses the convergence of the overall algorithm of Section 3.1.3.

### 3.1.1 Boundary Conditions

Since we are applying the overall method to simulations of biochemical networks in eukaryotic cells, which are cells with a nuclear membrane, we formulate our boundary conditions for this type of domain. Denote the entirety of the cell by $\Omega$, and the cell membrane (i.e., exterior boundary) as $\partial\Omega$. A eukaryotic cell will also have a nucleus, $\Omega_n \subset \Omega$, a closed volume contained completely within the interior of the cell. The nuclear membrane, $\partial\Omega_n$, encloses the nucleus, partitioning the cell's interior into two distinct compartments.

Passage through the cellular membrane will not be allowed, so that the exterior boundary will have a no–flux Neumann condition. This can, of course, be changed to a more general flux condition if necessary. The nuclear membrane will be impermeable to certain species, requiring again a no–flux Neumann condition, while allowing a passive flux for others. This second condition will be modeled by having the nuclear membrane flux proportional to the jump in probability density, or concentration, across the membrane. Note that this boundary condition assumes molecules cross the nuclear membrane independently of each other. The boundary condition may be derived from a more detailed model of the nuclear membrane as containing channels, called nuclear pores, through which certain species may diffuse. The nuclear membrane is thin relative to the size of a eukaryotic cell, and hence the diffusive motion of molecules within the membrane will equilibrate rapidly. This implies that the diffusive flux within the membrane can be assumed spatially constant. In addition, the number of nuclear pores is large enough that we approximate them as a fixed background density within the membrane. Combining these two approximations, and idealizing the membrane as infinitely thin, implies that the flux through

the nuclear membrane is proportional to the difference in probability density, or concentration, across the membrane. Note that in certain situations this boundary condition would need to be modified to a more physically detailed model. One such example would be if the number of molecules crossing the nuclear membrane can become large enough to saturate the nuclear pores.

Consider a single particle moving by classical Brownian motion within the cell. Let $p(\boldsymbol{x}, t)$ denote the probability density for the position of the particle. Then within both the nucleus, $\Omega_n$, and the cytoplasm, $\Omega \setminus \Omega_n$, $p(x, t)$ will satisfy equation (2.14). (Here $\Omega \setminus \Omega_n$ denotes the set of points within $\Omega$ that are not also contained in $\Omega_n$). Let $[p]_n$ denote the jump in $p(\boldsymbol{x}, t)$ across the nuclear membrane. Define by $\rho$ the nuclear membrane permeability, and by $D$ the diffusion constant of the particle. Let $\boldsymbol{\eta}$ denote the outward pointing normal to a given surface. Then, incorporating the assumed boundary conditions, $p(\boldsymbol{x}, t)$ satisfies

$$\begin{aligned} \frac{\partial p}{\partial t} &= D\Delta p, && \text{in } \Omega, \\ \frac{\partial p}{\partial \boldsymbol{\eta}} &= 0, && \text{on } \partial\Omega, \\ -D\frac{\partial p}{\partial \boldsymbol{\eta}} &= -\rho\,[p]_n\,, && \text{on } \partial\Omega_n, \end{aligned} \tag{3.1}$$

with the initial condition $p(\boldsymbol{x}, 0) = \delta(\boldsymbol{x} - \boldsymbol{x}_0)$, where $\boldsymbol{x}_0$ is the known initial position of the particle.. A discretization of these equations that has the general form of (2.13), will determine the jump rates in the reaction–diffusion master equation.

The corresponding multiple species, deterministic reaction–diffusion model for the assumed boundary conditions follows. Let $\left[C^l\right]_n$ denote the jump in $C^l$ across the nuclear membrane, $\rho^l$ the nuclear membrane permeability, and $D^l$

the diffusion constant of the $l$'th species. Then

$$\begin{aligned}
\frac{\partial C^l(\boldsymbol{x},t)}{\partial t} &= D^l \Delta C^l + \sum_{k=1}^{K} \nu_k^l \, \tilde{a}^k(\boldsymbol{C}(\boldsymbol{x},t),\boldsymbol{x}), && \text{in } \Omega, \\
\frac{\partial C^l(\boldsymbol{x},t)}{\partial \boldsymbol{\eta}} &= 0, && \text{on } \partial\Omega, \\
-D^l \frac{\partial C^l(\boldsymbol{x},t)}{\partial \boldsymbol{\eta}} &= -\rho^l \left[C^l\right]_n, && \text{on } \partial\Omega_n,
\end{aligned} \tag{3.2}$$

with the initial condition, $C^l(\boldsymbol{x},0) = C_0(\boldsymbol{x})$.

### 3.1.2 Numerical Discretization

For simplicity, we discretize (3.1) instead of the deterministic reaction–diffusion formulation (3.2). We may do this because our purpose is not to obtain a numerical scheme for the deterministic equations but instead to obtain the jump rates for use in our stochastic simulation, and, as was shown in Section 2.4.1, the jump rates are the same whether we use (3.1) or the full deterministic reaction–diffusion system (3.2). For the remainder of this section, we use the word "cell" to refer to a cell of the Cartesian computational mesh, and we specify "biological cell" when that is what we mean. We embed $\Omega$ in a Cartesian mesh with cell centers $\boldsymbol{x_i}$, and mesh width $h$. There are three different domains contained in this description: the nuclear space, $\Omega_n$, the cytoplasm, $\Omega \setminus \Omega_n$, and the space exterior to the biological cell. The total computational domain within which the biological cell is embedded is taken to be a square.

Define three separate solutions to (3.1), corresponding to each of the three domains: $p^{\text{nuc}}$, the value of $p(x,t)$ within $\Omega_n$, $p^{\text{cyt}}$, the value of $p(x,t)$ within $\Omega \setminus \Omega_n$, and $p^{\text{ext}}$, the value of $p$ outside the biological cell. Since the particle is assumed to never leave $\Omega$, $p^{\text{ext}}$ will be zero. Denote by $p^{\alpha}$ the value of the

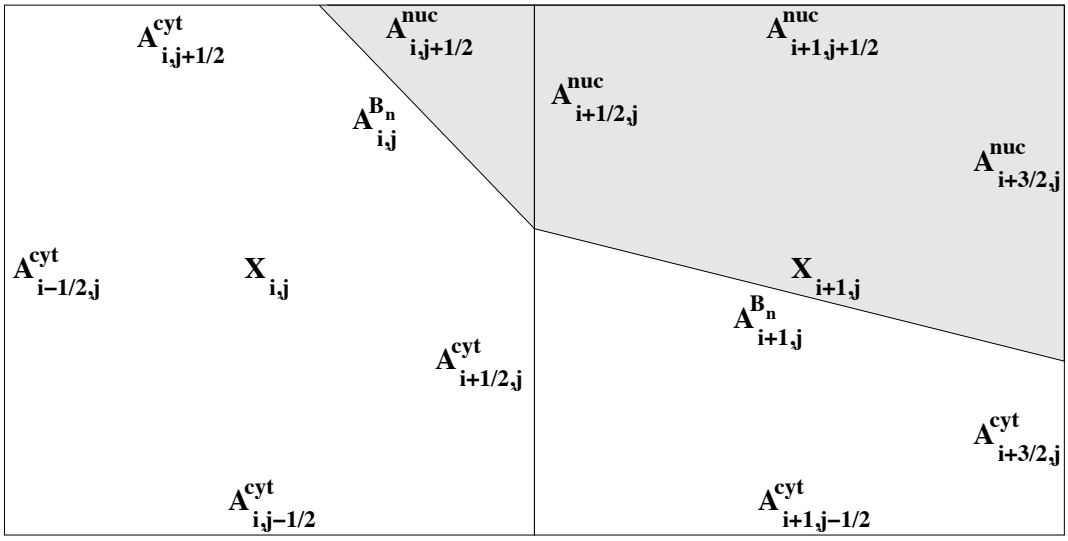


Figure 3.1: 2D Cartesian mesh cells cut by nuclear membrane. The darker region represents the portion of $\Omega_n$, the nuclear space, within the mesh cells. The lighter region represents the portion of $\Omega \setminus \Omega_n$, the cytoplasm, within the mesh cells. $A^{\text{cyt}}_{i+1/2,j}$ gives the length of the piece of the face connecting cells $(i,j)$ and $(i+1,j)$ that is within the cytoplasmic domain. The remaining $A^{\alpha}_{i,j}$ values, for $\alpha$ a given domain, are defined similarly. $A^{B_n}_{i,j}$ is the length of the piece of the nuclear membrane within the cell $(i,j)$. $X_{i,j}$ gives the center of the Cartesian cell at location $(i,j)$. Also, $V^{\alpha}_{i,j}$ (not shown) gives the area of the portion of cell $(i,j)$ within the domain $\alpha$.

solution for domain $\alpha$, where $\alpha \in \{\text{nuc}, \text{cyt}, \text{ext}\}$. Each of these solutions are assumed to be smoothly extendable across the boundaries of their region of definition. Note that the actual solution $p(x,t)$ will not be smooth across either the nuclear or cellular membrane, but its value on either side of each of these membranes can be smoothly extended to the other side.

For spatial dimension $d$, let $\boldsymbol{i} \in \mathbb{Z}^d$ denote the index vector for mesh cells. With the smooth extension assumption, a cell–centered solution value, $p_{\boldsymbol{i}}^{\alpha}$, can always be defined within cells containing some portion of the domain $\alpha$. For a cell completely within this domain only one solution value will be considered, $p_{\boldsymbol{i}}^{\alpha}$. If a cell is split by one of the membranes then two cell–centered solution values will be stored for the cell. It is assumed that at most one boundary intersects a given cell. For example, in Figure 3.1, which shows the 2D case for simplicity, cell $\boldsymbol{i} = (i,j)$ is split by the nuclear membrane, hence, there would be two solution values stored for this cell, $p_{\boldsymbol{i}}^{\text{nuc}}$, and $p_{\boldsymbol{i}}^{\text{cyt}}$. These two solution values are subsequently used to approximate the boundary condition on the membrane. They also allow, in the master equation formulation, separate probabilities of the particle being in either portion of the cell. Again, as the particle can not cross $\partial\Omega$, $p_{\boldsymbol{i}}^{\text{ext}} = 0$ for all $\boldsymbol{i}$. As we know $p_{\boldsymbol{i}}^{\text{ext}}$, multiple values need not be stored for cells cut by $\partial\Omega$. If the particle could cross the cellular membrane, then $p_{\boldsymbol{i}}^{\text{ext}}$ would not necessarily be zero, and multiple values would be needed in cells split by $\partial\Omega$.

Figure 3.1 defines several geometric quantities associated with cells that are used in the numerical discretization. Let $\boldsymbol{e}_k$ denote the unit vector along the $k$'th coordinate axis of $\mathbb{R}^d$. Define by

$$\boldsymbol{F}(x,t) = -D\nabla p, \tag{3.3}$$

the probability flux vector per unit area. Let $\boldsymbol{F}^\alpha$ be the flux vector of the domain $\alpha$ solution, and $(F_k)^\alpha$ the $k$'th component of $\boldsymbol{F}^\alpha$. $\boldsymbol{\eta}^\alpha$ will denote the outward pointing, with respect to domain $\alpha$, normal to a given surface. Following the conservative discretization method in [30], for all cells, $\boldsymbol{i}$, in which $p^\alpha_{\boldsymbol{i}}$ is defined:

$$\begin{aligned}
\frac{dp^\alpha_{\boldsymbol{i}}}{dt} &= -(\nabla\cdot\boldsymbol{F^\alpha})_i, \qquad (3.4)\\
&\approx -\frac{1}{V^\alpha_{\boldsymbol{i}}}\int_{V^\alpha_{\boldsymbol{i}}}\nabla\cdot\boldsymbol{F^\alpha}\,dV = -\frac{1}{V^\alpha_{\boldsymbol{i}}}\int_{\partial V^\alpha_{\boldsymbol{i}}}\boldsymbol{F^\alpha}\cdot\boldsymbol{\eta^\alpha}\,dS,\\
&= -\frac{1}{V^\alpha_{\boldsymbol{i}}}\left(\sum_{\pm}\sum_{k=1}^{d}\int_{A^\alpha_{\boldsymbol{i}\pm\boldsymbol{e}_k}}\boldsymbol{F^\alpha}\cdot\boldsymbol{\eta^\alpha}\,dS + \int_{B_n}\boldsymbol{F^\alpha}\cdot\boldsymbol{\eta^\alpha}\,dS + \int_{B_e}\boldsymbol{F^\alpha}\cdot\boldsymbol{\eta^\alpha}\,dS\right),\\
&\approx -\frac{1}{V^\alpha_{\boldsymbol{i}}}\left(\sum_{k=1}^{d}\left(A^\alpha_{\boldsymbol{i}+\frac{1}{2}\boldsymbol{e}_k}(F_k)^\alpha_{\boldsymbol{i}+\frac{1}{2}\boldsymbol{e}_k} - A^\alpha_{\boldsymbol{i}-\frac{1}{2}\boldsymbol{e}_k}(F_k)^\alpha_{\boldsymbol{i}-\frac{1}{2}\boldsymbol{e}_k}\right) + A^{B_n}_{\boldsymbol{i}}\boldsymbol{F}^{B_n}_{\boldsymbol{i}}\cdot\boldsymbol{\eta}^{B_n}_{\boldsymbol{i}}\right).
\end{aligned}$$

Here, $B_n = \partial\Omega_n \cap \partial V^\alpha_{\boldsymbol{i}}$, and $B_e = \partial\Omega \cap \partial V^\alpha_{\boldsymbol{i}}$. The surface integral over $B_e$ is identically zero due to the no–flux boundary condition at $\partial\Omega$. If a non–zero flux boundary condition is specified instead, then the integral would contribute another term of the form

$$-\frac{1}{V^\alpha_{\boldsymbol{i}}}A^{B_e}_{\boldsymbol{i}}\boldsymbol{F}^{B_e}_{\boldsymbol{i}}\cdot\boldsymbol{\eta}^{B_e}_{\boldsymbol{i}}$$

in the last line of (3.4).

To give a valid Reaction–Diffusion master equation the fluxes are chosen as the standard full–face centered difference

$$(F_k)^\alpha_{\boldsymbol{i}\pm\frac{1}{2}\boldsymbol{e}_k} = \mp D\,\frac{p^\alpha_{\boldsymbol{i}\pm\boldsymbol{e}_k} - p^\alpha_{\boldsymbol{i}}}{h}.$$

From the nuclear membrane boundary condition

$$\boldsymbol{F}^{B_n}_{\boldsymbol{i}}\cdot\boldsymbol{\eta}^{B_n}_{\boldsymbol{i}} = -\rho\,[p]^{B_n}_{\boldsymbol{i}}\,.$$

To enforce this jump condition the cell–centered solution value for the domain on the other side of the nuclear membrane is used. For example, if $\alpha$ = nuc

then $p_{\boldsymbol{i}}^{\alpha'}$ is used, where $\alpha' = \text{cyt}$. Vice–versa, if $\alpha = \text{cyt}$, then $\alpha' = \text{nuc}$. Using this definition, the boundary condition is approximated by choosing

$$\rho\,[p]_{\boldsymbol{i}}^{B_n} \equiv \rho\left(p_{\boldsymbol{i}}^{\alpha'} - p_{\boldsymbol{i}}^{\alpha}\right).$$

With all the flux terms specified, the final discretization is then

$$\frac{dp_{\boldsymbol{i}}^{\alpha}}{dt} = \frac{D}{V_{\boldsymbol{i}}^{\alpha} h}\left(\sum_{\pm}\sum_{k=1}^{d} A_{\boldsymbol{i}\pm\frac{1}{2}\boldsymbol{e}_k}^{\alpha}\left(p_{\boldsymbol{i}\pm\boldsymbol{e}_k}^{\alpha} - p_{\boldsymbol{i}}^{\alpha}\right)\right) + \frac{A_{\boldsymbol{i}}^{B_n}\rho}{V_{\boldsymbol{i}}^{\alpha}}\left(p_{\boldsymbol{i}}^{\alpha'} - p_{\boldsymbol{i}}^{\alpha}\right). \tag{3.5}$$

For cells that do not intersect any boundary the discretization reduces to the standard five(seven)–point discrete Laplacian in 2D(3D).

Defining the probability of the particle being in the domain $\alpha$ portion of the $\boldsymbol{i}$'th cell as

$$Q_{\boldsymbol{i}}^{\alpha}(t) = p_{\boldsymbol{i}}^{\alpha} V_{\boldsymbol{i}}^{\alpha} \approx \text{Prob}\{\boldsymbol{X}(t) \in V_{\boldsymbol{i}}^{\alpha} | \boldsymbol{X}(0) = \boldsymbol{x}_0\}, \tag{3.6}$$

the discretization can be rewritten as

$$\frac{dQ_{\boldsymbol{i}}^{\alpha}}{dt} = \frac{D}{h}\left(\sum_{\pm}\sum_{k=1}^{d} \frac{A_{\boldsymbol{i}\pm\frac{1}{2}\boldsymbol{e}_k}^{\alpha}}{V_{\boldsymbol{i}\pm\boldsymbol{e}_k}^{\alpha}} Q_{\boldsymbol{i}\pm\boldsymbol{e}_k}^{\alpha} - \frac{A_{\boldsymbol{i}\pm\boldsymbol{e}_k}^{\alpha}}{V_{\boldsymbol{i}}^{\alpha}} Q_{\boldsymbol{i}}^{\alpha}\right) + A_{\boldsymbol{i}}^{B_n}\rho\left(\frac{Q_{\boldsymbol{i}}^{\alpha'}}{V_{\boldsymbol{i}}^{\alpha'}} - \frac{Q_{\boldsymbol{i}}^{\alpha}}{V_{\boldsymbol{i}}^{\alpha}}\right). \tag{3.7}$$

The first term in (3.7) represents diffusive motion between computational cells, while the second represents motion across the nuclear membrane within one computational cell. Let the two components of a split computational cell be represented as separate computational cells. In this form, all movement between computational cells within the same domain is by diffusive jumps, while movement between computational cells of different domains is by jumps determined by the membrane fluxes. Despite the appearance of the membrane flux terms, this equation, with an appropriate index relabeling to account for the multiple components of a split computational cell, still has the same form as (2.12). Hence, all motion is still represented as first order reactions, with jump rates given by the coefficients of the $Q_{\{\cdot\}}^{\{\cdot\}}$ terms.

Taking $A^{\alpha}_{\boldsymbol{ij}}$ to be the area of the domain $\alpha$ face shared by cells $\boldsymbol{i}$ and $\boldsymbol{j}$, then the jump rate from the domain $\alpha$ component of cell $\boldsymbol{j}$ to the domain $\alpha$ component of cell $\boldsymbol{i}$ is:

$$k^{\alpha}_{\boldsymbol{ij}} = \frac{DA^{\alpha}_{\boldsymbol{ij}}}{hV^{\alpha}_{\boldsymbol{j}}}. \tag{3.8}$$

For strictly interior cells this reduces to

$$k^{\alpha}_{\boldsymbol{ij}} = \frac{D}{h^2}.$$

The jump rate across the nuclear membrane in cell $\boldsymbol{i}$, from domain $\alpha'$ to domain $\alpha$ is

$$k^{\alpha\alpha'}_{\boldsymbol{i}} = \frac{A^{B_n}_{\boldsymbol{i}}\rho}{V^{\alpha'}_{\boldsymbol{i}}}. \tag{3.9}$$

A similar equation holds for the jump from domain $\alpha$ to domain $\alpha'$. Note that $k^{\alpha}_{\boldsymbol{ij}}$ and $k^{\alpha}_{\boldsymbol{ji}}$ are unequal in general because $V^{\alpha}_{\boldsymbol{i}}$ may not be equal to $V^{\alpha}_{\boldsymbol{j}}$. Similarly, $k^{\alpha\alpha'}_{\boldsymbol{i}}$ and $k^{\alpha'\alpha}_{\boldsymbol{i}}$ will also differ as $V^{\alpha}_{\boldsymbol{i}}$ may not be equal to $V^{\alpha'}_{\boldsymbol{i}}$.

There is a fundamental difference in the scaling between equation (3.8), which scales like $1/h^2$, and (3.9), which scales like $1/h$. This difference arises because the flux for diffusive motion is proportional to the *gradient* of the density, while the flux across the nuclear membrane is proportional to the *difference* in the density across the membrane.

A consequence of the conservative discretization form is that total probability is conserved:

$$\sum_{\alpha}\sum_{\boldsymbol{i}\in\alpha}\frac{dQ^{\alpha}_{\boldsymbol{i}}}{dt} = \sum_{\alpha}\sum_{\boldsymbol{i}\in\alpha}\frac{dp^{\alpha}_{\boldsymbol{i}}}{dt}V^{\alpha}_{\boldsymbol{i}} = 0.$$

The master equation approximation will also satisfy the principle of detailed balance: the statement that at thermodynamic equilibrium the unidirectional probability flux from cell $\boldsymbol{i}$ to cell $\boldsymbol{j}$ is equal to the unidirectional probability flux

from cell $\boldsymbol{j}$ to cell $\boldsymbol{i}$. We expect detailed balance to hold, as (3.1) forms a closed and isolated system due to the no–flux cellular membrane condition and passive nuclear membrane flux (no active transport). Letting $p^{eq}(x,t) = p^{eq}$ be the constant equilibrium solution to the continuous problem, then $(Q^{eq})_{\boldsymbol{i}}^{\alpha} = p^{eq} V_{\boldsymbol{i}}^{\alpha}$ will be the equilibrium probability of the Brownian particle being in the domain $\alpha$ component of cell $\boldsymbol{i}$. For $A_{\boldsymbol{ij}}^{\alpha}$ the area of the domain $\alpha$ face between cells $\boldsymbol{i}$ and $\boldsymbol{j}$, the detailed balance condition is

$$\begin{aligned} & k_{\boldsymbol{ji}}^{\alpha}(Q^{eq})_{\boldsymbol{i}}^{\alpha} = k_{\boldsymbol{ij}}^{\alpha}(Q^{eq})_{\boldsymbol{j}}^{\alpha}, \\ \iff \quad & \frac{DA_{\boldsymbol{ij}}^{\alpha}}{hV_{\boldsymbol{i}}^{\alpha}}(Q^{eq})_{\boldsymbol{i}}^{\alpha} = \frac{DA_{\boldsymbol{ij}}^{\alpha}}{hV_{\boldsymbol{j}}^{\alpha}}(Q^{eq})_{\boldsymbol{j}}^{\alpha}, \\ \iff \quad & \frac{(Q^{eq})_{\boldsymbol{i}}^{\alpha}}{V_{\boldsymbol{i}}^{\alpha}} = \frac{(Q^{eq})_{\boldsymbol{j}}^{\alpha}}{V_{\boldsymbol{j}}^{\alpha}}, \end{aligned}$$

which holds by the definitions of $(Q^{eq})_{\boldsymbol{i}}^{\alpha}$ and $(Q^{eq})_{\boldsymbol{j}}^{\alpha}$. For jumps across a membrane between domains $\alpha$ and $\alpha'$,

$$\begin{aligned} & k_{\boldsymbol{i}}^{\alpha'\alpha}(Q^{eq})_{\boldsymbol{i}}^{\alpha} = k_{\boldsymbol{i}}^{\alpha\alpha'}(Q^{eq})_{\boldsymbol{i}}^{\alpha'}, \\ \iff \quad & \frac{A_{\boldsymbol{i}}^{B_n}\rho}{V_{\boldsymbol{i}}^{\alpha}}(Q^{eq})_{\boldsymbol{i}}^{\alpha} = \frac{A_{\boldsymbol{i}}^{B_n}\rho}{V_{\boldsymbol{i}}^{\alpha'}}(Q^{eq})_{\boldsymbol{i}}^{\alpha'}, \\ \iff \quad & \frac{(Q^{eq})_{\boldsymbol{i}}^{\alpha}}{V_{\boldsymbol{i}}^{\alpha}} = \frac{(Q^{eq})_{\boldsymbol{i}}^{\alpha'}}{V_{\boldsymbol{i}}^{\alpha'}}, \end{aligned}$$

which again holds by the definitions of $(Q^{eq})_{\boldsymbol{i}}^{\alpha}$ and $(Q^{eq})_{\boldsymbol{i}}^{\alpha'}$. Note that an active transport boundary condition at the cellular membrane could make the system open, in which case detailed balance would no longer be expected to hold. Moreover, an active transport mechanism at the nuclear membrane would also prevent the system from coming to thermodynamic equilibrium and would result in a steady state in which the above relationships across the nuclear membrane would be violated. This would not effect the rate constants for other (passive)

processes however, which would therefore still satisfy the conditions derived from the principle of detailed balance.

For comparison to our discretization, note that in [30] $(F_k)_{\boldsymbol{i}\pm\frac{1}{2}\boldsymbol{e}_k}$ is chosen to be the standard centered difference approximation when the $k$'th face does not intersect a boundary. This leads to the five(seven)–point Laplacian as the discretization for strictly interior cells. For faces cut by the boundary, [30] interpolates between the centered difference flux in neighboring cells to approximate the flux at the midpoint of the cut face. This method leads to a second order accurate approximation to the Laplacian, but does not give a valid master equation for the continuous time–discrete space discretization. To see why, note that the general form of the master equation for the probability, $Q_i$, of being at site $i$ with transition probability per unit time $W_{ji} \geqslant 0$, is given by (A.1). In general interpolation will introduce negative weights $W_{ji}$ or $W_{ij}$ into the $i$'th equation. Furthermore, interpolation violates the condition that if the $i$'th equation contains a term $W_{ij}Q_j$ then the $j$'th equation should contain a term $-W_{ij}Q_j$.

An alternative discretization method is presented in [18] that accounts for the boundary by using the standard five(seven)–point Laplacian at all locations and adding an extra forcing term. As the master equation has no forcing terms this method would not give an equation that could be realized by the Gillespie Method.

### 3.1.3 Overall Method

Using the discretization from the previous Section, realizations of the stochastic process described by the reaction–diffusion master equation can be created using

the Gillespie Method. The overall simulation algorithm is:

1. Initialization:

   (a) Given the membrane locations, calculate $A^{\alpha}_{\boldsymbol{i}\pm\boldsymbol{e}_k}$, $V^{\alpha}_{\boldsymbol{i}}$, and $A^{B_n}_{\boldsymbol{i}}$, for each location, $\boldsymbol{i}$, each direction, $\boldsymbol{e}_k$, and each domain, $\alpha$.

   (b) From equations (3.8) and (3.9) calculate the jump rates for all species, within all Cartesian cells containing some part of $\Omega$.

   (c) For each piece of a Cartesian cell, calculate the rates of all chemical reactions that can occur there. For reactions with volume dependent rates use $V^{\alpha}_{\boldsymbol{i}}$ to change the rate constants to units of reciprocal time.

2. Time Evolution:

   (a) Simulate individual realizations of the stochastic process described by the reaction–diffusion master equation using the Gillespie Method. Diffusive and transmembrane solute motion are represented as first order reactions, using the jump rates calculated in step (1b). Within each component of a cell, the rates from step (1c) are used to simulate chemical reactions.

3. Output:

   (a) To estimate moments or distributions, use statistics from many simulations.

### 3.1.4 Convergence of the Numerical Discretization

The convergence of the discretization provided by (3.5) is illustrated in 2D for both the Poisson equation and diffusion equation with circular boundaries. The method was found to converge between first and second order spatially. Let $(\boldsymbol{u}_h)_{\boldsymbol{i}}^{\alpha}$ denote the numerical solution to the Poisson problem, and $\boldsymbol{u}_h$ the vector whose components are given by $(\boldsymbol{u}_h)_{\boldsymbol{i}}^{\alpha}$. Define the maximum norm, $\|\boldsymbol{u}_h\|_\infty$, as

$$\|\boldsymbol{u}_h\|_\infty = \max_{\alpha,\boldsymbol{i}\in\alpha} |(\boldsymbol{u}_h)_{\boldsymbol{i}}^{\alpha}| .$$

A volume weighted two norm, $\|\boldsymbol{u}_h\|_2^w$, is defined as

$$\|\boldsymbol{u}_h\|_2^w = \left( \sum_{\alpha} \sum_{\boldsymbol{i}\in\alpha} ((\boldsymbol{u}_h)_{\boldsymbol{i}}^{\alpha})^2 \, V_{\boldsymbol{i}}^{\alpha} \right)^{\frac{1}{2}} .$$

Let $(\boldsymbol{u}_h^n)_{\boldsymbol{i}}^{\alpha}$ denote the numerical solution to the diffusion equation at time $t_n$, $\boldsymbol{u}_h^n$ the solution vector at time $t_n$, and $\boldsymbol{u}_h$ the solution over all spatial locations, domains, and times. The maximum norm over all time is defined as $\max_n \|\boldsymbol{u}_h^n\|_\infty$. As in Section 3.1.1, $\partial\Omega$ will denote the cell membrane, or outer boundary, while $\partial\Omega_n$ will denote the nuclear membrane, or inner boundary. In all of the examples considered in this section, the two boundaries are concentric circles with radii 1 and 1/2, respectively. The domain into which the circles are embedded is taken, for a given mesh width $h$, to be the square centered at the origin with sides of length $2 + 4h$. This provides a separation between the boundary of the computational domain, and the embedded boundaries.

Figure 3.2(a) shows the convergence of the discretization for the Poisson equation with just the outer boundary. The equations are

$$\begin{aligned} \Delta u &= f(\boldsymbol{x}), \quad \text{in } \Omega, \\ \frac{\partial u}{\partial \boldsymbol{\eta}} &= 0, \qquad \text{on } \partial\Omega, \end{aligned} \tag{3.10}$$

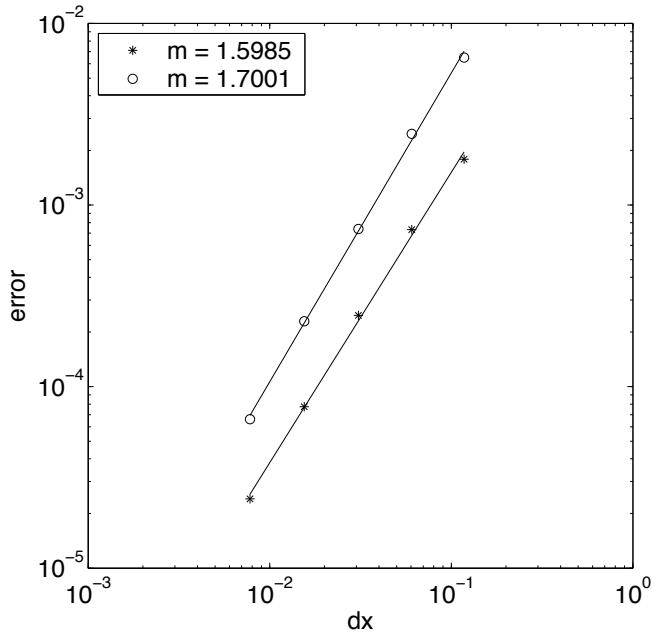


(a) Error for equation (3.10), with exact solution (3.11)

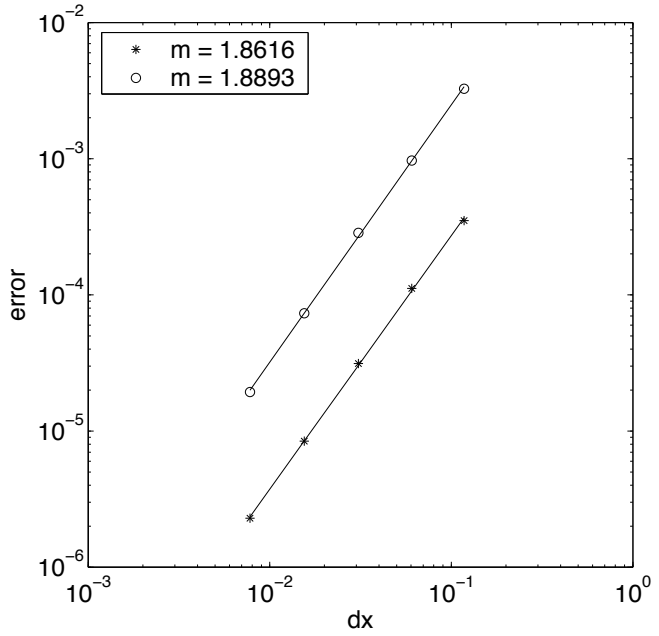


(b) Error for equation (3.10), with exact solution (3.12)

Figure 3.2: Continued on next page. See next page for legend.

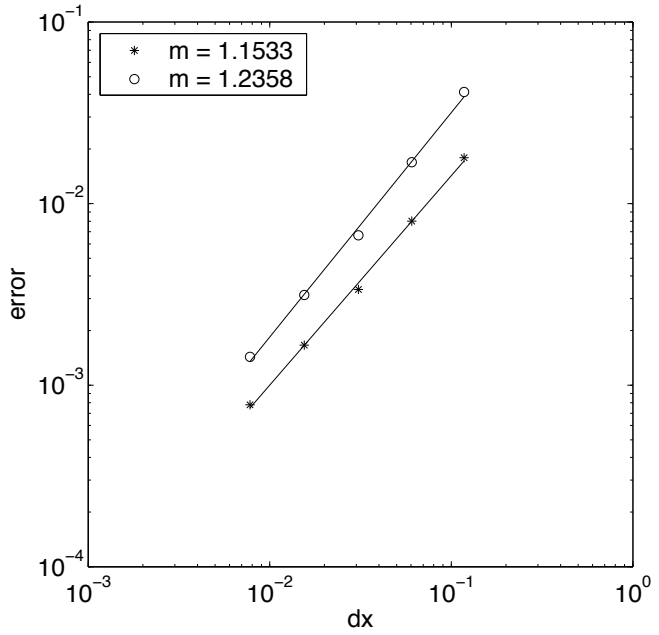


(c) Error for equation (3.13), with exact solution (3.14)

Figure 3.2: Convergence results for Poisson equation solutions; star is two norm error, and circle is maximum norm error. These errors are plotted against the mesh width $dx$ on log–log plots. The empirical order of accuracy is $m$, which is the slope of the best fit straight line in each case.

where $f(\boldsymbol{x})$ was chosen so that the exact solution was

$$u = \frac{r^4}{4} - \frac{r^3}{3}, \quad r \leq 1, \tag{3.11}$$

with $u = 0$ for $r > 1$. The two norm error converged at order 1.6, while the maximum norm error converged at order 1.7.

An angular dependence was added to $f(\boldsymbol{x})$ to give the exact solution

$$u = \left(\frac{r^4}{4} - \frac{r^3}{3}\right)\cos\theta, \quad r \leq 1, \tag{3.12}$$

with $u = 0$ for $r > 1$. Figure 3.2(b) shows the convergence of the errors for this problem. The $\theta$ dependence actually improves the convergence, so that the two norm error is order 1.86, while the maximum norm error now converges at order 1.89.

Figure 3.2(c) shows the convergence of the discretization for the Poisson equation with both boundaries. The equations are

$$\begin{aligned} \Delta u &= f(\boldsymbol{x}), && \text{in } \Omega, \\ \frac{\partial u}{\partial \boldsymbol{\eta}} &= 0, && \text{on } \partial\Omega, \\ -\frac{\partial u}{\partial \boldsymbol{\eta}} &= \pi \left[u\right]_n, && \text{on } \partial\Omega_n, \end{aligned} \tag{3.13}$$

where $f(\boldsymbol{x})$ was chosen so that the exact solution was

$$u = \begin{cases} \cos \pi r + \sin \pi r & \text{in } \Omega_n, \\ \cos \pi r & \text{in } \Omega \setminus \Omega_n, \\ 0 & \text{outside } \Omega. \end{cases} \tag{3.14}$$

The jump condition at the interior boundary reduces the order of convergence to 1.15 in the two norm, and 1.23 in the maximum norm.

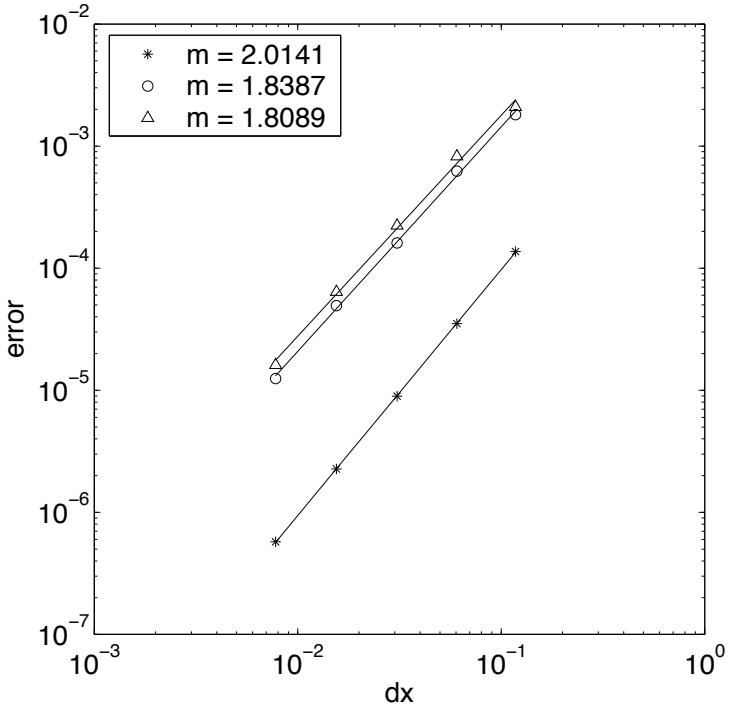


(a) Error for equation (3.15), with exact solution (3.16)

Figure 3.3: Continued on next page. See next page for Legend.

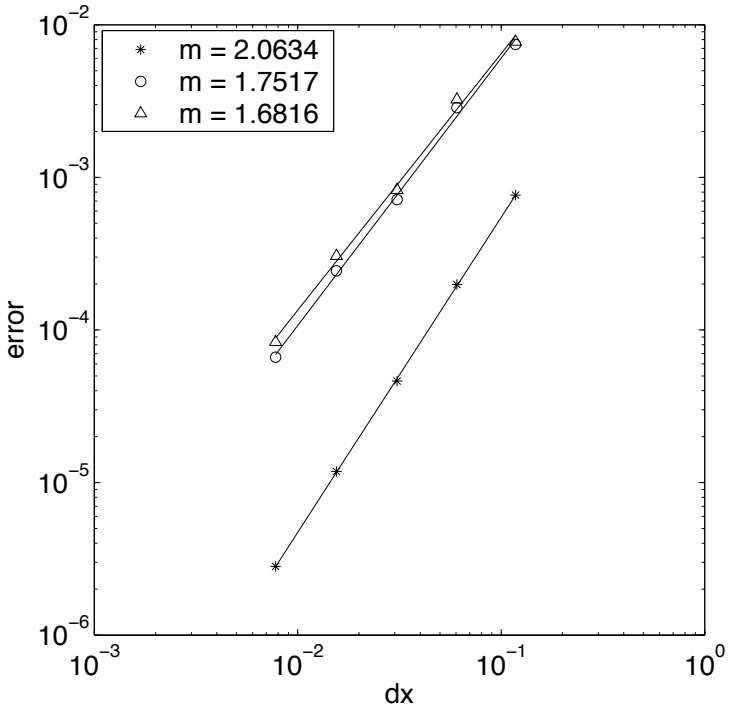


(b) Error for equation (3.17), with exact solution (3.18)

Figure 3.3: Convergence results for diffusion equation solutions; star is two norm error at $t_f$, circle is the maximum norm error at $t_f$, and diamond is the maximum of the maximum norm error over all time. These errors are plotted against the mesh width $dx$ on log–log plots. The empirical order of accuracy is $m$, which is the slope of the best fit straight line in each case.

Figure 3.3(a) shows the convergence of the discretization for the diffusion equation with just the exterior boundary. The final time, at which the two norm and maximum norm errors were measured was taken to be $t_f = .025$. At this time the solution was still far from equilibrium. $\Delta t/h$ was fixed at about $t_f/L$, where $L$ was the diameter of the outer boundary. For the examples in Figure 3.3, $\Delta t/h \approx .013$. The time integration was performed using the second order, $L_0$ stable, implicit Runge–Kutta method mentioned in [30]. Similar results were obtained for a Crank–Nicholson discretization. The equations are

$$\begin{aligned} \frac{\partial u}{\partial t} &= \Delta u + f(\boldsymbol{x}, t), \quad \text{in } \Omega, \\ \frac{\partial u}{\partial \boldsymbol{\eta}} &= 0, \qquad\qquad\quad \text{on } \partial\Omega, \end{aligned} \tag{3.15}$$

where $f(\boldsymbol{x})$ was chosen so that the exact solution was

$$u = \left( \frac{r^4}{4} - \frac{r^3}{3} \right) e^{-20t}, \quad r \leq 1, \tag{3.16}$$

with $u = 0$ for $r > 1$. At $t_f$, the two norm error converged at about order 2.01, and the maximum norm error converged at about order 1.84. The maximum over all time points of the maximum norm converged at about order 1.81.

Figure 3.3(b) shows the convergence of the discretization for the diffusion equation with both boundaries. Note that the same time discretization was used as above, again with $\Delta t/h \approx .013$. The equations are

$$\begin{aligned} \frac{\partial u}{\partial t} &= \Delta u + f(\boldsymbol{x}, t), \quad \text{in } \Omega, \\ \frac{\partial u}{\partial \boldsymbol{\eta}} &= 0, \qquad\qquad\quad \text{on } \partial\Omega, \\ -\frac{\partial u}{\partial \boldsymbol{\eta}} &= [u]_n, \qquad\qquad \text{on } \partial\Omega_n, \end{aligned} \tag{3.17}$$

where $f(\boldsymbol{x}, t)$ was chosen so that the exact solution was

$$u = \begin{cases} \left(\frac{br^4}{4} + \frac{ar^3}{3} + \frac{ar^5}{5}\right) e^{-20t} & \text{in } \Omega_n, \\ \left(\frac{r^3}{3} - \frac{r^4}{4}\right) e^{-20t} & \text{in } \Omega \setminus \Omega_n, \\ 0 & \text{outside } \Omega. \end{cases} \tag{3.18}$$

$a$ and $b$ were chosen to satisfy the jump boundary condition at $r = 1/2$. At $t_f$ the two norm error converged at about order 2.06, and the maximum norm error converged at about order 1.75. The maximum over all time points of the maximum norm converged at about order 1.68.

### 3.1.5 Convergence of the Overall Method

The overall method presented in Section 3.1.3 has two sources of error associated with it: sampling error, and error due to the spatial discretization. The Gillespie method provides exact realizations of the stochastic process defined by the reaction–diffusion master equation, hence the error in any individual realization is due solely to the spatial discretization. From the central limit theorem, for a fixed mesh size, we expect the error between the mean population levels from $N$ simulations and the means of the reaction–diffusion master equation, to be approximately $O(1/\sqrt{N})$. Note that the constant in the $O(1/\sqrt{N})$ term will depend on the mesh size. With a sufficient number of samples the joint probability distribution, for a fixed mesh size, can be estimated to any desired accuracy, but the required number of samples might be very large.

As an example, consider a single particle moving within a 2D biological cell. Assume the cell has a circular cellular membrane of radius 1, and a circular nuclear membrane of radius 1/2. The particle's dynamics are assumed to be

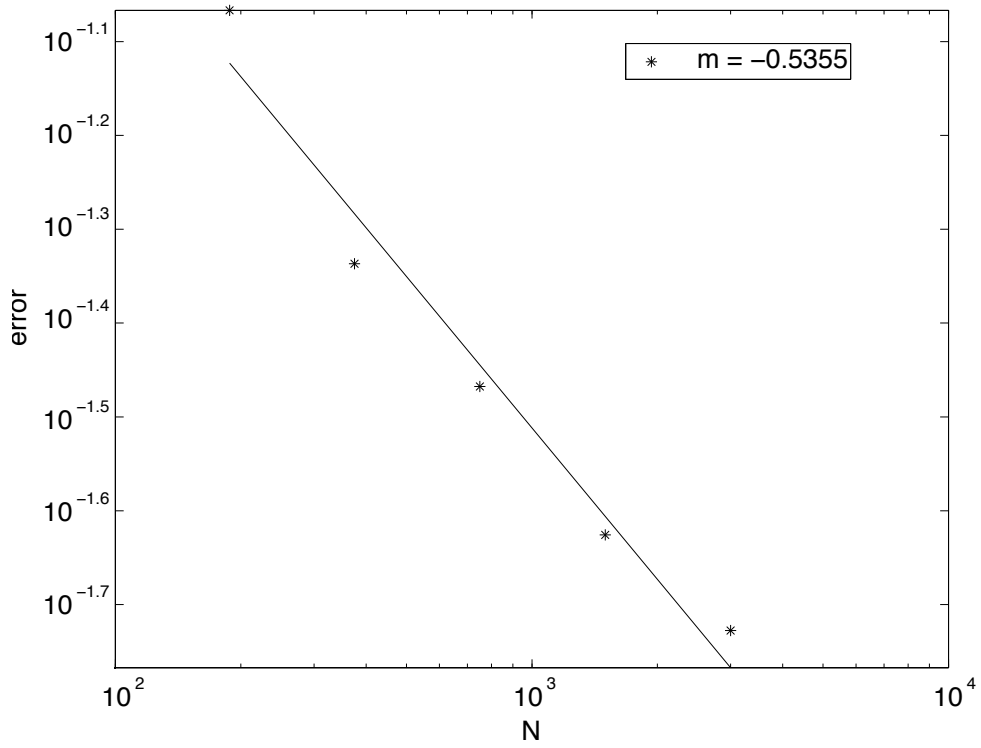


Figure 3.4: Convergence of the mean of Gillespie simulations to the numerical solution to (3.1). Here the error is given by the maximum absolute difference over all times and spatial locations between the Gillespie simulation estimate, and the numerical solution. A 37 by 37 mesh was used with mesh width 2/33, $D = 1$, and $\rho = 1$. The particle was started at the center of the domain for all simulations. $m$ gives the slope of the best fit line to the data.

given by (3.1), with $D = 1$ and $\rho = 1$. Since there is only one particle, the mean number of the particle in a given region is just the probability of the particle being in that region. As the reaction–diffusion master equation is in terms of the population levels of the particle at different locations, its mean should converge to the solution of (3.1) as $h$ goes to zero. Figure 3.4 shows the maximum error over all times between the mean of $N$ Gillespie simulations and the numerical solution to (3.1), as the number of samples is increased. Here $h$ is fixed at $2/33$, for a 37 by 37 mesh. Notice that the error decreases like $1/\sqrt{N}$.

Having obtained the distribution given by the reaction–diffusion master equation, there is still the question of how accurate a representation of the dynamics of the system it gives. It is not clear that the reaction–diffusion master equation has a well–defined continuum limit as $h$ goes to zero. Instead, it is generally considered valid only for a range of $h$ values, and there are several simultaneous physical conditions which $h$ should satisfy. First, $h$ should be significantly larger than the mean free path, $\lambda$, between the elastic collisions driving diffusion. This condition ensures that the system can be considered in local equilibrium within a computational cell because of many non–reactive collisions. Note, however, that to ensure that the system is accurately resolving local behavior, and also that the approximation of diffusion as jumps between cells is reasonable, $h$ should be significantly smaller than the length scale of the entire system, $L$. Summarizing these constraints,

$$L \gg h \gg \lambda.$$

As we now show, $h$ also needs to be chosen large enough (!) that the system can be considered in local equilibrium and well mixed within each mesh cell on the

time scale of the fastest bimolecular reactions. This assumption underlies the use of stochastic chemical kinetics independently within each mesh cell. For this to hold, the time scale for the particle to diffuse throughout a mesh cell should be much faster than the time scale for the fastest bimolecular chemical reaction. The time scale to diffuse throughout a region of length scale $h$ is approximately $h^2/D$. For a bimolecular reaction, the time scale with rate constant $k$ is $h^3/k$ for a mesh cell of volume $h^3$. (Recall that the units of the rate constant of a bimolecular reaction are volume per unit time.) Hence, it is necessary that,

$$\frac{h^3}{k} \gg \frac{h^2}{D},$$

which implies that,

$$h \gg \frac{k}{D}.$$

Thus, the rate constant for a bimolecular reaction places a fundamental lower limit on the spatial size of mesh cells. Fortunately, for cellular processes and the molecules involved in them, $k/D$ is generally not large enough to impose a significant restriction on $h$. In summary, letting $k$ denote the rate constant of the fastest bimolecular reaction, then

$$L \gg h \gg \max\left(\lambda, \frac{k}{D}\right).$$

In these inequalities $D$ is the diffusion coefficient of a particular molecular species and $k$ refers to the fastest bimolecular reaction in which that species participates. Such inequalities must hold simultaneously for all species under consideration. Note that a first order reaction does not restrict the mesh size in any manner since it generally represents an internal molecular event, and is not dependent on the system being well–mixed locally.

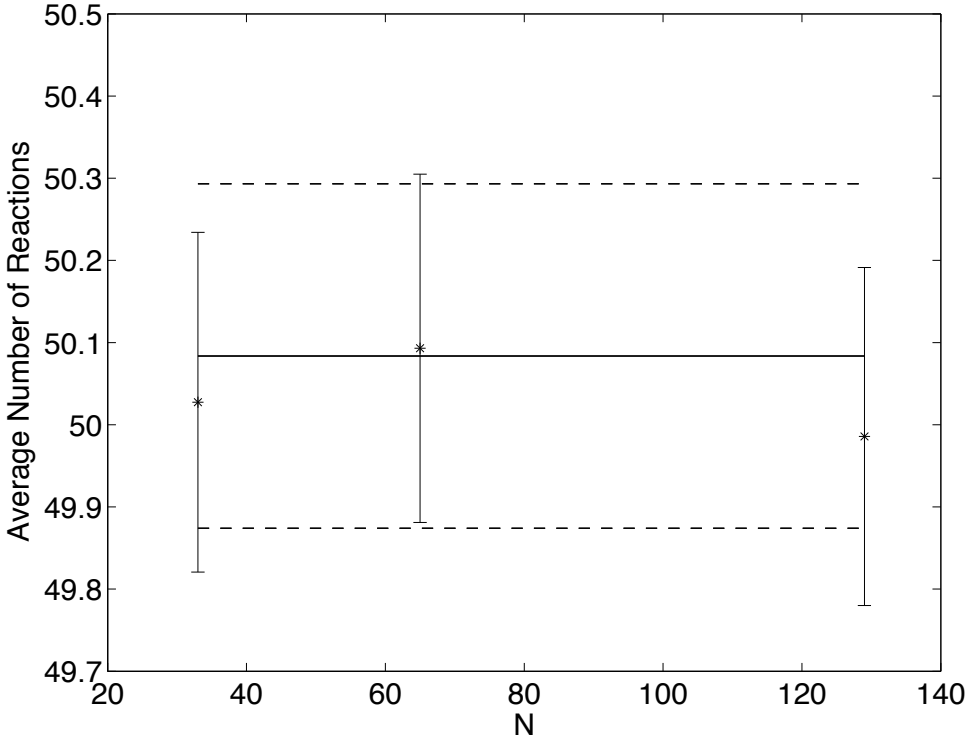


Figure 3.5: Average number of reactions in stochastic diffusion simulations, given by stars, compared to the exact solution for the expected number of reactions of the spatially homogeneous chemical master equation, solid straight line. Error bars give 99.7 percent confidence intervals about the data points. The error bars are calculated using the sampled variance. $N$ gives the number of mesh points in each direction. For each data point, 3000 sample realizations were used to calculate the average number of reactions. The dashed lines give the predicted 99.7 percent confidence interval, for 3000 samples, about the exact mean using the exact variance of the well–mixed master equation. Data is from $t = .1$, a time at which approximately half the $A$, and half the $B$ chemicals have been converted to $C$. Note the drastically expanded vertical scale.

As of yet, the reaction–diffusion master equation has not been derived from more microscopic physical models. Its validity has been verified numerically in [6] through comparison with microscopic hard sphere models that track individual particle positions and momenta. One might also hope that, for sufficiently fast diffusion, the results from the reaction–diffusion master equation applied to an initially well–mixed system would agree over a range of $h$ values with the spatially homogeneous chemical master equation. For example, consider the simple chemical reaction $A + B \to C$, within a 1 unit by 1 unit square. The exact solution, at any time, for the average number of reactions in the spatially homogeneous chemical master equation is given in [24]. This reduces the statistical error in the problem to that in estimating the average number of reactions from the reaction–diffusion master equation. 100 molecules of $A$ and 100 of $B$ are each started randomly distributed throughout the domain. No–flux boundary conditions were assumed for the diffusion of chemicals, but periodic boundary conditions were also tested with no significant impact on the results. With bimolecular rate constant, .0001, and a diffusion constant of 100 for each species, $k/D = .000001$. Hence, by the preceding arguments $h$ should only need to be greater than .000001 for the reaction–diffusion master equation to be valid. Figure 3.5 shows that as the number of mesh points, $N$, is increased, the average number of reactions from spatial simulations agrees with the exact number of reactions given by the spatially homogeneous chemical master equation to statistical error.

## 3.2 Determining Active Transport Jump Rates

We now return to the active transport model of Section 2.5 and derive expressions for the physical jump rates $\kappa_{ij}^l$. The same methodology as in the previous section is used, developing an embedded boundary discretization of equation (2.42) to obtain the rates. In the subsequent analysis we assume the reader is familiar with the notation of the previous section, particularly the geometrical mesh quantities defined in Figure 3.1. We begin by defining the active transport flux,

$$\boldsymbol{F}(\boldsymbol{x},t) = \rho(\boldsymbol{x},t)\,\boldsymbol{v}(\boldsymbol{x}).$$

As equation (2.42) is a conservation law, the analysis of equation (3.4) holds. For simplicity, we assume that particles can not move through membranes by active transport so that all membrane fluxes are zero. With this assumption, we find that

$$\frac{d\rho_{\boldsymbol{i}}^{\alpha}}{dt} \approx -\frac{1}{V_{\boldsymbol{i}}^{\alpha}}\left(\sum_{k=1}^{d}\left(A_{\boldsymbol{i}+\frac{1}{2}\boldsymbol{e}_k}^{\alpha}(F_k)_{\boldsymbol{i}+\frac{1}{2}\boldsymbol{e}_k}^{\alpha} - A_{\boldsymbol{i}-\frac{1}{2}\boldsymbol{e}_k}^{\alpha}(F_k)_{\boldsymbol{i}-\frac{1}{2}\boldsymbol{e}_k}^{\alpha}\right)\right). \tag{3.19}$$

Note, by definition the active transport flux satisfies

$$(F_k)_{\boldsymbol{i}\pm\frac{1}{2}\boldsymbol{e}_k}^{\alpha} = (\rho v_k)_{\boldsymbol{i}\pm\frac{1}{2}\boldsymbol{e}_k}^{\alpha},$$

where $v_k$ denotes the $k$'th component of $\boldsymbol{v}$. We approximate this term by upwinding, letting

$$(\rho v_k)_{\boldsymbol{i}\pm\frac{1}{2}\boldsymbol{e}_k}^{\alpha} = \rho_{\boldsymbol{i}\pm\frac{1}{2}\boldsymbol{e}_k-\frac{1}{2}\boldsymbol{e}_k}^{\alpha}\max\left(0,(v_k)_{\boldsymbol{i}\pm\frac{1}{2}\boldsymbol{e}_k}^{\alpha}\right) + \rho_{\boldsymbol{i}\pm\frac{1}{2}\boldsymbol{e}_k+\frac{1}{2}\boldsymbol{e}_k}^{\alpha}\min\left(0,(v_k)_{\boldsymbol{i}\pm\frac{1}{2}\boldsymbol{e}_k}^{\alpha}\right). \tag{3.20}$$

Rewriting equation (3.19) we then find

$$\frac{d\rho_{\boldsymbol{i}}^{\alpha}}{dt} \approx -\frac{1}{V_{\boldsymbol{i}}^{\alpha}} \sum_{\pm} \sum_{k=1}^{d} \pm \Bigg( A^{\alpha}_{\boldsymbol{i}\pm\frac{1}{2}\boldsymbol{e}_k} \Bigg[ \rho^{\alpha}_{\boldsymbol{i}\pm\frac{1}{2}\boldsymbol{e}_k - \frac{1}{2}\boldsymbol{e}_k} \max\left(0, (v_k)^{\alpha}_{\boldsymbol{i}\pm\frac{1}{2}\boldsymbol{e}_k}\right) + \rho^{\alpha}_{\boldsymbol{i}\pm\frac{1}{2}\boldsymbol{e}_k + \frac{1}{2}\boldsymbol{e}_k} \min\left(0, (v_k)^{\alpha}_{\boldsymbol{i}\pm\frac{1}{2}\boldsymbol{e}_k}\right) \Bigg] \Bigg). \quad (3.21)$$

Using equation (3.6), the probability of the particle being in the domain $\alpha$ component of the $\boldsymbol{i}$'th mesh cell, $Q_{\boldsymbol{i}}^{\alpha}$, is

$$\frac{dQ_{\boldsymbol{i}}^{\alpha}}{dt} = \sum_{\pm} \sum_{k=1}^{d} \pm \Bigg( \frac{A^{\alpha}_{\boldsymbol{i}\pm\frac{1}{2}\boldsymbol{e}_k}}{V^{\alpha}_{\boldsymbol{i}\pm\frac{1}{2}\boldsymbol{e}_k - \frac{1}{2}\boldsymbol{e}_k}} Q^{\alpha}_{\boldsymbol{i}\pm\frac{1}{2}\boldsymbol{e}_k - \frac{1}{2}\boldsymbol{e}_k} \max\left(0, (v_k)^{\alpha}_{\boldsymbol{i}\pm\frac{1}{2}\boldsymbol{e}_k}\right) + \frac{A^{\alpha}_{\boldsymbol{i}\pm\frac{1}{2}\boldsymbol{e}_k}}{V^{\alpha}_{\boldsymbol{i}\pm\frac{1}{2}\boldsymbol{e}_k + \frac{1}{2}\boldsymbol{e}_k}} Q^{\alpha}_{\boldsymbol{i}\pm\frac{1}{2}\boldsymbol{e}_k + \frac{1}{2}\boldsymbol{e}_k} \min\left(0, (v_k)^{\alpha}_{\boldsymbol{i}\pm\frac{1}{2}\boldsymbol{e}_k}\right) \Bigg).$$

This has the form of a master equation, and hence we find that the jump rate, $\kappa^{\alpha}_{\boldsymbol{i}+\boldsymbol{e}_k,\boldsymbol{i}}$, to go from the domain $\alpha$ component of the $\boldsymbol{i}$'th mesh cell to the neighboring mesh cell, $\boldsymbol{i} + \frac{1}{2}\boldsymbol{e}_k$, satisfies,

$$\kappa^{\alpha}_{\boldsymbol{i}+\boldsymbol{e}_k,\boldsymbol{i}} = \begin{cases} \dfrac{A^{\alpha}_{\boldsymbol{i}+\frac{1}{2}\boldsymbol{e}_k}}{V_{\boldsymbol{i}}} \left| (\boldsymbol{v}_k)^{\alpha}_{\boldsymbol{i}+\frac{1}{2}\boldsymbol{e}_k} \right|, & \text{if } (v_k)^{\alpha}_{\boldsymbol{i}+\frac{1}{2}\boldsymbol{e}_k} \geq 0, \\ 0, & \text{else.} \end{cases} \quad (3.22)$$

Likewise, the jump rate to the neighbor, $\boldsymbol{i} - \boldsymbol{e}_k$ satisfies

$$\kappa^{\alpha}_{\boldsymbol{i}-\boldsymbol{e}_k,\boldsymbol{i}} = \begin{cases} \dfrac{A^{\alpha}_{\boldsymbol{i}-\frac{1}{2}\boldsymbol{e}_k}}{V_{\boldsymbol{i}}} \left| (\boldsymbol{v}_k)^{\alpha}_{\boldsymbol{i}-\frac{1}{2}\boldsymbol{e}_k} \right|, & \text{if } (v_k)^{\alpha}_{\boldsymbol{i}-\frac{1}{2}\boldsymbol{e}_k} \leq 0, \\ 0, & \text{else.} \end{cases} \quad (3.23)$$

Note that both these jump rates scale like $\frac{1}{h}$, for mesh width $h$ (as opposed to the diffusive jump rates which scale like $\frac{1}{h}$). This is expected since active transport is being modeled as an advection process, and hence only involves one derivative of the density, $\rho(\boldsymbol{x}, t)$. With these choices of jump rates our overall discretization method will remain conservative.

# Chapter 4

# Application to Gene Expression

## 4.1 Transcription, Translation, Transport Model

As an application of the method presented in Section 3.1.3 we present a model of transcription, nuclear export, translation, and nuclear import in eukaryotes. While the model is simplified, and uses transcription and translation models that are more appropriate for a prokaryotes, it demonstrates the feasibility of the method in simulating biological networks. Section 4.1.1 describes the basic molecular cell biology necessary to understand the biochemical reaction model of Section 4.1.2. Section 4.1.3 shows the time evolution of one realization of the model.

### 4.1.1 Background Biology

The process by which a functional protein is produced from a segment of DNA that codes for it, called a gene, is a complex series of chemical events. In a coarsest description, the gene is first *transcribed* to produce a copy of itself called an mRNA. The mRNA is a linear sequence of nucleotides, every three of which comprise an element of a code representing an amino acid. The mRNA is then *translated* by special cellular machinery whereby the linear sequence of nucleotides are read, and the corresponding sequence of amino acids that the mRNA codes for are assembled. The polypeptide chain of amino acids typically undergoes further chemical and structural modifications to then form a functional protein.

For eukaryotes this situation is more complicated: transcription occurs in the nucleus and translation occurs in the cytoplasm of the cell. Between transcription and translation there is then an additional step that is required involving the movement of the mRNA out of the nucleus. This nuclear export process requires a series of chemical events; it can not occur simply through diffusion of the mRNA. Similarly, those proteins that influence gene expression must by imported into the nucleus to be effective.

Large protein complexes form pores in the nuclear membrane through which all trans–membrane traffic flows. These nuclear pore complexes are normally only wide enough for small molecules of less than 9 nanometers to pass through by free diffusion. Large molecules, such as mRNAs and most proteins, require the assistance of nuclear export and import receptors, which allow the pores effectively to dilate so that molecules of up to 26 nanometers can pass [1].

We shall be interested in the export of newly transcribed mRNA from the

nucleus, and the import of the resulting protein product back into the nucleus. These two pathways are believed to be distinct in the nuclear receptors used, and in the biasing factors that confer directionality to the process (so that, for example, newly exported mRNA does not get re–imported into the nucleus). Since the general mRNA export pathway is still unsettled, we shall use the same pathway for modeling mRNA export and protein import. This pathway is driven by a nuclear membrane RanGTP gradient that confers directionality to the movement of cargo across the membrane. A subset of the full RanGTP cycle model presented in [37] is used to account for the movement of receptors and their cargo. The RanGTP nuclear transport process is sometimes referred to as "active" because there is an energy expenditure in maintaining the gradient of RanGTP across the nuclear membrane. In contrast, the actual movement of cargo across the nuclear membrane is believed to be passive. Note that this pathway is used for the export of some mRNAs, for example, the export of incompletely spliced HIV mRNA encoding viral structural proteins [9].

The basic model presented in the next section is built on the pathway of transcription of one gene to produce mRNA, nuclear export of the mRNA, translation of the mRNA within the cytoplasm, and import of the resulting protein product back into the nucleus. Protein import plays an important role in many transcriptional networks, allowing the protein product of one gene to bind and regulate the expression of another. Several important steps in the transcription–translation cycle for eukaryotes are not modeled, including splicing, the opening of the chromatin to allow physical access to the gene, and the assembly of the transcription initiation complex.

### 4.1.2 Chemical Model

The eukaryotic cell is modeled in 2D as two concentric circles, representing the plasma and nuclear membranes. The plasma membrane radius is taken to be $11.81\,\mu$m, while the nuclear membrane radius is $5\,\mu$m. The transcription and translation models used are based on those presented in [12]. Specifically, the gene of interest has several states. $DNA$ denotes that the gene is free of RNA polymerase II, hereafter RNAP, the enzyme which reads the nucleotides comprising the gene and then incorporates the corresponding nucleoside triphospate into the growing mRNA transcript. $DNA^0$ will denote that the RNAP is bound to the gene's promoter and ready to begin transcription. $DNA^l$ will denote that the first $l$ of the nucleotides forming the gene have been read and incorporated into the mRNA, with $M$ giving the total number of nucleotides in the gene. Finally, the number of mRNA molecules within spatial computational cell $i$ is given by $mRNA_i$. For simplicity, the gene is assumed to be localized in the center of the nucleus, which will have index $i_{\text{center}}$. The concentration of both RNAP and the nucleoside triphospates that are added to the mRNA transcript are assumed fixed so that transitions between the different DNA states are first order reactions. With these definitions, the transcriptional reactions, all defined solely at the cell center, are then:

$$\begin{aligned} DNA &\rightarrow DNA^0, \\ DNA^{l-1} &\rightarrow DNA^l, \quad l = 1, \ldots, M-1, \\ DNA^{L-1} &\rightarrow mRNA_{i_{\text{center}}} + DNA. \end{aligned}$$

The rates for these reactions are respectively: $.05\,\text{s}^{-1}$, $30\,\text{s}^{-1}$, and $30\,\text{s}^{-1}$. The number of nucleotides in the gene, $M$, is chosen to be 999.

Newly transcribed mRNA is assumed to diffuse freely throughout the nucleus until entering the export pathway. The mRNA export model is based on the RanGTP export system. Denote by $NR$, the nuclear export receptor to which mRNA can bind, by $Rt$, RanGTP, by $Rd$, RanGDP, by $Rb$, RanBP1, and by $NR$–$Rt$, nuclear receptor complexed with RanGTP. All five are assumed to be at steady state concentrations, and uniformly distributed throughout the nucleus and cytoplasm. Note that the steady state concentrations are not assumed to be the same within the nucleus and cytoplasm, simply within each individually. Steady state concentrations and subsequent reaction rates were based on the data in [37]. The export process consists of three reactions, beginning with the binding of the export receptor–RanGTP complex to nuclear mRNA. Once this has occurred, the nuclear membrane is assumed to be permeable to the complex. At all locations within the cytoplasm the complex can then bind RanBP1, which subsequently induces the release of the mRNA from the complex. The reactions are:

$$\begin{aligned} mRNA_i + NR\text{–}Rt_i &\rightarrow mRNA\text{–}NR\text{–}Rt_i, && \text{within nucleus,} \\ mRNA\text{–}NR\text{–}Rt_i + Rb_i &\rightleftarrows mRNA\text{–}NR\text{–}Rt\text{–}Rb_i, && \text{within cytoplasm,} \\ mRNA\text{–}NR\text{–}Rt\text{–}Rb_i &\rightarrow mRNA_i + NR_i + Rb_i + Rd_i, && \text{within cytoplasm.} \end{aligned}$$

Using the assumption of constant concentrations, we can reduce these reactions to the following four:

$$\begin{aligned} mRNA_i &\rightarrow mRNA\text{–}NR\text{–}Rt_i, && \text{within nucleus,} \\ mRNA\text{–}NR\text{–}Rt_i &\rightleftarrows mRNA\text{–}NR\text{–}Rt\text{–}Rb_i, && \text{within cytoplasm,} \\ mRNA\text{–}NR\text{–}Rt\text{–}Rb_i &\rightarrow mRNA_i, && \text{within cytoplasm.} \end{aligned}$$

The rates for these reactions are respectively: $1184.5\,\mathrm{s}^{-1}$, $298.93\,\mathrm{s}^{-1}$ for the forward, $.5\,\mathrm{s}^{-1}$ for the reverse, and $51.19\,\mathrm{s}^{-1}$.

Once the mRNA is free within the cytoplasm, it can then associate with ribosomes, the molecular machines on which translation occurs. The ribosomes are assumed to be uniformly distributed throughout the cytoplasm as a constant background concentration. The translation process begins with the binding of a mRNA to a ribosome to form a complex that is ready to translate, denoted by $mRNA_i^0$. As the ribosomes are very large, it is assumed that the translation process is immobile. Translation then consists of a series of elongation steps by which the mRNA is moved through the ribosome, read, and each set of three nucleotides is translated into the appropriate amino acid. This amino acid is then added to the growing polypeptide that will become the protein. Let $mRNA^l$ denote that $l$ amino acids have been incorporated into the polypeptide chain, $l = 1, \ldots, N$, where $N = M/3$. Denote by $P$ protein. Assuming all amino acid concentrations are spatially homogeneous and at steady state, the translation process reduces to the following set of reactions:

$$\begin{aligned}
mRNA_i &\to mRNA_i^0, && \text{within cytoplasm,}\\
mRNA_i^{l-1} &\to mRNA_i^l, \quad l = 1, \ldots, N-1, && \text{within cytoplasm,}\\
mRNA_i^{N-1} &\to P_i + mRNA_i, && \text{within cytoplasm.}
\end{aligned}$$

The rates for these reactions are respectively: $.5\,\mathrm{s}^{-1}$, $33\,\mathrm{s}^{-1}$, and $33\,\mathrm{s}^{-1}$.

Protein may freely diffuse within both the nucleus and the cytoplasm, however, it may not freely cross the nuclear membrane. Instead, it uses the RanGTP nuclear import process to enter the nucleus. This process consists of two reactions: protein binding to nuclear import receptor within the cytoplasm, and

unbinding of protein from the receptor upon binding of RanGTP within the nucleus. The reactions are then:

$$\begin{aligned} P_i + NR_i &\rightarrow P\text{–}NR_i, && \text{within cytoplasm,} \\ P\text{–}NR_i + Rt_i &\rightarrow P_i + NR\text{–}Rt_i, && \text{within nucleus.} \end{aligned}$$

Using the constant concentration assumption, these reactions can be reduced to the following first order reactions:

$$\begin{aligned} P_i &\rightarrow P\text{–}NR_i, && \text{within cytoplasm,} \\ P\text{–}NR_i &\rightarrow P_i, && \text{within nucleus.} \end{aligned}$$

The rate for these reactions are respectively: $1218.25\,\mathrm{s}^{-1}$, and $1.23\,\mathrm{s}^{-1}$.

A feedback mechanism is incorporated into the model by allowing the protein to repress the expression of its own gene. Denoting by $DNA_{\mathrm{rep}}$ the repressed state of the gene, the reactions are

$$DNA + P_{i_{center}} \rightleftarrows DNA_{\mathrm{rep}}$$

Here the forward reaction rate is, $.01\,\mu\mathrm{m}^3\mathrm{s}^{-1}$, and the reverse rate is $.01\,\mathrm{s}^{-1}$.

Finally, mRNA is assumed to be able to be degraded within the cytoplasm with rate $.2\,\mathrm{s}^{-1}$, and protein anywhere with rate $.0025\,\mathrm{s}^{-1}$. Table 4.1 gives the diffusion and nuclear membrane permeability rates for the different species in the model. Note that because of the finite diffusion coefficients, this model will give different statistics than the corresponding well-mixed model. For example, in the nuclear export model the time for an mRNA–nuclear export receptor complex to diffuse throughout the nucleus is approximately

$$\frac{r_{\mathrm{nuc}}^2}{D} = 250 \text{ s.}$$

| Species | $D$ $\mu\mathrm{m}^2\,\mathrm{s}^{-1}$ | $\rho$ $\mu\mathrm{m}\,\mathrm{s}^{-1}$ |
|---|---|---|
| $mRNA$ | .1 | 0 |
| $mRNA^l$ | 0 | 0 |
| $mRNA$–$NR$–$Rt$ | .1 | .17 |
| $mRNA$–$NR$–$Rt$–$Rb$ | .1 | 0 |
| $P$ | 20.0 | 0 |
| $P$–$NR$ | 20.0 | 1.87 |

Table 4.1: Diffusion constant, $D$, and nuclear membrane permeability, $\rho$, for each species.

In contrast, the time scale for that complex to leave the nucleus in the well-mixed model would be approximately

$$\frac{\frac{4}{3}\pi r_{\mathrm{nuc}}^3}{4\pi r_{\mathrm{nuc}}^2\,\rho} = 9.8 \text{ s}.$$

With the assumed biological constants the two step export process, finding the nuclear membrane and then passing through it, is strongly diffusion limited. Therefore, a well–mixed model with infinitely fast diffusion would ignore the long time scale for an export complex to *find* the nuclear membrane, much less to get through it. This would result in a substantially faster export process than biologically occurs.

### 4.1.3 Numerical Results

Figures 4.1 and 4.2 show the time evolution of one realization of the model described in the previous section, using an underlying 37 by 37 Cartesian mesh with a mesh width of approximately .72 microns. Within the simulations we

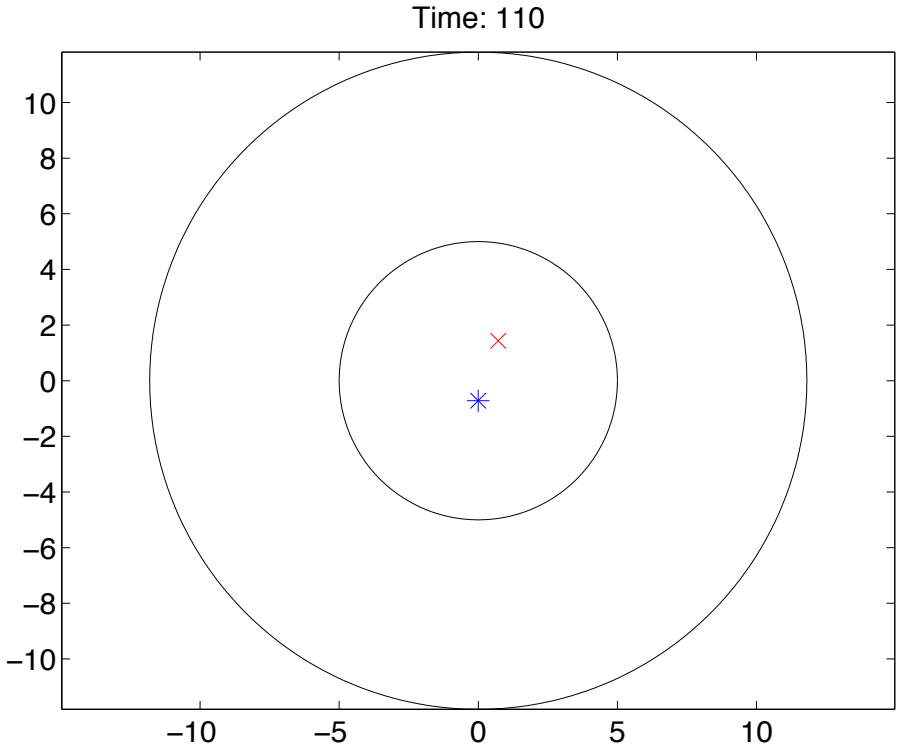


(a)

Figure 4.1: Continued on next page.

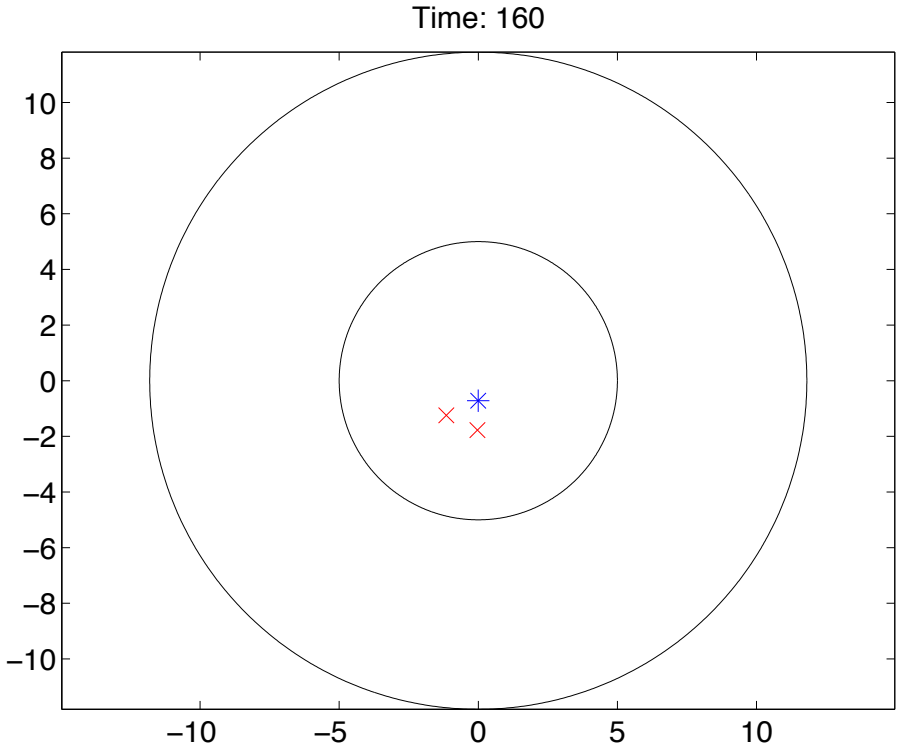


(b)

Figure 4.1: Continued on next page.

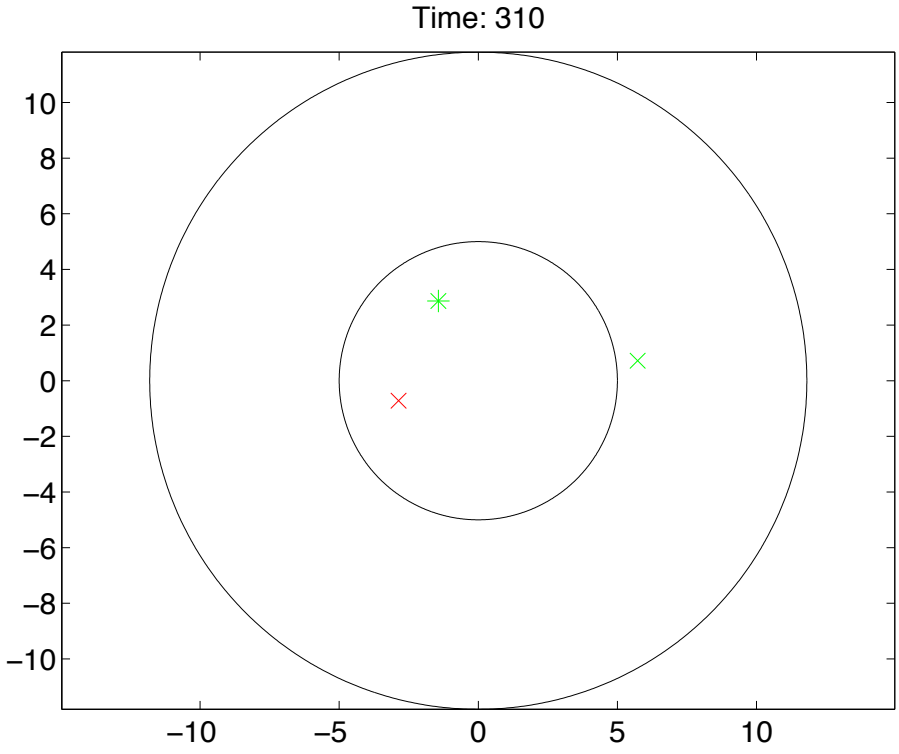


(c)

Figure 4.1: Continued on next page.

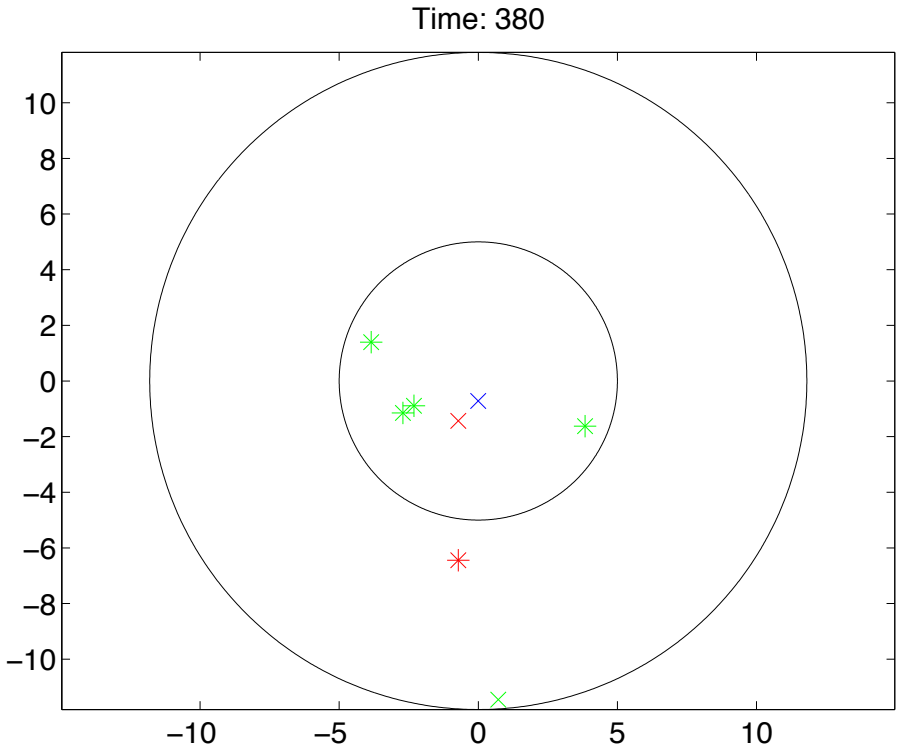


(d)

Figure 4.1: Evolution of one realization of the model from Section 4.1.2 over several minutes. A blue star denotes the unbound DNA, and a blue "x" that the DNA is repressed. During transcriptional states the DNA is not displayed. Red stars denote mRNA, and red "x's" mRNA bound to nuclear receptor and RanGTP. mRNAs coupled to nuclear receptors, RanGTP, and RanBP1 are not present in the images shown. During translation mRNAs are not displayed. Green stars denote proteins, and a green "x" represents protein bound to nuclear receptor. Time is in seconds.

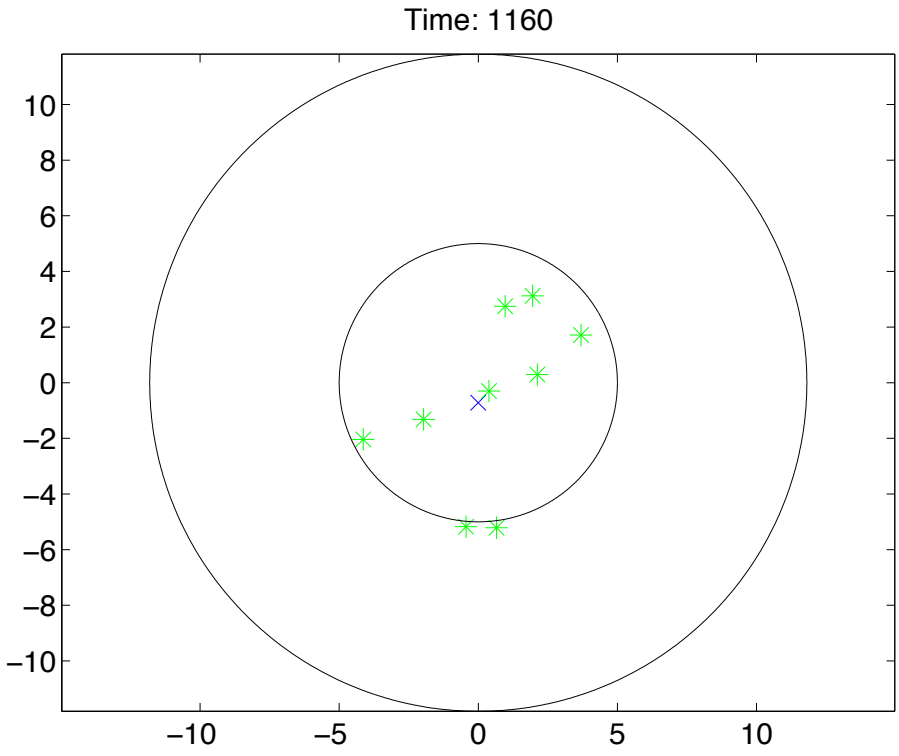


(a)

Figure 4.2: Continued on next page.

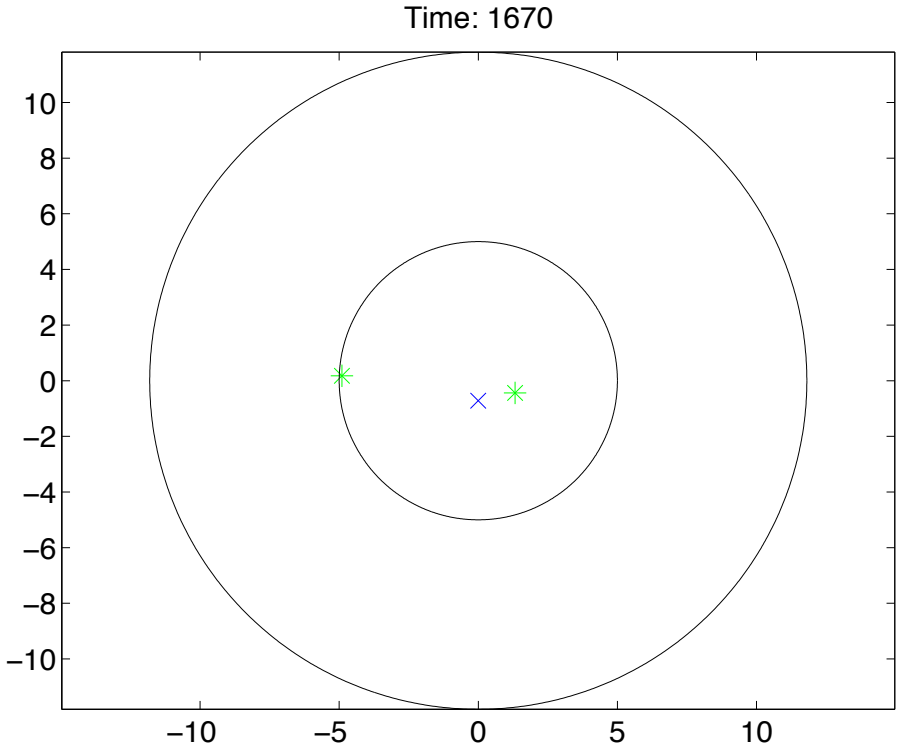


(b)

Figure 4.2: Continued on next page.

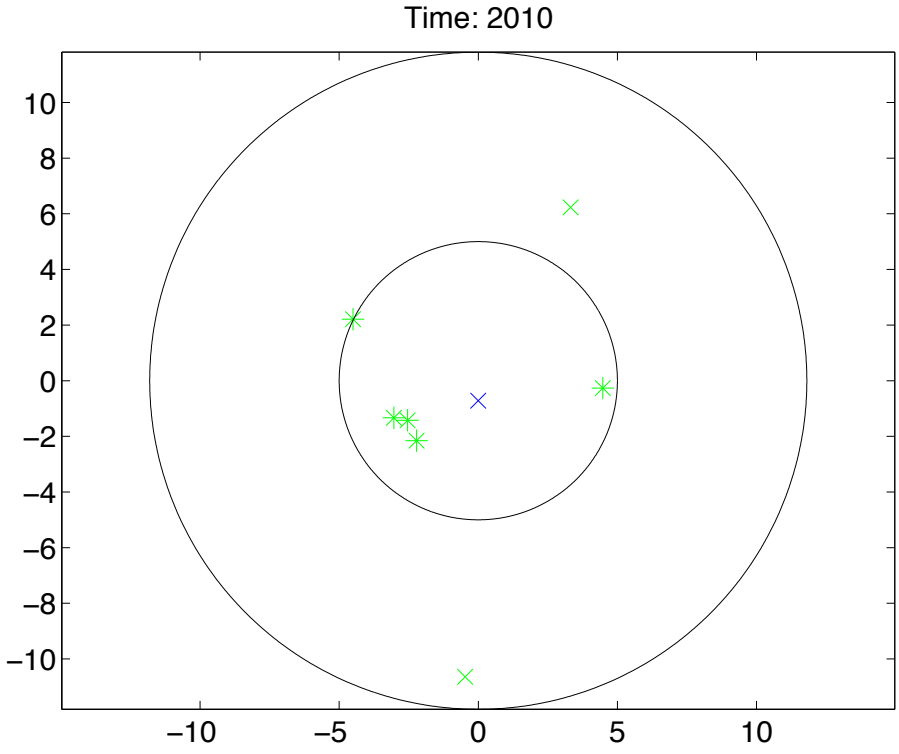


(c)

Figure 4.2: Continued on next page.

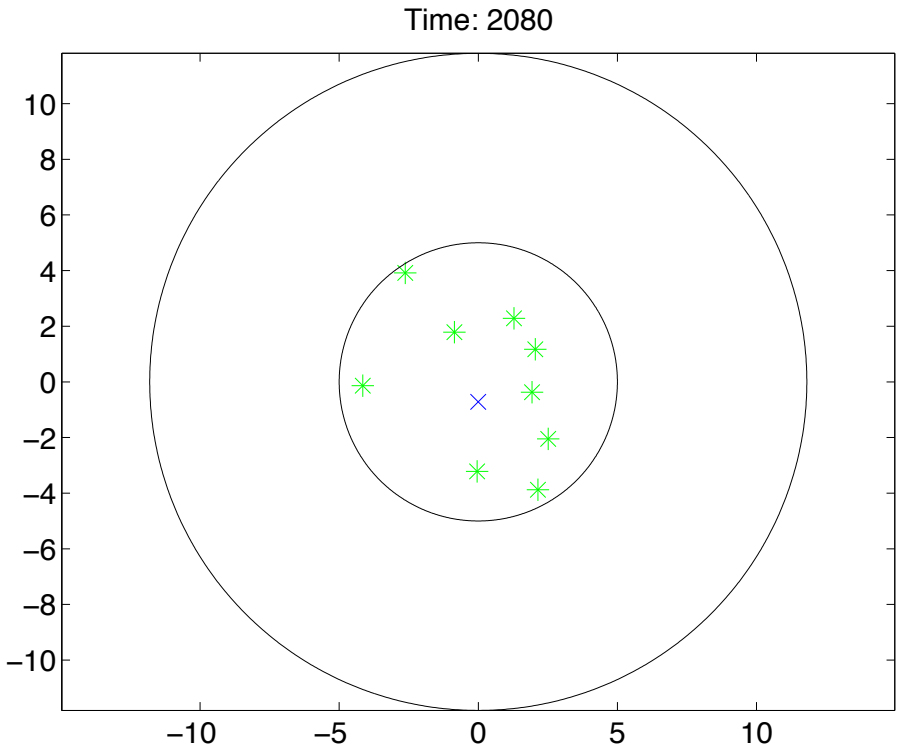


(d)

Figure 4.2: Evolution of one realization of the model from Section 4.1.2 over a half hour. Symbols have the same codes as in Figure 4.1.

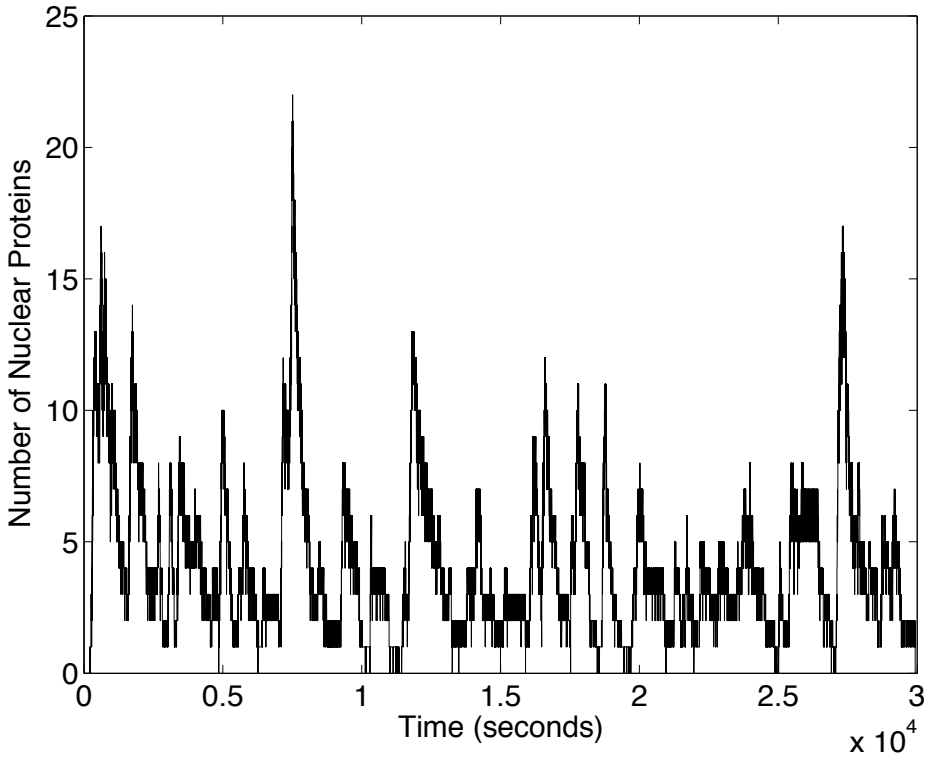


Figure 4.3: Total number of nuclear proteins in one realization of the model from Section 4.1.2. Simulation occurred over 30,000 seconds, with data points at one second intervals.

calculate the number of molecules of each chemical species within each mesh cell. We assume that *within* each individual mesh cell particles are well–mixed, and as such the marker for every molecule in each figure is placed randomly within the mesh cell containing that molecule. Initially there are no mRNAs or proteins within the system, and the DNA is in the unbound state. Figure 4.1 shows the evolution of the system over several minutes. By Figure 4.1(a) the first mRNA has been fully transcribed and, because of the fast binding rate, is bound to a nuclear export receptor. The DNA is unbound, waiting for the next transcription cycle to begin. After 160 seconds, a second mRNA has been transcribed and bound with a nuclear receptor. The DNA is again unbound. By 310 seconds several proteins have been translated. One is diffusing within the cytoplasm bound to a nuclear receptor, while the other has already undergone the nuclear import process and is diffusing freely within the nucleus. Notice there is only one visible mRNA, as the second is undergoing translation within the cytoplasm and hence not displayed. The DNA is also not visible as it is undergoing transcription. Finally, after 380 seconds, several proteins have accumulated within the nucleus, with one binding to and inhibiting the DNA. A free mRNA is diffusing within the cytoplasm, along with a nuclear receptor coupled protein.

By allowing the protein to feed back and inhibit the transcription of its gene, we create a system in which protein production occurs in bursts. Figure 4.2 shows that a large amount of protein is built up in the nucleus by 1160 seconds, and that the DNA is in the repressed state. The higher protein levels increase the probability of the gene becoming repressed, and because the on rate for binding is sufficiently fast, and the off rate sufficiently slow, by 1670

seconds the overall protein population has shrunk from 10 to just 2. This is due in part to the fast decay rates of the mRNA. As the DNA is repressed, no mRNAs are transcribed to replace those that quickly decay, and hence the protein population simply decays away over time. Once the protein population becomes sufficiently low, as in Figure 4.2(b), it becomes more unlikely that protein will find the DNA to bind and repress it, and hence, the DNA is able to enter the transcription cycle. By 2010 seconds at least one mRNA has been transcribed and subsequently translated several times, as the nuclear protein level has increased. The production of mRNA followed by its subsequent translation produces new proteins, and consequently the nuclear protein population rises thereafter. By 2080 seconds, 10 protein molecules are within the nucleus.

Figure 4.3 shows the total number of nuclear proteins in one realization, over 30,000 seconds. The total number is given by the amount of free, receptor–bound, and DNA–bound proteins within the nucleus at a fixed time. Note that the number of proteins tends to quickly jump up to a given amount, and then more slowly decay to either one or zero proteins. When only one protein is present for large periods of time, it is usually bound to the DNA, thereby repressing the gene (data not shown).

# Chapter 5

# The Three–Dimensional Point Binding Interaction

In Chapter 4 a model for transcription, translation, and nuclear transport was presented. In the model, the protein product of the expressed gene could rebind to a regulatory region controlling the gene's promoter and negatively inhibit further transcription. In this bound state the protein then prevented transcription from initiating. This binding interaction was modeled by assuming that both the gene and the regulatory region were isolated within the same mesh cell. As the reaction–diffusion master equation model assumes that particles are well–mixed locally, this implied that the binding interaction occurred through the same mechanism as a normal bimolecular reaction, but only within the specified mesh cell containing the gene. It is not clear if the solution to this model will converge in the continuum limit as the numerical mesh size is reduced to zero. We therefore investigate in this chapter whether this point binding model converges as the numerical mesh size is reduced. While convergence of the

reaction–diffusion master equation for the point binding interaction is not necessary to create useful models involving point binding reactions, it is a desirable property. (For example, one could always *try* to fit kinetic parameters to achieve desired results for a particular mesh size, however, there is no guarantee that this approach would always work).

Another reason to study the 3D point binding reaction is its strong relation to the binding of diffusing molecules. For example, consider the reaction A + B $\rightarrow$ C at rate $k$, with one initial molecule of A and one initial molecule of B. Assume that the domain in which the particles are diffusing is all of $\mathbb{R}^3$. In the Fock Space formulation of Section 2.4.4, we then find that the probability the particle of species A is in mesh cell $\boldsymbol{i}$ and the particle of species B is in mesh cell $\boldsymbol{i}'$, $F^{(1,1,0)}(\boldsymbol{i}, \boldsymbol{i}', t)$, satisfies

$$\frac{dF^{(1,1,0)}}{dt}(\boldsymbol{i}, \boldsymbol{i}', t) = \Big( \left[ D^{\mathrm{A}} \Delta_h^a + D^{\mathrm{B}} \Delta_h^b \right] F^{(1,1,0)} \Big)(\boldsymbol{i}, \boldsymbol{i}', t) - \frac{k}{h^3} \delta_{\boldsymbol{i}\boldsymbol{i}'} F^{(1,1,0)}(\boldsymbol{i}, \boldsymbol{i}', t). \tag{5.1}$$

Here $\Delta_h^a$ denotes the standard second order discrete Laplacian acting on the coordinates of the A particle, and $\Delta_h^b$ denotes the discrete Laplacian acting on the coordinates of the species B particle. Coupled to this equation there would be a second equation describing the motion of the species C particle, once the reaction has occurred. $F^0(\boldsymbol{i}, t)$, the probability for the species C particle to be in the $\boldsymbol{i}$'th mesh cell, satisfies

$$\frac{dF^0}{dt}(\boldsymbol{i}, t) = \left( D^{\mathrm{C}} \Delta_h^c F^0 \right)(\boldsymbol{i}, t) + \frac{k}{h^3} F^{(1,1,0)}(\boldsymbol{i}, \boldsymbol{i}, t).$$

We now consider the separation vector, $\boldsymbol{i} - \boldsymbol{i}'$, for the two particles of species

A and B. Define the probability of the separation vector having the value $\boldsymbol{j}$,

$$\begin{aligned} P(\boldsymbol{j},t) &= \sum_{\boldsymbol{i}-\boldsymbol{i}'=\boldsymbol{j}} F^{(1,1,0)}(\boldsymbol{i},\boldsymbol{i}'), \\ &= \sum_{\boldsymbol{i}\in R^3} F^{(1,1,0)}(\boldsymbol{i},\boldsymbol{i}-\boldsymbol{j}). \end{aligned}$$

Let $\mathbf{0}$ denote the zero vector. We do not show here, but one can derive from equation (5.1) that $P(\boldsymbol{j},t)$ satisfies

$$\frac{dP}{dt}(\boldsymbol{j},t) = (D\Delta_h P)(\boldsymbol{j},t) - \frac{k}{h^3}\delta_{\boldsymbol{j}\mathbf{0}} P(\boldsymbol{j},t), \tag{5.2}$$

where $D = D^{\mathrm{A}} + D^{\mathrm{B}}$. Note that this equation is the same as the Fock Space formulation that would correspond to a reaction–diffusion master equation model for the binding of *single* diffusing particle to a *fixed* binding site at the origin.

The notion of a true continuum 3D point binding interaction, which we might hope the reaction–diffusion master equation point binding model provides an approximation to, is problematic. In both a continuum formulation, and for fine enough mesh sizes in the discrete master equation model, when the number of diffusing substrate molecules is small the probability of any one actually finding and binding to the target location is low. We therefore discuss several different ways to model, and regularize, the continuum 3D point binding interaction in Section 5.1. Note that the reaction–diffusion master equation model already contains such a regularization by allowing binding to occur as a well–mixed reaction once a substrate molecule is within the mesh cell containing the target site. Several regularized models of the interaction in continuous, three–dimensional space are discussed. In Section 5.2 we study the existence of a continuum limit for equation (5.2). We conclude in Section 5.3 by investigating the convergence of a discrete approximation of the continuum point binding

model developed in [34]. The specific discrete model considered has the benefit of being a master equation, and hence could be incorporated directly into the reaction–diffusion master equation formulation.

## 5.1 Continuum Point Binding Models

There are a number of different methods by which the binding of a diffusing molecule in three–dimensional space to a small fixed location can be modeled in continuous space formulations. One common technique involves regularizing the problem through the addition of a finite binding radius about the target point. This changes the problem to that of binding to a 2D surface in 3D. Such formulations can then be numerically simulated through Langevin type simulations, however, due to the small size of the binding target it remains difficult for diffusing particles to ever encounter the binding radius. Another similar method is the use of an interaction potential with small support to represent the reaction. This type of method again suffers from the difficultly of the diffusing particle ever encountering the region in which the potential is defined. Both of these mechanisms have been used by other modelers, see for example [3]. Note that one other drawback to each of these methods is the introduction of new parameters to the original reaction–diffusion problem. For example, both methods require the introduction of reaction–radii to describe the extent of the binding surface, or support of the potential. Moreover, the numerical implementation of these types of models can often become complex, requiring methods for detecting particle–target encounters, and detecting particle–geometry collisions.

Alternatively, it is possible to formulate a continuum point binding interac-

tion using the differential operator

$$D\Delta - k\delta(\boldsymbol{x} - \boldsymbol{x}_0),$$

where the target point is taken to be at $\boldsymbol{x}_0$. This operator can be defined rigorously, see [2]. The probability density, $\rho(\boldsymbol{x}, t)$, for the diffusing particle to be at the point $\boldsymbol{x}$ then satisfies

$$\frac{\partial \rho}{\partial t}(\boldsymbol{x}, t) = D\Delta\rho(\boldsymbol{x}, t) - k\delta(\boldsymbol{x} - \boldsymbol{x}_0)\rho(\boldsymbol{x}, t). \tag{5.3}$$

Equation (5.3) has also been given a rigorous mathematical meaning, see for example [10]. We note that the formal continuum limit taken in Section 2.4.4 would give (5.3) as the limit of equation (5.2), however, this formal limit may not necessarily be correct.

The three preceding point binding models all have the draw back of having a small interaction radius for binding to the target point. In practical terms, discrete approximations to these equations would appear to either require very fine computational meshes, with mesh sizes *smaller* than the scale of the interaction radius, or require special techniques to account for the binding interaction. In [3], where no spatial mesh is used, binding radii are increased from probable physical sizes, and instead chosen such that well–mixed equilibrium binding rates are recovered.

One method for avoiding the problem of a small interaction radius is to take advantage of the biology of the binding interaction. For example, consider the previously mentioned model of gene expression developed in Chapter 4. There, binding of gene regulatory proteins to regulator sites on DNA was represented as a point binding reaction. In actuality, the exact mechanism by which regulatory proteins bind specific sites on DNA is unknown. DNA itself is a one-dimensional

object when considered on the scale of the entire nucleus, however, DNA is wound up and surrounded by many bound proteins forming a large intertwined complex known as chromatin. The chromatin forms more three–dimensional like structure than isolated DNA. A number of authors, see for example [28] and [43], have studied the DNA binding problem, both experimentally and through modeling, but as of yet no definitive theory has been developed. Some models propose that regulatory site binding involves nonspecific binding of regulators to DNA, along which the regulators can then diffuse/slide to locate specific binding sites. Whether such a mechanism is physically possible is questionable because of the large number of occluding objects comprising the chromatin. Other models rely on the existence of measured interaction potentials for specific binding sites, however, these potentials are often fairly short range [28], and would not appear to eliminate the problem of how a single diffusing particle can locate and bind a specific point. Note that one mechanism that can reduce the singularity of binding a specific point is the existence of a large density of binding particles. Biologically, it may be that most regulatory proteins are simply present in a sufficiently large number to eliminate the singularity of the problem.

In Section 5.3 we describe another continuum model for this specific binding problem. We essentially assume that the diffusing regulatory molecule can bind to the surface of the chromatin, and diffuse within this surface until binding to an unfolded one–dimensional piece of DNA. Once bound to the DNA, the molecule can diffuse until reaching the binding site, or can unbind back to the chromatin. The exact model considered is an idealization of this biological model, due to Charles S. Peskin [34]. One benefit of this approach is

the elimination of the short scale binding interaction and associated reaction–radii parameters. This allows the use of numerical meshes with length scales of the same order as those in Chapter 4. The model does have the drawback of requiring additional binding parameters for attachment to chromatin and DNA. Diffusion constants for movement within the chromatin and DNA are also required. A beneficial feature of this continuum model is that it can be approximated by a convergent spatial discretization that has the form of a master equation. This allows the incorporation of the model into the reaction–diffusion master equation formulation.

## 5.2 Continuum Limit of a Point Binding Model

We now numerically examine the behavior of equation (5.2) as $h \to 0$. As we shall see, ascertaining the existence of a continuum limit to this equation appears to require a more sophisticated analysis than the simple convergence study based on numerically refining the computational mesh presented here. The domain in which we solve (5.2) is taken to be the three–dimensional periodic cube, $\Omega = [0, L)^3$. To make explicit the dependence of the numerical solution on $h$, we denote the solution to this equation, at the location $(i, j, k)$ at time $t$, by $(P_h)_{ijk}(t)$. In all numerical simulations within this section we use biologically relevant rate constants, taking the diffusion constant, $D = 10\,\mu\mathrm{m}^2\,\mathrm{s}^{-1}$, and the length of the periodic domain, $L = 24\,\mu\mathrm{m}$. The binding rate to the point binding site is taken to be $k = 1\,\mu\mathrm{m}^3\,\mathrm{s}^{-1}$. For each simulation, the diffusing substrate particle is started at the origin, and therefore a discrete approximation to the

delta function is used as the initial condition. The approximation chosen is that

$$(P_h)_{ijk}(0) = \frac{1}{h^3}\delta_{i0}\,\delta_{j0}\,\delta_{k0}.$$

The point binding site is placed at $\boldsymbol{x}_0 = (12, 0, 0)\,\mu$m. All simulations use $N = 33 \times 3^M$ mesh points, for $M = 0$, 1, or 2. Note that this corresponds to refining the mesh width by factors of 3. This choice insures that the mesh cell containing the binding site remains centered at $(12, 0, 0)$. It also ensures that a region represented by a fixed collection of mesh cells on the coarsest mesh can be exactly represented by a collection of mesh cells on any finer mesh. This allows the calculation of the probability of the particle being in specific regions at a fixed time, over a range of mesh widths. One disadvantage of this setup is that the cell center of the mesh cell initially containing the particle changes as the mesh is refined. This condition, along with the choice of delta function approximation, leads to reduced first order convergence of the numerical solutions to (5.2) for standard diffusion, $k = 0$. (See Table 5.2).

For each simulation, time integration was performed using the Crank–Nicholson like, second order $L_0$–stable method of [39]. All simulations were run to a final time of .42 s, with

$$dt = \frac{.42}{300 \times 3^m},$$

where $m = 0$ when $N = 33$, $m = 1$ when $N = 99$, and $m = 2$ when $N = 297$.

Finally, denote by $\Lambda^{N\leftarrow 3N}$ the averaging operator that maps a mesh function on a $(3N)^3$ mesh to a mesh function on a $N^3$ mesh. $\Lambda^{N\leftarrow 3N}$ is defined by

$$(\Lambda^{N\leftarrow 3N} P_{h/3})_{ijk} = \frac{1}{27}\sum_{i'=3i}^{3i+2}\sum_{j'=3j}^{3j+2}\sum_{k'=3k}^{3k+2}(P_{h/3})_{i'j'k'}.$$

We first examine the numerical convergence of the discrete approximation for both $k = 0$ and $k = 1$. We define four measures of error, the maximum norm error of the discrete density,

$$e^{\infty}(N,t) = \max_{ijk} \left| (\Lambda^{N \leftarrow 3N} P_{h/3})_{ijk}(t) - (P_h)_{ijk}(t) \right|,$$

the discrete $L^2$ error of the density,

$$e^{2}(N,t) = \left( \sum_{ijk} \left[ (\Lambda^{N \leftarrow 3N} P_{h/3})_{ijk}(t) - (P_h)_{ijk}(t) \right]^2 h^3 \right)^{1/2},$$

the error in the probability for the particle to still be diffusing at time $t$,

$$e^{\text{diff}}(N,t) = \left| \sum_{ijk} \left[ (\Lambda^{N \leftarrow 3N} P_{h/3})_{ijk}(t) - (P_h)_{ijk}(t) \right] h^3 \right|,$$

and the error in the probability for the particle to still be diffusing at time $t$ *and* not be in the mesh cell containing the binding site,

$$\bar{e}^{\,\text{diff}}(N,t) = \left| \sum_{\substack{ijk, \\ (i,j,k) \neq (\lfloor N/2 \rfloor, 0, 0)}} \left[ (\Lambda^{N \leftarrow 3N} P_{h/3})_{ijk}(t) - (P_h)_{ijk}(t) \right] h^3 \right|.$$

Here $\lfloor N/2 \rfloor$ denotes the greatest integer less than or equal to $N/2$, hence, $(\lfloor N/2 \rfloor, 0, 0)$ labels the mesh cell containing the binding site. The final error measure is used to see how the solution is behaving away from the binding site.

Table 5.1 shows each error measure evaluated at $t = .42$ s, for both $k = 0$ and $k = 1$, when $N = 33$ and $N = 99$. Note that to five digits the first two error measures appear identical when comparing the $k = 0$ and $k = 1$ cases. In actuality the errors only agree to seven or eight digits. This indicates that the discrete densities for the binding problem and regular diffusion are very close

| | $k=0$ | $k=1$ |
|---|---|---|
| $e^{\infty}(33,.42)$ | 2.5566e-4 | 2.5566e-4 |
| $e^{\infty}(99,.42)$ | 7.8685e-5 | 7.8685e-5 |
| $e^{2}(33,.42)$ | 3.1568e-3 | 3.1568e-3 |
| $e^{2}(99,.42)$ | 1.0386e-3 | 1.0386e-3 |
| $e^{\text{diff}}(33,.42)$ | 1.0071e-5 | 1.0119e-5 |
| $e^{\text{diff}}(99,.42)$ | 1.5031e-8 | 1.0242e-7 |
| $\bar{e}^{\,\text{diff}}(33,.42)$ | 9.8426e-6 | 9.8949e-6 |
| $\bar{e}^{\,\text{diff}}(99,.42)$ | 4.7987e-6 | 4.7099e-6 |

Table 5.1: Numerical measures of error associated with equation (5.2), for $k=0$ and $k=1$.

in value, and that the effect of the binding reaction for physical values of $k$ is quite small. Notice, however, that the last two error measures, which depend on the probability of the particle being in a region as opposed to the probability density, agree to fewer non–zero digits. (Though their actual value is several orders of magnitude smaller than the first two error measures).

With the previous error definitions, we now define the numerical convergence rates. For example, the numerical convergence rate for the maximum norm error is given by

$$r^{\infty}(N,t) = \log_3\left(\frac{e^{\infty}(N,t)}{e^{\infty}(3N,t)}\right).$$

The other convergence rates, $r^2$, $r^{\text{diff}}$, and $\bar{r}^{\,\text{diff}}$ are defined similarly.

Table 5.2 gives the observed numerical convergence rates for $k=0$ and $k=1$. The rates are evaluated at the final simulation time of $t=.42$, a time when the solution is still far from equilibrium. Notice that the maximum norm

| | $k=0$ | $k=1$ |
|---|---|---|
| $r^{\infty}(33,.42)$ | 1.073 | 1.073 |
| $r^{2}(33,.42)$ | 1.012 | 1.012 |
| $r^{\text{diff}}(33,.42)$ | 5.923 | 4.181 |
| $\bar{r}^{\,\text{diff}}(33,.42)$ | .654 | .676 |

Table 5.2: Empirical numerical convergence rates associated with equation (5.2), for $k=0$ and $k=1$.

and two norm rates, like the observed errors, agree to four digits for $k=0$ and $k=1$. Moreover, the rates indicate that in both cases the discrete density is converging at first order when varied between the chosen mesh sizes. The last two rates, those depending on convergence of the particle's probability to be in a region, are noticeably different when $k=0$ and $k=1$.

To see if the discrete solution when $k=0$ was approaching the discrete solution to the diffusion equation for $k=1$, as $h$ was refined, we examined the error between the $k=0$ and $k=1$ solutions for fixed values of $N$. For a fixed mesh width, $h$, let $\rho_h$ be the solution to the discrete diffusion equation, i.e., the $k=0$ case, and let $\hat{\rho}_h$ denote the solution to the point binding problem with $k=1$. Five of the error measures that were examined include the discrete maximum norm error,

$$\alpha^{\infty}(N,t) = \max_{ijk} \left| (\rho_h)_{ijk}(t) - (\hat{\rho}_h)_{ijk}(t) \right|,$$

the relative maximum norm error,

$$\alpha_{\text{r}}^{\infty}(N,t) = \max_{ijk} \left| \frac{(\rho_h)_{ijk}(t) - (\hat{\rho}_h)_{ijk}(t)}{(\rho_h)_{ijk}(t)} \right|,$$

| | $N = 33$ | $N = 99$ | $N = 297$ |
|---|---|---|---|
| $\alpha^{\infty}(N, .42)$ | 7.9172e-8 | 6.9265e-8 | 3.1348e-8 |
| $\alpha_{\mathrm{r}}^{\infty}(N, .42)$ | 4.7148e-2 | 6.3757e-2 | 3.0736e-2 |
| $\alpha^{2}(33, .42)$ | 5.7235e-8 | 6.2309e-8 | 3.7231e-8 |
| $\alpha^{\mathrm{diff}}(33, .42)$ | 1.8595e-7 | 2.3448e-7 | 1.4709e-7 |
| $\bar{\alpha}^{\,\mathrm{diff}}(33, .42)$ | 1.5549e-7 | 2.0784e-7 | 1.3503e-7 |

Table 5.3: Error between $k = 0$ and $k = 1$ solutions to equation (5.2) for varying mesh sizes.

the discrete two norm error,

$$\alpha^{2}(N,t) = \left( \sum_{ijk} \left| (\rho_h)_{ijk}(t) - (\hat{\rho}_h)_{ijk}(t) \right|^2 h^3 \right)^{1/2},$$

the error in the total probability for the particle to be unbound,

$$\alpha^{\mathrm{diff}}(N,t) = \left| \sum_{ijk} \left[ (\rho_h)_{ijk}(t) - (\hat{\rho}_h)_{ijk}(t) \right] h^3 \right|,$$

and the error for the particle to be unbound and outside the mesh cell containing the binding site on the coarsest mesh,

$$\bar{\alpha}^{\,\mathrm{diff}}(N,t) = \left| \sum_{ijk \in I(N)} \left[ (\rho_h)_{ijk}(t) - (\hat{\rho}_h)_{ijk}(t) \right] h^3 \right|.$$

Here $I(N)$ denotes those mesh cells, for $N = 33$, 99, or 297, that are outside the volume representing the $N = 33$ mesh cell containing the binding site.

Table 5.3 shows for each error measure the error between the $k = 0$ and $k = 1$ solutions as $N$ is varied. Aside from the pointwise maximum norm error, none of the errors strictly decrease as $N$ is increased. Each of the other error

measures increases as $N$ is refined to 99 and then decrease as $N$ is further increased to 297.

Based on the preceding sets of convergence rates and numerical errors, the point binding interaction does appear to converge as the mesh width is refined through the *chosen* set of values. It is unclear if this apparent convergence will continue as the mesh is further refined. Over the entire chosen range of mesh values, the solution when $k = 1$ is not converging to the solution to the standard diffusion equation, however, when going directly from $N = 33$ to $N = 297$ all the error measures between the two solutions decrease. Clearly, more investigation is need to answer whether the solution to equation (5.2) is converging as $h \to 0$.

## 5.3 Dimensional Hierarchy Model

We now investigate an alternative model of the point binding interaction due to Charles S. Peskin [34]. The continuum problem for a diffusing particle to locate a point binding site is regularized by having binding occur through a hierarchy of different dimensional surfaces. Previous authors have studied diffusive models with binding to surfaces [43], but the current model provides a novel mechanism to locate and bind a specific point. When diffusing in 3D, the particle is assumed to either continue diffusing or bind to a 2D surface. Within this surface, the particle may then freely diffuse, unbind and return to 3D diffusion, or bind to a specific curve (within the surface). Similarly, within the curve the particle can unbind and return to diffusing within the 2D surface, diffuse along the curve, or bind to a specific point on the curve, the point at which the binding reaction occurs. For comparison, note that the point binding reaction in the

reaction–diffusion master equation formulation involves binding directly to the point in question from 3D diffusion (see equation (5.2)). Also, see Section 5.1 for a discussion of alternative methods to regularize the point binding problem.

A canonical formulation of the proposed model is given by diffusion of a point particle within a periodic 3D box, $\Omega_3 = [-L/2, L/2)^3$. The 2D binding surface is taken to be the plane $\Omega_2 \equiv \{(x, y, 0)\} \in \Omega_3$, with the 1D binding curve the line $\Omega_1 \equiv \{(x, 0, 0)\} \in \Omega_2$, and the binding point the origin. The diffusing particle is assumed to have a separate diffusion constant within each surface, $D_1$, $D_2$, and $D_3$, each having units of length$^2$/time. Transition rates to unbind from a lower dimensional surface to a higher dimensional surface are given by $k_{01}$, $k_{12}$, and $k_{23}$, each having units of time$^{-1}$. Equilibrium rate constants for moving between two successive surfaces are given by $K_{10}$, $K_{21}$, and $K_{32}$, each having units of length. With this definition, the transition rates to bind a lower dimensional surface are then $k_{01}K_{10}$, $k_{12}K_{21}$, and $k_{23}K_{32}$, each having units of length/time.

We define $\rho_0(t)$ to be the probability the diffusing particle is bound at the reaction point, and consider a hierarchy of probability densities, $\rho_1(x, t)$, $\rho_2(x, y, t)$, and $\rho_3(x, y, z, t)$. Each probability density, $\rho_d$, gives the probability density for the particle to be diffusing in the $d$ dimensional surface $\Omega_d$. For example, $\rho_2(x, y, t)$ satisfies

$$\text{Prob}\{\text{particle is in } \Omega_2\} = \int_{\Omega_2} \rho_2(x, y, t) dx dy.$$

Reaction fluxes are defined by

$$\begin{aligned} f_{01}^{\pm}(t) &= \frac{1}{2}\left(\rho_0(t) - \rho_1(0^{\pm},t)K_{10}\right)k_{01}, \\ f_{12}^{\pm}(x,t) &= \frac{1}{2}\left(\rho_1(x,t) - \rho_2(x,0^{\pm},t)K_{21}\right)k_{12}, \\ f_{23}^{\pm}(x,y,t) &= \frac{1}{2}\left(\rho_2(x,y,t) - \rho_3(x,y,0^{\pm},t)K_{32}\right)k_{23}. \end{aligned} \tag{5.4}$$

Letting $\Delta_d$ denote the $d$ dimensional Laplacian, the equations of evolution are (see [34]):

$$\begin{aligned} \frac{\partial \rho_0}{\partial t}(t) + f_{01}^{+}(t) + f_{01}^{-}(t) &= 0, \\ \frac{\partial \rho_1}{\partial t}(x,t) + f_{12}^{+}(x,t) + f_{12}^{-}(x,t) &= D_1\Delta_1\rho_1(x,t), \\ \frac{\partial \rho_2}{\partial t}(x,y,t) + f_{23}^{+}(x,y,t) + f_{23}^{-}(x,y,t) &= D_2\Delta_2\rho_2(x,y,t), \\ \frac{\partial \rho_3}{\partial t}(x,y,z,t) &= D_3\Delta_3\rho_3(x,y,z,t). \end{aligned} \tag{5.5}$$

We assume periodic boundary conditions on the exterior boundary of each surface. Interior boundary conditions giving the flux between successive surfaces are then

$$\begin{aligned} D_1\frac{\partial \rho_1}{\partial x}(0^{-},t) &= f_{01}^{-}(t), & -D_1\frac{\partial \rho_1}{\partial x}(0^{+},t) &= f_{01}^{+}(t), \\ D_2\frac{\partial \rho_2}{\partial y}(x,0^{-},t) &= f_{12}^{-}(x,t), & -D_2\frac{\partial \rho_2}{\partial y}(x,0^{+},t) &= f_{12}^{+}(x,t), \\ D_3\frac{\partial \rho_3}{\partial z}(x,y,0^{-},t) &= f_{23}^{-}(x,y,t), & -D_3\frac{\partial \rho_3}{\partial z}(x,y,0^{+},t) &= f_{23}^{+}(x.y,t). \end{aligned} \tag{5.6}$$

Note that assuming a symmetric initial condition of the form,

$$\begin{aligned} \rho_1(x,0) &= \rho_1(-x,0), \\ \rho_2(x,y,0) &= \rho_2(\pm x,-y,0), \\ \rho_3(x,y,z,0) &= \rho_3(\pm x,\pm y,-z,0), \end{aligned} \tag{5.7}$$

implies that

$$f_{01}^{+} = f_{01}^{-}, \quad f_{12}^{+} = f_{12}^{-}, \quad f_{23}^{+} = f_{23}^{-}, \tag{5.8}$$

for all time.

### 5.3.1 Numerical Model

We use the numerical method of Chapter 3 to develop a spatially discrete approximation to the diffusion hierarchy model. We again assume a cubic domain, with sides of length $L$. Let $N$ denote the number of mesh cells in a given dimension, and $h = L/N$ the mesh width. Mesh cell centers are then given by

$$(x_i, y_j, z_k) = (ih, jh, kh) - \frac{L}{2} + \frac{h}{2}, \quad i, j, k = 0 \dots N-1.$$

Since we assume periodicity, we make the identification $x_N = x_0$, $y_N = y_0$, and $z_N = z_0$. For $N$ even all boundaries lie on mesh cell faces, leading to a simplified embedded boundary discretization. We therefore restrict to even $N$ for all subsequent results. The discretization of $\rho_3(x, y, z, t)$ is denoted by $\left(\rho_3^h\right)_{ijk}(t)$, and similarly the corresponding 2D and 1D mesh variables are $\left(\rho_2^h\right)_{ij}(t)$ and $\left(\rho_1^h\right)_i(t)$ (we subsequently drop the explicit $t$ dependence).

A discrete, one dimensional, delta function is defined as,

$$\delta_i^h = \begin{cases} \frac{1}{h}, & i = 0, \\ 0, & \text{else.} \end{cases}$$

Denoting $0_h^+ = N/2$, and $0_h^- = N/2 - 1$, the discrete reaction fluxes corresponding to (5.4) are then given by

$$\left(f_{01}^h\right)^{\pm} = \frac{1}{2}\left(\rho_0^h - \left(\rho_1^h\right)_{0_h^{\pm}} K_{10}\right) k_{01}, \tag{5.9}$$

$$\left(f_{12}^h\right)_i^{\pm} = \frac{1}{2}\left(\left(\rho_1^h\right)_i - \left(\rho_2^h\right)_{i,0_h^{\pm}} K_{21}\right) k_{12}, \tag{5.10}$$

$$\left(f_{23}^h\right)_{ij}^{\pm} = \frac{1}{2}\left(\left(\rho_2^h\right)_{i,j} - \left(\rho_3^h\right)_{i,j,0_h^{\pm}} K_{32}\right) k_{23}. \tag{5.11}$$

We let $\Delta_d^h$ denote the standard second order, $d$ dimensional, periodic discrete Laplacian. The discrete diffusion operators in dimension $d = 1, 2, 3$, are then

defined to be

$$\begin{aligned}
\left(L_1^h \rho_1^h\right)_i &= D_1 \left(\Delta_1^h \rho_1^h\right)_i \\
&\quad - \left(\left(\rho_1^h\right)_{N/2} - \left(\rho_1^h\right)_{N/2-1} - \left(f_{01}^h\right)^-\right) \delta^h_{i-(N/2-1)} \\
&\quad - \left(\left(\rho_1^h\right)_{N/2-1} - \left(\rho_1^h\right)_{N/2} - \left(f_{01}^h\right)^+\right) \delta^h_{i-N/2},
\end{aligned} \tag{5.12}$$

$$\begin{aligned}
\left(L_2^h \rho_2^h\right)_{ij} &= D_2 \left(\Delta_2^h \rho_2^h\right)_{ij} \\
&\quad - \left(\left(\rho_2^h\right)_{i,N/2} - \left(\rho_1^h\right)_{i,N/2-1} - \left(f_{12}^h\right)_i^-\right) \delta^h_{j-(N/2-1)} \\
&\quad - \left(\left(\rho_2^h\right)_{i,N/2-1} - \left(\rho_2^h\right)_{i,N/2} - \left(f_{12}^h\right)_i^+\right) \delta^h_{j-N/2},
\end{aligned} \tag{5.13}$$

$$\begin{aligned}
\left(L_3^h \rho_3^h\right)_{ijk} &= D_3 \left(\Delta_3^h \rho_3^h\right)_{ijk} \\
&\quad - \left(\left(\rho_3^h\right)_{i,j,N/2} - \left(\rho_3^h\right)_{i,j,N/2-1} - \left(f_{23}^h\right)_{ij}^-\right) \delta^h_{k-(N/2-1)} \\
&\quad - \left(\left(\rho_3^h\right)_{i,j,N/2-1} - \left(\rho_2^h\right)_{i,j,N/2} - \left(f_{23}^h\right)_{ij}^+\right) \delta^h_{k-N/2}.
\end{aligned} \tag{5.14}$$

We note that these forms of the operators are easily transformed to Fourier space. With these definitions, the spatial discretization of (5.5) is then given by

$$\begin{aligned}
\frac{d\rho_0^h}{dt} + \left(f_{01}^h\right)^+ + \left(f_{01}^h\right)^- &= 0, \\
\frac{d\left(\rho_1^h\right)_i}{dt} + \left(f_{12}^h\right)_i^+ + \left(f_{12}^h\right)_i^- &= D_1 \left(L_1^h \rho_1^h\right)_i, \\
\frac{d\left(\rho_2^h\right)_{ij}}{dt} + \left(f_{23}^h\right)_{ij}^+ + \left(f_{23}^h\right)_{ij}^- &= D_2 \left(L_2^h \rho_2^h\right)_{ij}, \\
\frac{d\left(\rho_3^h\right)_{ijk}}{dt} &= D_3 \left(L_3^h \rho_3^h\right)_{ijk}.
\end{aligned} \tag{5.15}$$

Assuming a symmetric initial condition of the form (5.7) will imply that the discrete reaction fluxes also satisfy (5.8).

Note that equation (5.15) has the form of a master equation, with three different types of jump rates. Diffusive jump rates for moving within each $d$–dimensional surface are given by $D_d/h^2$. Unbinding from a $d-1$ dimensional

surface to a $d$–dimensional surface has the jump rate $k_{(d-1)\,d}$. Binding rates from a $d$–dimensional surface to a $d-1$ dimensional surface, for mesh cells that border the $d-1$ dimensional surface, are given by $k_{(d-1)\,d}\,K_{d\,(d-1)}/h$.

### 5.3.2 Numerical Results

As we do not have an exact closed–form solution to equation (5.5), we now consider the the convergence of equation (5.15) as the numerical mesh width, $h$, is reduced. For simplicity we examine this convergence numerically. The specific problem we consider is that of starting a particle at the point binding site, and then calculating the time evolution of the probability densities for the particle's position as the particle subsequently unbinds, and later rebinds. We assume that after the particle rebinds for the first time, it can not subsequently unbind. We therefore expect the bound density, $\rho_0(t)$, to approach 1 as $t \to \infty$. To keep track of the probability that the particle has not unbound at time $t$, and that it has rebound, we split the density $\rho_0(t)$ in two. Denote by $\rho_0(t)$ the probability that the particle has not unbound at time $t$, and by $\rho_0^*(t)$ the probability that the particle has *rebound* to the target point after having been unbound. In the continuum formulation, the equations of evolution now become

$$\begin{aligned}
\frac{\partial \rho_0}{\partial t}(t) &= -k_{01}\rho_0(t), \\
\frac{\partial \rho_0^*}{\partial t}(t) &= \frac{1}{2}k_{01}K_{10}\left(\rho_1(0^+,t) + \rho_1(0^-,t)\right), \\
\frac{\partial \rho_1}{\partial t}(x,t) + f_{12}^+(x,t) + f_{12}^-(x,t) &= D_1\Delta_1\rho_1(x,t), \\
\frac{\partial \rho_2}{\partial t}(x,y,t) + f_{23}^+(x,y,t) + f_{23}^-(x,y,t) &= D_2\Delta_2\rho_2(x,y,t), \\
\frac{\partial \rho_3}{\partial t}(x,y,z,t) &= D_3\Delta_3\rho_3(x,y,z,t).
\end{aligned} \tag{5.16}$$

Notice that these changes do not effect any of the spatially defined densities. We then find that equation (5.15) becomes

$$\begin{aligned}
\frac{\partial \rho_0^h}{\partial t} &= -k_{01}\rho_0^h, \\
\frac{\partial \rho_0^{*\,h}}{\partial t} &= \frac{1}{2}k_{01}K_{10}\left(\left(\rho_1^h\right)_{0_h^+} + \left(\rho_1^h\right)_{0_h^-}\right), \\
\frac{d\left(\rho_1^h\right)_i}{dt} + \left(f_{12}^h\right)_i^+ + \left(f_{12}^h\right)_i^- &= D_1\left(L_1^h\,\rho_1^h\right)_i, \\
\frac{d\left(\rho_2^h\right)_{ij}}{dt} + \left(f_{23}^h\right)_{ij}^+ + \left(f_{23}^h\right)_{ij}^- &= D_2\left(L_2^h\,\rho_2^h\right)_{ij}, \\
\frac{d\left(\rho_3^h\right)_{ijk}}{dt} &= D_3\left(L_3^h\,\rho_3^h\right)_{ijk}.
\end{aligned} \tag{5.17}$$

Our initial condition is then $\rho_0^h(0) = 1$, with the other densities zero at time zero.

For all simulations we take the diffusion constants, $D_1$, $D_2$, and $D_3$ to each have the value $10\,\mu\mathrm{m}^2\mathrm{s}^{-1}$. The length, $L$, of the periodic box is taken to be $24\,\mu\mathrm{m}$, and the unbinding rate constants, $k_{d-1\,d}$, are all chosen to be $1\,\mathrm{s}^{-1}$. To discretize equation (5.17) in time we use the Crank–Nicholson like, second order $L_0$–stable method of [39]. We begin by showing the particle does indeed rebind as $t \to \infty$, i.e., that

$$\lim_{t\to\infty} \rho_0^{*\,h}(t) = 1.$$

Letting $K_{d\,d-1} = 10\,\mu\mathrm{m\,s}^{-1}$ for each equilibrium rate constant, and taking $N = 64$, we can see in Figure 5.1 that $\rho_0^{*\,h}(t)$ approaches 1 as $t$ increases.

We now consider the numerical convergence, as $h \to 0$, of the solutions to equations (5.17). In the following, we take $K_{d\,d-1} = 1\,\mu\mathrm{m\,s}^{-1}$. Recall that $h = L/N$. The numerical time step, $dt$, was chosen to satisfy

$$\begin{aligned}
dt &= \frac{64}{25N}, \\
&\approx \frac{h}{10}.
\end{aligned}$$

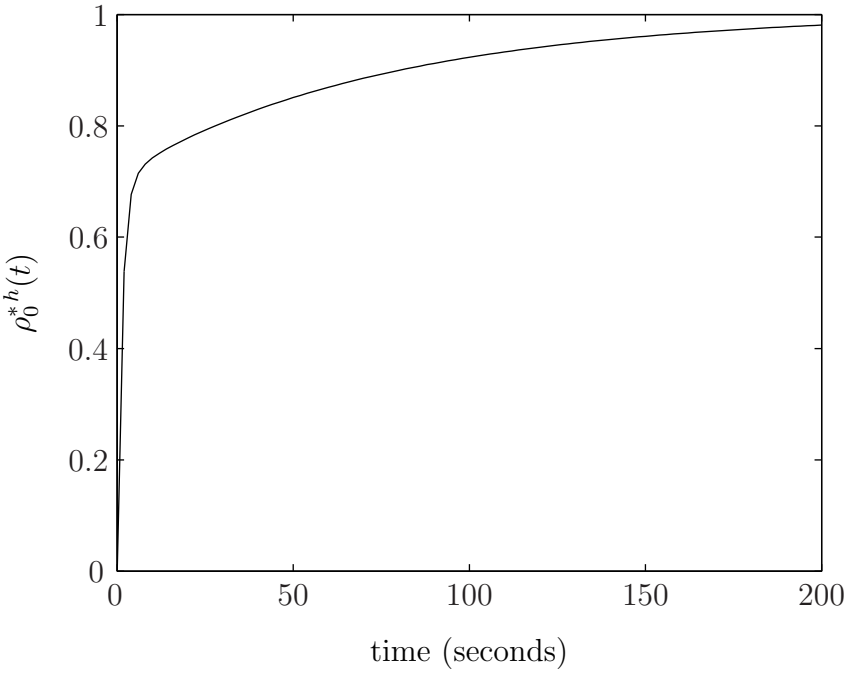


Figure 5.1: Long time behavior of $\rho_0^{*h}$, for $K_{10} = K_{21} = K_{32} = 0$ and $dt = .1\,\mathrm{s}$.

Recalling that $N$ is assumed even, denote by $\Lambda_d^{N\leftarrow 2N}$ the averaging operator that maps a $d$–dimensional mesh function defined on a $(2N)^d$ mesh to a mesh function on a $N^d$ mesh. For example, $\Lambda_2^{N\leftarrow 2N}$ is defined by

$$(\Lambda_2^{N\leftarrow 2N}\rho_2^{h/2})_{ij} = \frac{1}{4}\left((\rho_2^{h/2})_{2i\,2j} + (\rho_2^{h/2})_{2i+1\,2j} + (\rho_2^{h/2})_{2i\,2j+1} + (\rho_2^{h/2})_{2i+1\,2j+1}\right).$$

$\Lambda_1^{N\leftarrow 2N}$ and $\Lambda_3^{N\leftarrow 2N}$ are the defined similarly.

We consider three measures of the relative error in subsequent numerical

solutions, the maximum point wise error,

$$e^{\infty}(N,t) = \max\left[\left|{\rho_0^*}^{h/2}(t) - {\rho_0^*}^{h}(t)\right|, \left|\rho_0^{h/2}(t) - \rho_0^h(t)\right|,\right.$$
$$\max_i \left|\left(\Lambda_1^{N\leftarrow 2N}\rho_1^{h/2}\right)_i(t) - \left(\rho_1^h\right)_i(t)\right|,$$
$$\max_{ij} \left|\left(\Lambda_2^{N\leftarrow 2N}\rho_2^{h/2}\right)_{ij}(t) - \left(\rho_2^h\right)_{ij}(t)\right|,$$
$$\left.\max_{ijk} \left|\left(\Lambda_3^{N\leftarrow 2N}\rho_3^{h/2}\right)_{ijk}(t) - \left(\rho_3^h\right)_{ijk}(t)\right|\right],$$

the discrete $L^2$ error,

$$\begin{aligned} e^2(N,t) = &\left|{\rho_0^*}^{h/2}(t) - {\rho_0^*}^{h}(t)\right| + \left|\rho_0^{h/2}(t) - \rho_0^h(t)\right| \\ &+ \left(\sum_i \left|\left(\Lambda_1^{N\leftarrow 2N}\rho_1^{h/2}\right)_i(t) - \left(\rho_1^h\right)_i(t)\right|^2 h\right)^{1/2} \\ &+ \left(\sum_{ij} \left|\left(\Lambda_2^{N\leftarrow 2N}\rho_2^{h/2}\right)_{ij}(t) - \left(\rho_2^h\right)_{ij}(t)\right|^2 h^2\right)^{1/2} \\ &+ \left(\sum_{ijk} \left|\left(\Lambda_3^{N\leftarrow 2N}\rho_3^{h/2}\right)_{ijk}(t) - \left(\rho_3^h\right)_{ijk}(t)\right|^2 h^3\right)^{1/2}, \end{aligned}$$

and the maximum error over all time steps of $\rho_0^{*h}$,

$$e^*(N,K) = \max_{k=0\ldots K}\left|{\rho_0^*}^{h/2}(t_k) - {\rho_0^*}^{h}(t_k)\right|.$$

Using these error measures, the empirical numerical convergence rates are then defined to be

$$r^{\infty}(N,t) = \log_2\left(\frac{e^{\infty}(N,t)}{e^{\infty}(2N,t)}\right),$$
$$r^2(N,t) = \log_2\left(\frac{e^2(N,t)}{e^2(2N,t)}\right),$$
$$r^*(N,K) = \log_2\left(\frac{e^*(N,K)}{e^*(2N,K)}\right).$$

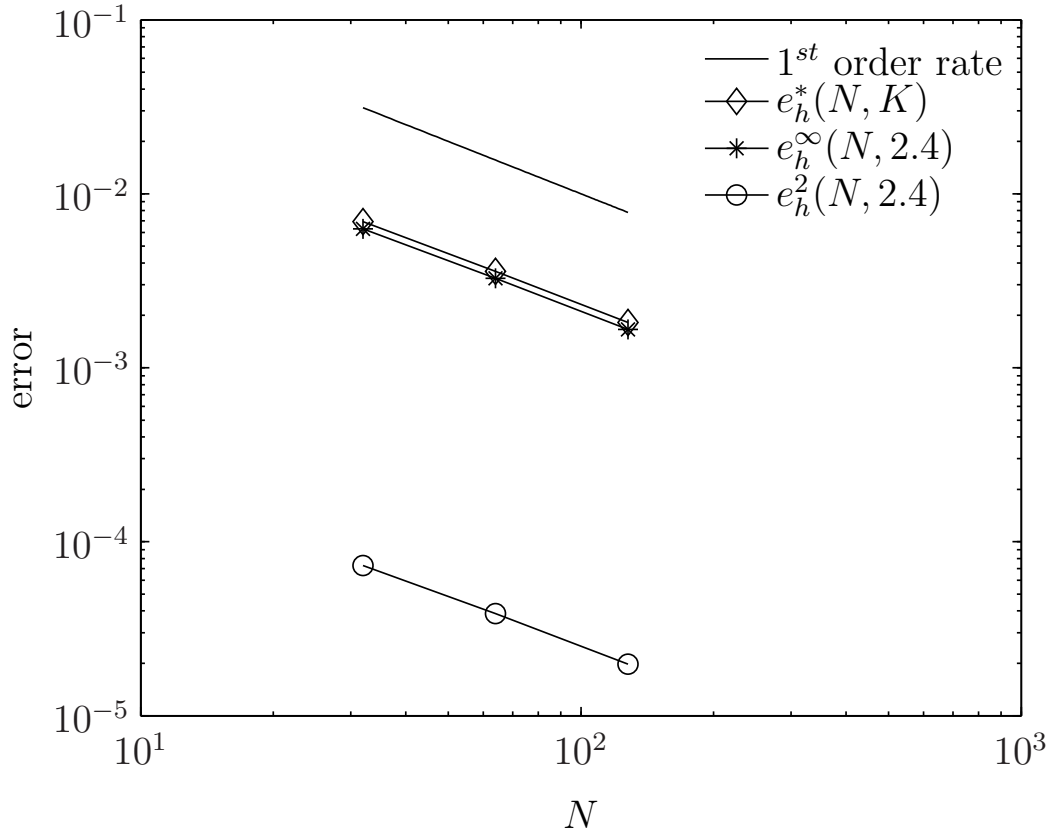


Figure 5.2: Numerical Error in equation (5.17) vs. $N$. The number of *sampled times*, $K = 26$. Note that the number of time steps varied for each mesh size as $dt \approx h/10$.

| | $N = 32$ | $N = 64$ |
|---|---|---|
| $r^*(N, 26)$ | .95 | .976 |
| $r^\infty(N, 2.4)$ | .95 | .976 |
| $r^2(N, 2, 4)$ | .911 | .976 |

Table 5.4: Empirical numerical convergence rates associated with Figure 5.2.

Figure 5.2 shows that each of the error measures converges approximately first order as the mesh spacing is refined from $N = 32$ to $N = 256$. The error in the discrete $L_h^2$ norm is several orders of magnitude smaller than the pointwise error. In addition, note that the error in the maximum norm, $e^\infty$, is almost exactly the same as $e^*$. At $t = 2.4\,\mathrm{s}$, the maximum pointwise error over all the densities and spatial locations actually equals the error in ${\rho_0^*}^h(2.4)$. In general, the pointwise error at each time, over all the densities, appears to be largest for ${\rho_0^*}^h(t)$ (data not shown). Table 5.4 shows the empirical convergence rates associated with Figure 5.2. Note that the rates for $e^*$ and $e^\infty$ are the same to three decimal places. Further, all three convergence rates are approximately one, indicating first order convergence of the numerical discretization. This is expected, as the approximation to the boundary conditions contained in equations (5.12),(5.13), and (5.14) is only first order in the flux, and zero'th order for the actual diffusion operator.

# Chapter 6

# Conclusion

## 6.1 Future extensions

There are a number of future research directions that we are currently pursuing. Foremost is the application of the reaction–diffusion active transport formulation to more realistic biological models than that of Chapter 4. One interesting application is in studying the temperature and ATP dependence of mRNA diffusion. It has been observed experimentally that the diffusion constant of nuclear mRNAs changes more than would be predicted from the Einstein Relation when the temperature of eukaryotic cells is lowered. Moreover, changing the ATP concentration in such cells also appears to affect measured diffusion coefficients [8]. One proposed mechanism for these effects involves speculation that free mRNAs within the nucleus can undergo non–specific DNA binding. It is known that from the end of transcription through the beginning of nuclear export mRNAs are coupled to RNA helicases. RNA helicases help unwind RNA in an ATP dependent manner, hence, the change in the mRNA diffusion constant may be

due to changes in the enzymatic activity of bound RNA helicases.

Another research direction is in developing a more comprehensive biological model of eukaryotic gene expression. This would require adding several new processes including splicing, chromatin dynamics, and transcription factor assembly. With a more realistic model the importance, or lack of importance, of spatial movement in gene expression could then be studied. A related project would be to study the effect of the geometry of organelles and chromatin on the dynamics of gene expression. The nucleus is not a well–mixed environment, nor is it simply an empty sphere as modeled in Chapter 4. It would be interesting to see if different geometries have a noticeable effect on the overall expression process.

Studying the robustness of solutions to the reaction–diffusion master equation as mesh size is varied would be very useful in determining its value as as modeling tool. It may be that different scalings or functional forms for the reaction terms in the master equation are necessary to accurately approximate more microscopic reaction models. In this same direction, studying the relationship between more microscopic models, such as the continuum Fock Space formulation of [11], and the reaction–diffusion master equation may aide in determining appropriate functional forms for reaction terms in the master equation. Moreover, it would be appealing to rigorously derive the reaction–diffusion master equation from a more microscopic model, either directly as a discrete approximation to some continuum model, or indirectly as an asymptotic approximation for a range of numerical mesh sizes.

We have not yet explored the reaction–active transport formulation described in Sections 2.5 and 3.2. Examining the interplay between active trans-

port and diffusion, and the effects of adding both means of spatial movement, could provide an interesting picture on the spatial dynamics within real biological cells. Different components of the gene expression process are known to involve active transport, such as the movement of mRNAs that are localized within the cytoplasm. This interplay has not yet been modeled, but would be an important component of any detailed spatial model of gene expression.

## 6.2 Summary

We have developed a numerical method for solving the reaction–diffusion master equation in complex geometries, and shown how to extend this method to incorporate the active transport of molecules within biological cells. An abstract model of eukaryotic gene expression was developed and solved using this master equation approach, demonstrating the computational feasibility of the method. This model provides a first component in developing a realistic, spatial model of eukaryotic gene expression. The connection between the reaction–diffusion master equation and single particle stochastic reaction–diffusion models was also studied, and it was shown that the reaction–diffusion master equation is equivalent to a discrete Fock Space formulation that tracks individual molecules. We have also investigated the convergence of the point binding reaction as used to model DNA binding interaction in Chapter 4. An alternative model of the point binding reaction was examined in Section 5.3, and a convergent discrete master approximation to this model developed.

# Appendix A

# General Master Equation

We derive here the Master Equation for a general discrete state, continuous time Markov process. Let $\{x_i\}_{i\in\mathbb{N}}$ denote the possible states, and $X(t)$ the stochastic process. We define

$$P(x_i, t_2 \mid x_j, t_1) = Prob\left[X(t_2) = x_i, \text{ given that } X(t_1) = x_j\right].$$

From the Markov property one can derive the Chapman–Kolmogorov equation [17] [40] [26] which states,

$$\frac{dP(x_i, t_2 \mid x_j, t_0)}{dt} = \sum_{k\in\mathbb{N}} P(x_i, t_2 \mid x_k, t_1)\, P(x_k, t_1 \mid x_j, t_0).$$

We now assume that there exist transition weights, $W_{ij}(t)$, such that

$$\lim_{\Delta t\to 0} \frac{P(x_i, t+\Delta t \mid x_j, t)}{\Delta t} = W_{ij}(t).$$

Intuitively, this states the the probability to transition from state $x_j$ at time $t$ to state $x_i$ at a short time later, $t+\Delta t$, is simply $W_{ij}(t)\Delta t$. Using this assumption,

and the Chapman–Kolmogorov equation, one has that

$$\begin{aligned}\frac{dP(x_i,t \mid x_{i_0},0)}{dt} &= \lim_{\Delta t\to 0}\frac{P(x_i,t+\Delta t \mid x_{i_0},0)-P(x_i,t \mid x_{i_0},0)}{\Delta t},\\ &= \lim_{\Delta t\to 0}\frac{1}{\Delta t}\sum_{j\in\mathbb{N}:j\neq i}\Big(P(x_i,t+\Delta t \mid x_j,t)\,P(x_j,t \mid x_{i_0},0)\\ &\qquad - P(x_j,t+\Delta t \mid x_i,t)\,P(x_i,t \mid x_{i_0},0)\Big),\end{aligned}$$

which simplifies to

$$\frac{dP(x_i,t \mid x_{i_0},0)}{dt} = \sum_{j\in\mathbb{N}:j\neq i}\Big(W_{ij}(t)P(x_j,t \mid x_{i_0},0) - W_{ji}(t)P(x_i,t \mid x_{i_0},0)\Big). \tag{A.1}$$

Here we have made use of the fact that

$$P(x_i,t \mid x_{i_0},0) = \sum_{j\in\mathbb{N}:j\neq i} P(x_j,t+\Delta t \mid x_i,t)\,P(x_i,t \mid x_{i_0},0).$$

Equation (A.1) is called the Master Equation for the process $X(t)$.

A more intuitive derivation of the Master Equation is given formally by noticing that the probability to be in the state $x_i$ at time $t+\Delta t$ is simply the sum of two terms. The first term is the probability of being in other states $x_j$ at time $t$ and transitioning to state $x_i$ by time $t+\Delta t$. The second is the probability of being in state $x_i$ at time $t$ and remaining till time $t+\Delta t$. Mathematically this is expressed as

$$\begin{aligned}P(x_i,t+\Delta t \mid x_{i_0},0) = &\sum_{j\in\mathbb{N}:j\neq i}\Big(W_{ij}(t)P(x_j,t \mid x_{i_0},0)\Delta t\Big)\\ &+\Big(1-\sum_{j\in\mathbb{N}:j\neq i}W_{ji}(t)\Delta t\Big)P(x_i,t \mid x_{i_0},0).\end{aligned}$$

Rearranging and taking the limit as $\Delta t\to 0$ gives equation (A.1).

There are several important properties of the structure of (A.1) which we use in deriving our stochastic reaction–diffusion method. Foremost is that all the

jump rates, $W_{ij}(t)$, must be non–negative. In addition, the term $W_{ij}(t)P(x_j, t \mid x_{i_0}, 0)$ appears twice with opposite sign: once in the equation for $P(x_i, t \mid x_{i_0}, 0)$ and once in the equation for $P(x_j, t \mid x_{i_0}, 0)$. This implies that the amount of probability that flows per unit time into state $i$ due to transitions from state $j$ to $i$, is exactly the amount of probability that flows per unit time out of state $j$ due to these same transitions. Finally, note that the coefficient of $P(x_i, t \mid x_{i_0}, 0)$ on the right hand side of (A.1) is non–positive and its absolute value has the form

$$W_i(t) = \sum_{j \in \mathbb{N}: j \neq i} W_{ji}(t).$$

# Appendix B

# Basic Combinatorics Results

Consider the vector of integers, $\boldsymbol{m} = (m_1, \ldots, m_M)$, where $M$ gives the number of components of $\boldsymbol{m}$. Suppose $\boldsymbol{m}$ contains $N$ distinct values, and assume that the number of each of the $N$ distinct values is given by $(n_1, \ldots, n_N)$. Therefore,

$$M = \sum_{i=1}^{N} n_i.$$

Denote by $\tilde{\sigma}(\boldsymbol{m})$ the set of all distinct vectors generated by permutations of the componenets of $\boldsymbol{m}$. Then,

**Theorem B.0.1.** *The number of elements in* $\tilde{\sigma}(\boldsymbol{m})$ *is*

$$M! \prod_{i=1}^{N} \frac{1}{n_i!}.$$

Let $\sigma(\boldsymbol{m})$ denote the set of all vectors, including multiple copies, generated by permutations of the components of $\boldsymbol{m}$. $\sigma(\boldsymbol{m})$ contains $M!$ elements. Then,

**Theorem B.0.2.** *For any function* $f(\boldsymbol{m})$,

$$\sum_{\tilde{\boldsymbol{m}} \in \tilde{\sigma}(\boldsymbol{m})} f(\tilde{\boldsymbol{m}}) = \left( \prod_{i=1}^{N} \frac{1}{n_i!} \right) \sum_{\tilde{\boldsymbol{m}} \in \sigma(\boldsymbol{m})} f(\tilde{\boldsymbol{m}}).$$

# Bibliography

[1] B. Alberts, A. Johnson, J. Lewis, M. Raff, K. Roberts, and P. Walter. *Molecular Biology of the Cell*. Garland Science, New York, 4th edition, 2002.

[2] S. Albeverio and P. Kurasov. *Singular Perturbations of Differential Operators*. Number 271 in London Mathematical Society Lecture Note Series. Cambridge University Press, New York, 2000.

[3] S. S. Andrews and D. Bray. Stochastic simulation of chemical reactions with spatial resolution and single molecule detail. *Physical Biology*, 1:137–151, 2004.

[4] A. Arkin and H. H. McAdams. Stochastic mechanisms in gene expression. *Proc. Natl. Acad. Sci. USA*, 94:814–819, February 1997.

[5] A. Arkin, J. Ross, and H. H. McAdams. Stochastic kinetic analysis of developmental pathway bifurcation in phage $\lambda$–infected escherichia coli cells. *Genetics*, 149:1633–1648, August 1998.

[6] F. Baras and M. M. Mansour. Reaction-diffusion master equation: A comparison with microscopic simulations. *Phys. Rev. E*, 54(6):6139–6147, December 1996.

[7] W. J. Blake, M. Kaern, C. R. Cantor, and J. J. Collins. Noise in eukaryotic gene expression. *Nature*, 422:633–637, April 2003.

[8] A. Calapez and et al. The intranuclear mobility of messenger rna binding proteins is atp dependent and temperature sensitive. *J. Cell Biol.*, 159(5):795–805, 2002.

[9] B. R. Cullen. Nuclear mRNA export: insights from virology. *TRENDS Biochem. Sci.*, 28(8):419–424, August 2003.

[10] G. F. Dell'Antonio, R. Figari, and A. Teta. Diffusion of a particle in presence of $N$ moving point sources. *Annales de l'Institut Henri Poincaré*, 69(4):413–424, 1998.

[11] M. Doi. Second quantization representation for classical many-particle system. *J. Phys. A: Math. Gen.*, 9:1465–1477, 1976.

[12] D. A. Drew. A mathematical model for prokaryotic protein synthesis. *B. Math. Biol.*, 63:329–351, 2001.

[13] M. B. Elowitz, A. J. Levine, E. D. Siggia, and P. S. Swain. Stochastic gene expression in a single cell. *Science*, 297:1183–1186, August 2002.

[14] H. Eyring, H. Walter, and G. E. Kimball. *Quantum Chemistry*. John Wiley & Sons, New York, 1967.

[15] D. Fusco, N. Accornero, B. Lavoie, S. Shenoy, J. Blanchard, R. Singer, and E. Bertrand. Single mRNA molecules demonstrate probabilistic movement in living mammalian cells. *Curr. Biol.*, 13:161–167, January 2003.

[16] C. W. Gardiner. Correlations in stochastic models of chemical reactions. *J. Stat. Phys.*, 14:307, 1976.

[17] C. W. Gardiner. *Handbook of Stochastic Methods: For Physics, Chemistry, and the Natural Sciences*, volume 13 of *Springer Series in Synergetics*. Springer Verlag, New York, 2nd edition, 1996.

[18] F. Gibou, R. P. Fedkiw, L. Cheng, and M. Kang. A second-order-accurate symmetric discretization of the Poisson equation on irregular domains. *J. Comput. Phys.*, 176:205–227, 2002.

[19] M. A. Gibson and J. Bruck. Efficient exact stochastic simulation of chemical systems with many species and many channels. *J. Phys. Chem. A*, 104:1876–1899, 2000.

[20] D. T. Gillespie. Exact stochastic simulation of coupled chemical-reactions. *J. Phys. Chem.*, 81(25):2340–2361, 1977.

[21] D. T. Gillespie. A rigourous derivation of the chemical master equation. *Physica A*, 188:404–425, 1992.

[22] D. T. Gillespie. The chemical langevin equation. *J. Phys. Chem.*, 113(1):297–306, 2000.

[23] S. A. Isaacson and C. S. Peskin. Incorporating diffusion in complex geometries into stochastic chemical kinetics simulations. *Siam J. Sci. Comput.*

Accepted, preprint of this paper and movies of gene expression and regulation model available at `http://www.math.nyu.edu/~isaacsas`.

[24] K. Ishida. Stochastic model for bimolecular reaction. *J. Chem. Phys.*, 41(8):2472–2478, October 1964.

[25] E. R. Kandel. The molecular biology of memory storage: A dialogue between genes and synapses. *Science*, 294:1030–1038, November 2001.

[26] S. Karlin and H. Taylor. *A First Course in Stochastic Processes*. Academic Press, New York, 2nd edition, 1975.

[27] B. N. Kholodenko, G. C. Brown, and J. B. Hoek. Diffusion control of protein phosphorylation in signal transduction pathways. *Biochem. J.*, 350:901–907, 2000.

[28] F. Kühner, L. T. Costa, P. M. Bisch, S. Thalhammer, W. M. Heckl, and G. H. E. Lexa-dna bond strength by single molecule force spectroscopy. *Biophysical Journal*, 87:2683–2690, October 2004.

[29] R. D. Levin. *Quantum Mechanics of Molecular Rate Processes*. Oxford University Press, London, 1969.

[30] P. McCorquodale, P. Colella, and H. Johansen. A cartesian grid embedded boundary method for the heat equation on irregular domains. *J. Comput. Phys.*, 173:620–635, 2001.

[31] D. A. McQuarrie. Stochastic approach to chemical kinetics. *J. Appl. Prob.*, 4:413–478, 1967.

[32] D. A. McQuarrie and J. D. Simon. *Physical Chemistry: A Molecular Approach*. University Science Books, Sausalito, California, 1997.

[33] E. M. Ozbudak, M. Thattai, I. Kurtser, A. D. Grossman, and A. van Oudenaarden. Regulation of noise in the expression of a single gene. *Nat. Genet.*, 31:69–73, May 2002.

[34] C. S. Peskin. Stochastic reaction and diffusion in a hierarchy of dimensions. Notes, 2005.

[35] T. Schlick. *Molecular Modeling and Simulation - An Interdisciplinary Guide*. Springer, New York, 2002.

[36] C. Schutte and F. A. Bornemann. Approximation properties and limits of the quantum-classical molecular dynamics model. In P. Deuflhard and J. e. a. Hermans, editors, *Computational Molecular Dynamics: Challenges, Methods, Ideas.*, volume 4 of *Lecture Notes in Computational Science and Engineering*, pages 380–395. Springer, 1998.

[37] A. E. Smith, B. M. Slepchenko, J. C. Schaff, L. M. Loew, and I. G. Macara. Systems analysis of ran transport. *Science*, 295:488–491, January 2002.

[38] D. A. Smith and R. E. Simmons. Models of motor-assisted transport of intracellular particles. *Biophys. J.*, 80(1):45–68, January 2001.

[39] E. H. Twizell, A. B. Gumel, and M. A. Arigu. Second-order, $L_0$-stable methods for the heat equation with time-dependent boundary conditions. *Advances in Computational Mathematics*, 6(3):333–352, 1996.

[40] N. G. Van Kampen. *Stochastic Processes in Physics and Chemistry*. North-Holland, Amsterdam, 2001.

[41] H. Wang, C. S. Peskin, and T. C. Elston. A robust numerical algorithm for studying biomolecular transport processes. *J. Theor. Biol.*, 221:491–511, 2003.

[42] J. Xing, H. Wang, and G. Oster. From continuum fokker-planck models to discrete kinetics models. *Biophys. J.*, 89:1551–1563, 2005.

[43] H. Zhou and A. Szabo. Enhancement of association rates by nonspecific binding to dna and cell membranes. *Phys. Rev. Lett.*, 93(17):178101, 2004.